NASA TECHNICAL MEMORANDUM

NASA TM X-71960

COPY NO.

NASA TM X-71960

LOW-SPEED WIND-TUNNEL TESTS OF A 1/9-SCALE MODEL OF A VARIABLE-SWEEP ADVANCED SUPERSONIC TRANSPORT

By

H. Clyde McLemore, Lysle P. Parlett

and William G. Sewall

May 1974

NATIONAL AERONAUTICS AND SPACE ADMINISTRATION

LANGLEY RESEARCH CENTER, HAMPTON, VIRGINIA 23665

1. Report No.	2. Government Accession No.	3. Recipient's Catalog No.
TM X-71960		

4. Title and Subtitle	5. Report Date
LOW-SPEED WIND-TUNNEL TESTS OF A 1/9-SCALE MODEL OF A VARIABLE-SWEEP ADVANCED SUPERSONIC TRANSPORT	May 1974
	6. Performing Organization Code

7. Author(s)	8. Performing Organization Report No.
H. Clyde McLemore, Lysle P. Parlett and William G. Sewall	

9. Performing Organization Name and Address	10. Work Unit No.
NASA Langley Research Center Hampton, VA 23665	743-65-12-03
	11. Contract or Grant No.
	13. Type of Report and Period Covered: Technical Memorandum

12. Sponsoring Agency Name and Address	14. Sponsoring Agency Code
National Aeronautics and Space Administration Washington, DC 20546	

15. Supplementary Notes

16. Abstract

Tests have been conducted in the Langley full-scale tunnel to determine the aerodynamic characteristics of a 1/9-scale variable-sweep advanced supersonic transport configuration. The model configurations investigated were the basic unflapped arrangement, and a takeoff and landing flap arrangement with several strake leading edge flow control devices. The tests were conducted for an angle-of-attack range from about -5° to 36° and a sideslip range from -5° to 10°. The tests were conducted for a range of Reynolds number from 3.92×10^{6} to 5.95×10^{6} corresponding to test velocities of about 54.5 knots and 81.7 knots, respectively.

17. Key Words (Suggested by Author(s)) (STAR category underlined)	18. Distribution Statement
Aerodynamics, Low Speed Stability and Control, Advanced Supersonic Transport, Variable Sweep	~~Foreign distribution excluded~~

19. Security Classif. (of this report)	20. Security Classif. (of this page)	21. No. of Pages	22. Price*
Unclassified	Unclassified	84	$4.00

LOW-SPEED WIND-TUNNEL TESTS OF A 1/9-SCALE MODEL OF A VARIABLE-SWEEP ADVANCED SUPERSONIC TRANSPORT

By H. Clyde McLemore, Lysle P. Parlett
and William G. Sewall
Langley Research Center

SUMMARY

Tests have been conducted in the Langley full-scale tunnel to determine the force and moment characteristics of a 1/9-scale variable-sweep advanced supersonic transport model.

The model, with or without flaps deflected, had a pitchup characteristic in the moderate to high angle-of-attack range. The pitchup appeared to be caused mainly by the wing strake, and deflecting the whole strake in incidence or modifying the leading edge of the strake by drooping it or by adding a slat provided a small improvement in longitudinal stability. The slatted-strake landing or takeoff configuration with T-tail provided longitudinal stability to angles of attack of 12° to 15°. Above these angles of attack the T-tail resulted in a severe pitchup. In general, the model had good lateral and directional stability characteristics through about 15° angle of attack, after which the stability deteriorated rapidly with increasing angle of attack and instability occurred near maximum lift.

INTRODUCTION

The present study is part of an overall effort by the NASA to provide the technology base for the development of advanced supersonic vehicles. The configuration concept which is the subject of this paper is a derivative of one studied in the National SST (supersonic transport) program (references 1 and 2) and traces its ancestry to the SCAT 16 configuration of the SCAT (supersonic commercial air transport) studies (reference 3). As studied in

the SST program, the concept exhibited one of the highest ratios of payload to gross weight of all those submitted for evaluation.

The dominant feature of the configuration is its non-integrated, variable-sweep wing. The variable-sweep feature was utilized to provide high levels of low-speed lift, good subsonic flight efficiency, and good supersonic cruise efficiency with a relatively small, highly loaded wing which would involve less structural design uncertainty than would the lightly loaded, large wings of competing concepts.

The primary reason for abandoning the non-integrated, variable-sweep concept during its development was a conflict between longitudinal stability criteria of that time, and effects of the engine exhaust on the horizontal tail. Placement of the horizontal tail in a high, or T-tail, position would have eliminated adverse thermal and acoustic effects of the jet on the tail and would have prevented a venturi-like suck-down of the horizontal tail as the exhaust jet streamed between it and the ground during takeoff rotation, both of which were problems for a low-tail configuration. However, a T-tail was generally known to produce a deep-stall problem as the tail dropped into the wake of the stalled wing and became ineffective. Because "stick pusher" or attitude-limiting systems, which are dependent upon attitude and pitch-rate sensing, were not then considered permissible in commercial aircraft, the contractor conducting the SST study ultimately took the alternate route of integrating the wing and horizontal tail, and suspending the engine nacelles from the latter, before abandoning the variable-sweep approach altogether. Since that time, developments in stability criteria and in aero-electronic technology and an increased emphasis on CCV (control-configured vehicles) have opened the path to serious study of a T-tail solution of the problems of the variable-sweep SST.

The purposes of the subject tests were: (1) to establish a comprehensive matrix of aerodynamic data from which the development of acceptable operating procedures in the critical low-speed regime may be explored, taking advantage of new criteria and developing propulsion and aero-electronic technologies, and (2) to explore means of alleviating those aerodynamic characteristics of the configuration that most adversely affect interdisciplinary trades.

The present investigation consisted of low-speed wind-tunnel tests to determine the static longitudinal, lateral, and directional stability characteristics of a 1/9-scale model of a variable-sweep advanced supersonic transport configuration. The tests were conducted in the Langley full-scale tunnel for a range of Reynolds number from 3.92×10^6 to 5.95×10^6 (corresponding to test velocities of about 54.5 knots and 81.7 knots, respectively). The tests were conducted for a range of angles of attack from about -5° to 36° and for sideslip angles of -5° to 10°. The model variables were: flap, slat, strake, strake leading edge devices, sweep-angle, a low-tail and a T-tail arrangement, and a straight and a drooped fuselage nose.

SYMBOLS

The data are referred to the stability system of axes. (See fig. 1). The origin of the axes was located to correspond with the model center of gravity which was at 50 percent of the mean aerodynamic chord of the 72° swept wing configuration (see fig. 2).

The dimensional quantities are given in the international System of Units (SI), and definitions and conversion to other unit systems are given in reference 4.

b	reference wing span ($\Lambda = 72^\circ$), 3.34 m
C_D	drag coefficient, Drag/qS
C_L	lift coefficient, Lift/qS
C_ℓ	rolling moment coefficient, $\frac{\text{Rolling moment}}{qSb}$
C_m	pitching moment coefficient, $\frac{\text{Pitching moment}}{qS\bar{c}}$
C_n	yawing moment coefficient, $\frac{\text{Yawing moment}}{qSb}$
C_Y	side force coefficient, Side force/qS
$\bar{c}$	reference mean aerodynamic chord ($\Lambda = 72^\circ$), 2.03 m
H.R.L.	horizontal reference line
i_s	strake incidence angle, degrees (nose down, negative)

i_t	horizontal-tail incidence angle, degrees (nose up, positive)
L.E.	leading edge
M_X	moments about X-axis, degrees
M_Y	moments about Y-axis, degrees
Y_Z	moments about Z-axis, degrees
q	free stream dynamic pressure, Newton/m^2
S	wing reference area ($\Lambda = 72^o$), 5.77 m^2
T	T-tail horizontal tail
X	longitudinal axis
Y	lateral axis
Z	vertical axis
C_{ℓ_β}	rate of change of C_ℓ with β for β range of $\pm 5^o$
C_{n_β}	rate of change of C_n with β for β range of $\pm 5^o$
C_{Y_β}	rate of change of C_Y with β for β range of $\pm 5^o$
α	angle of attack, degrees
β	angle of sideslip, degrees
δ_a	aileron droop angle, degrees
δ_f	flap deflection, degrees
δ_n	strake leading edge deflection, degrees
δ_s	wing slat deflection, degrees
Λ	wing leading edge sweep angle, degrees
ϕ	angle of roll, degrees
ψ	angle of yaw, degrees

MODEL

Drawings of the 1/9-scale model are shown in figures 2, 3, 4, and 5, and additional dimensional characteristics are given in table I. Photographs of the 1/9-scale model mounted for tests in the Langley full-scale tunnel and of a 1/135-scale model (1/15-scale of larger model) mounted in a 1/15-scale model of the full-scale tunnel are presented as figs. 6, 7, and 8. The 1/9-scale model was constructed of wood and fiberglass over an aluminum frame and was considered to be rigid for these low-speed tests. The models were constructed to simulate the shape of the elastic airplane in 1g flight of the aircraft for the 20°-sweep condition.

The model had a variable-sweep wing with outboard pivots, a single vertical tail, and an interchangeable horizontal tail (low tail or T-tail). The wing pivot was located 5.378m aft of the undrooped fuselage nose and at span station 0.70m. The horizontal tail was all-movable through an angle range from 5° to -20°. The wing sweep could be varied from 20° to 72° for the unflapped wing, from 20° to 30° for the takeoff flap arrangement, and could be set only at 20° for the landing flap arrangement. The takeoff flap configuration (designated $14^{\circ}/28^{\circ}$ and shown in figure 3) consisted of an intermediate large section (0.20c) deflected 14° and a smaller aft portion (0.12c) deflected 28°. The landing flap arrangement (designated $30^{\circ}/50^{\circ}$ and shown in figure 3) was the same as that for the takeoff case except that the mid and aft portions were deflected 30° and 50°, respectively. The wing outboard of the pivot had a leading edge slat (0.135c) deflected 10° for all of the takeoff flap tests and 30° for all landing flap tests. The center of gravity of the model was considered to be located at 50-percent of the mean aerodynamic chord of the 72°-swept configuration (5.220m aft of the undrooped fuselage nose). The model was unpowered but was equipped with flow-through nacelles having an equal inlet and exit areas. Several devices were used for delaying the formation of a leading edge vortex and the wing strake. These were: (1) a leading edge slat, (2) leading edge droop, and (3) deflecting the whole strake (nose downward). The geometric characteristics and angular deflections of these devices are shown in figures 4 and 5.

TESTS AND CORRECTIONS

Tests

Force tests were conducted on the 1/9-scale model in the Langley full-scale tunnel for a range of Reynolds number, based on a mean aerodynamic chord of 2.03m, of 3.92×10^6 to 5.95×10^6 (corresponding to velocities of about 54.5 knots and 81.7 knots, respectively) with most of the tests conducted at the lower value. Tests were conducted for angles of attack from about -5° to 36° and for sideslip angles from -5° to 10°. The model configuration variables are listed in table 2.

Wool tufts were attached to the upper surface to the wing, fuselage, and horizontal tail, and to the vertical tail to aid in the interpretation of the force test results.

Corrections

The test data have been corrected for tunnel air-flow angularity, buoyancy, and for strut tares. Wall corrections were found by theory and by experiment on the 1/135-scale model to be negligible and were not incorporated into the data. (Theory of ref. 5 showed at a lift coefficient of 1.0 an angularity of 0.35° and a dynamic pressure correction of 0.75 percent.)

PRESENTATION OF DATA

Type of Data	Figure Number
Longitudinal:	
Tuft studies	9, 10, 11, 12
Effect of Reynolds number	13
Effect of wing sweep	14, 15
Effect of horizontal tail position, clean	15
Effect of high lift devices	16
Effect of slatted strake, flaps down	17
Effect of removing strake	18
Effect of strake leading edge droop	19
Effect of strake leading edge device	20
Effect of strake incidence	21
Effect of strake leading edge arrangement	22
Effect of horizontal tail incidence	23, 24, 25
Lateral-Directional:	
Effect of β	26- 32
C_{Y_β}, C_{n_β}, C_{ℓ_β} versus α	33- 35

In a few instances it was desirable to compare longitudinal data for the slatted-strake take-off flap arrangement at $\beta = 0^\circ$ with data for other configurations, but these particular $\beta = 0^\circ$ data were not obtained. Upon examination of the data at $\beta = \pm 5^\circ$, however, it was determined that 5° of sideslip had very little effect on the longitudinal data; so slatted strake, takeoff flap data at $\beta = -5^\circ$ were used in place of $\beta = 0^\circ$ data in figures 17, 18, and 19, and it is so indicated in the figures.

RESULTS AND DISCUSSION

In order to expedite the publication of the data of this report, the data will be presented with only a cursory analysis. The analysis concentrates on the T-tail configuration since it was considered that the low-tail

configuration was tested only to afford a point of reference with previous work, or a basis for comparison, and not as an acceptable alternate tail position because of the aforementioned problems associated with excessive tail temperatures caused by the engine exhaust and suckdown of the horizontal tail when in proximity to the ground. Further, the data are generally analyzed with regard to the achievement of high lift and adequate stability and control for angles of attack up to that at which the outboard wing panels stall since this would seem to be the maximum usable angle of attack because stall of the outboard panels would normally indicate loss of damping in roll, loss of lateral control, and excessive buffeting.

Tuft studies.- As an aid in interpreting the force-and-moment characteristics, flow studies were made by observing the action of, and by photographing, wool tufts attached to the surfaces of the wings, fuselage, and tail for a few selected configurations--all with 20° wing sweep. The clarity of the photographs was quite poor, so the flow patterns were diagramed and are presented in figures 9 through 12 to illustrate the general air-flow characteristics of the model.

In general, the strake is seen to have attached flow throughout the angle-of-attack range investigated, but the presence of a leading edge vortex is evident. Modifications to the strake (i.e., slats, drooped leading edge, or strake incidence) improved the flow behind the strake by suppressing the leading edge vortex. The outboard wing panels are seen to be stalled at high angles of attack for all configurations, but the flaps remain unstalled. This stall of the outboard wing panels is an important point to note with regard to analysis of the force test data in that, although the outboard wing panels begin to stall at angles of attack between 18° and 22° and are usually completely stalled at an angle of attack of 26°, the force data (figures 13 to 25) show that the lift coefficients continue to rise to much higher angles of attack. These greater values of lift coefficient are evidently the result of increased vortex lift on the wing strake and would probably not be considered usable lift for an operational aircraft because, as pointed out previously, the prior outboard wing stall would probably have already resulted in loss of damping in roll, inadequate lateral control, and excessive buffeting.

One further point that should be made is that the wing slat did not function as well as expected, and it is felt that modifications to the slat deflection angle and slot geometry would have improved the airflow over the outboard wing for angles of attack greater than 22°. The tuft test data also show that side-slipping the model in general caused the flow to deteriorate over the advanced wing.

Reynolds number.- At the outset of the program, tests were conducted on the flapped configuration for a range of wind-tunnel speeds to determine whether there were appreciable effects of Reynolds number and to determine whether tests at speeds lower than maximum tunnel speed would be acceptable. These data on the effects of Reynolds number are shown in figure 13. The data show that variations in Reynolds number in the range from 3.92×10^6 to 5.95×10^6 had little effect on the aerodynamic characteristics - particularly to angles of attack of about 20°. Above this angle, $C_{L,max}$ was increased a small amount with increasing Reynolds number. The difference was considered to be negligible, however, for the purposes of the present investigation; and, since the test program could be expedited by using the lower velocity, the remainder of the tests was conducted at a Reynolds number of 3.92×10^6 (test velocity of about 54.5 knots).

Wing sweep.- The effects of wing-sweep angle on the aerodynamic characteristics of the clean configuration, with and without the T-tail and the low-tail arrangement, are shown in figures 14 and 15. Increasing wing-sweep angle is seen to decrease lift and lift curve slope in the angle of attack range to about 15°. The pitchup that begins at about 7° angle of attack for the 20° sweep condition for either horizontal-tail arrangement is also alleviated slightly by increasing wing-sweep angle.

High lift devices.- One point that should be noted at the beginning of the discussion is that the lift coefficients of the present investigation for a particular angle of attack appear to be unusually low. The reason for this characteristic is the manner in which C_L is defined. The fully swept planform area was selected as the reference area since this was the area used by previous investigators (governmental and industrial) concerned with the variable-sweep concept. One should note that the lift coefficients of the

present investigation would be increased by about 50 percent if the reference area had been that of the 20°-sweep configuration (the area being based on that described by extending the leading and trailing edge of the variable-sweep panels to the aircraft centerline).

The effect of wing high-lift devices (flaps and slats) on the aerodynamic characteristics for the basic-strake and for the slatted-strake configurations are shown in figure 16 for the two tail arrangements. The lift coefficient at all angles of attack is seen to be increased considerably by the addition of flaps and slats, and the longitudinal stability characteristics for the T-tail arrangement are about the same as for the flap-up condition, except that the onset of pitchup is delayed from about 7° angle of attack for the clean configuration to about 10° for the flap-down configurations with the T-tail. The pitch characteristics for the slatted-strake configuration are shown in figure 17. The slatted strake was considered to be part of the basic high-lift system since it had been indicated in reference 6 to be a recommended feature. The data of figure 17 show that for both the landing and takeoff configurations, use of the slatted strake provided an improvement in longitudinal stability. The pitchup for the flap-down, T-tail configurations was delayed to 12° or 15° angle of attack (as compared to about 10° for the basic-strake configuration) and was somewhat less severe at higher angles. Hence the slatted strake was considerably better than the basic strake in providing high usable lift values for the takeoff and for the landing configurations. Even with the slatted strake, however, the longitudinal instability was quite severe at the approximately 22° angle of attack at which the outboard wing panels stalled; so it would probably not be possible to use all the high lift coefficient that would be available from the point of view of wing stall.

Strake modifications.- Both the tuft studies of figures 9-12, and past experience with strakes similar to those of the present model, have indicated that the pitchup is associated with the loading of the strake. Hence, the effects of removing the slatted strake for the landing and takeoff flap arrangements were investigated and the results are shown in figure 18. The effects of removing the strake are seen to be an increase in longitudinal

stability, a marked delay in the onset and severity of the pitchup, and a loss of lift. Since the slatted strake had resulted in improved longitudinal stability and an increase in maximum usable lift coefficient, as compared with the basic strake, alternate strake modifications were investigated to determine whether other approaches to controlling strake flow would be perhaps more effective or more simple than use of the slat.

The effect of drooping the leading edge of the strake is shown in figures 19 and 20. Figure 19 shows that increasing the droop angle beyond 30° did not have any significant effect on either longitudinal stability or lift. Figure 20 shows a comparison of the aerodynamic characteristics for the 30° droop condition, the basic strake, and the slatted strake. These data show that the drooped leading edge was as effective as the strake slat in delaying the onset and reducing the severity of the pitchup.

It was reasoned further that if the strake was causing a large positive pitching moment at high angles of attack, then deflecting the whole strake, nose downward, should relieve the pitchup caused by the strake lift and should improve the longitudinal stability by improving the flow over the wing behind the strake. The effect of deflecting the whole strake up to $i_s = -15^{\circ}$ for the landing flap arrangement is shown in figure 21. These data show that increasing the incidence of the strake delayed the onset of the pitchup. The lift is virtually unaffected for angles of attack below 25°, and the drag is reduced significantly at the higher angles of attack. The data suggest the possibility of programing the strake incidence to vary on a one-to-one basis with angle of attack to delay the onset of pitchup to at least $\alpha = 15^{\circ}$, and probably further with higher strake incidence angles.

The overall effects of the various strake modifications for the takeoff flap arrangement are shown in figure 22. The whole strake was deflected only 5° for this flap arrangement, and it appears from the higher strake-deflection data of figure 21 that greater strake deflection angles would have increased the longitudinal stability of the takeoff flap arrangement and would probably have delayed the pitchup. Of the strake modifications investigated, however, the slatted strake appears to be the best arrangement for the takeoff flap configuration.

It should be noted that none of the strake modifications had a significant effect on the maximum lift coefficient or upon the maximum usable C_L, and none of the modifications enabled the use of the maximum lift that would be available if it were not for the pitchup. The significance of these data are that they show the strake to be the main contributor to the longitudinal instability, and this wing apex area should be the area for concentrated study to determine means of improving the longitudinal stability characteristics of the variable-sweep SST in its landing or takeoff modes.

Effect of horizontal tail deflection.- The effects on the aerodynamic characteristics of deflecting the horizontal tail are shown in figures 23-35. The horizontal tail is seen to be quite effective in providing longitudinal trim throughout the angle-of-attack range investigated for either the T-tail or the low-tail arrangement.

LATERAL AND DIRECTIONAL CHARACTERISTICS

The lateral and directional aerodynamic characteristics of the model with and without the tail installed for several values of wing leading-edge sweep and for several wing configurations are shown in figures 26-32. The comparable stability derivatives are shown in figures 33-35. The derivatives were obtained by determining the incremental change in the lateral and directional characteristics caused by a $\pm 5^\circ$ change in sideslip angle.

In general, the model had good lateral and directional characteristics through about 15° angle of attack, after which the stability deteriorated very rapidly and instability occurred at about 20° angle of attack (near $C_{L,max}$).

CONCLUDING REMARKS

The results of force tests in the Langley full-scale tunnel of a 1/9-scale variable-sweep advanced supersonic transport model show the following:

1. The model with or without flaps deflected had a pitchup characteristic in the moderate to high angle of attack range. The pitchup appeared to be caused mainly by the wing strake, and deflecting the whole strake in

incidence or modifying the strake leading edge by drooping it or by adding a slat provided a small improvement in longitudinal stability.

2. The slatted-strake landing or takeoff configuration with T-tail provided longitudinal stability to angles of attack of 12° to 15°. Above these angles of attack, however, the T-tail resulted in a severe pitchup.

3. Both the T- and low-tail provided good longitudinal control effectiveness throughout the angle-of-attack range investigated.

4. In general, the model had good lateral and directional stability characteristics through about 15° angle of attack, after which the stability decreased very rapidly with increasing angle of attack and instability occurred near maximum lift.

REFERENCES

1. Commercial Supersonic Transport Program. Phase II-A. Comprehensive Report Nov. 1, 1974. Contract No. FA-SS-64-4 The Boeing Company Airplane Division; Renton, Wash. USA.

2. Commercial Supersonic Transport Program. Phase II-C. Interim Aircraft Performance Assessment Report. Contract No. FA-SS-66-5. Nov. 15, 1965.

3. Proceedings of NASA Conference on Supersonic - Transport Feasibility Studies and Supporting Research, Sept. 17-19, 1963. NASA TM X-905.

4. Mechtly, E. A.: The International System of Units - Physical Constants and Conversion Factors (Second Revision) NASA SP-7012, 1973.

5. Heyson, Harry H.: Use of Superposition in Digital Computers to Obtain Wind-Tunnel Interference Factors for Arbitrary Configurations, With Particular Reference to V/STOL Models. NASA TR R-302, 1969.

6. Freeman, Delma C., Jr.: Low Subsonic Flight and Force Investigation of a Supersonic Transport Model with a Variable-Sweep Wing. NASA TN D-4726, Nov. 1968.

TABLE I.- MODEL DIMENSIONS

Wing - (All wing dimensions refer to the 72° sweep configuration)

Area	$5.77\ m^2$
Span	3.34 m
Aspect Ratio	1.93
Mean Aerodynamic Chord	2.03 m
Root Chord	4.13 m
Sweep of Wing Leading Edge	(Variable, 20°-72°)
Geometric Twist: (referenced to H.R.L.)	
Root	-1.33°
Tip (80% semispan, parallel to fuselage centerline)	-5.52°

Horizontal Tail	T-tail	Low-Tail
Area	$0.651 m^2$	$1.036 m^2$
Span	1.42 m	1.65 m
Mean Aerodynamic Chord	.50 m	.64 m
Incidence	-20°- $+5^{\circ}$	-20°- $+5^{\circ}$
Dihedral	$+10^{\circ}$	-10°

Moment Reference

Longitudinal Location	5.21 m from undeflected nose
Vertical Location	.063 m above H.R.L.

TABLE I.- (Concluded)

Vertical Tail	T-tail Configuration	Low-Tail Configuration
Area	0.823 m^2	0.509 m^2
Span	.76 m	.72 m
Sweep Angles		
Leading Edge	37^o	34^o
Trailing Edge	30^o	20^o
Root Chord	1.90 m	1.67 m
Tip Chord	.64 m	.27 m
Engines		
Engines are skewed 1.5^o from the X-axis with the exhaust nozzles pointing outward		
Spanwise Location of Engines	Inboard	Outboard
(to front of inlets)	2.54 m	5.46 m
Location relative to H.R.L.	-5.75^o	-4.25^o

TABLE II.- MODEL CONFIGURATION VARIABLES

CLEAN				
Λ	Strake	Wing Slat	Wing Flap	Tail
20° 30° 42° 72°	Off, On	Retracted	0°	Off, T Low

TAKE-OFF				
Λ	Strake	Wing Slat	Wing Flap	Tail
20°, 30°	Off, On Incidence: (0°, 5°, 10°,15°) L.E. Devices: (Slat, Droop L.E. of 0°,30°,60°,90°)	10°	$14^{\circ}/28^{\circ}$	Off, T Low Incidence: (5°, 0°, -5°,-10°, -20°)

LANDING				
Λ	Strake	Wing Slat	Wing Flap	Tail
20°	Off, On, Incidence: (0°,5°,10°,15°) L.E. Devices: (Slat, Droop L.E. of 0°,30°,60°,90°)	30°	$30^{\circ}/50^{\circ}$	Off, T Low Incidence: (5°,0°,-5°; -10°, -20°)

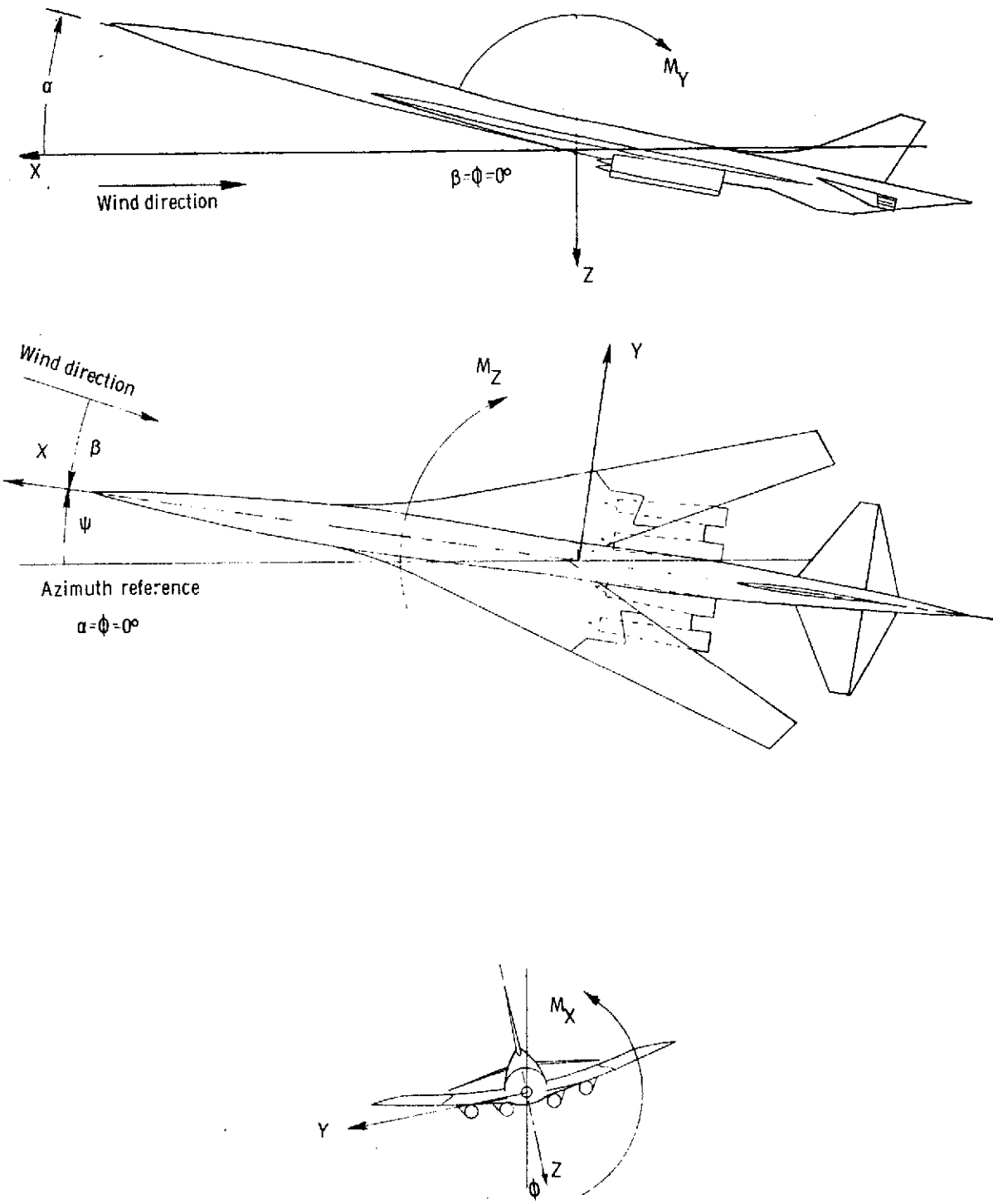

Figure 1.- System of axes used in investigation. Arrows indicate positive directions of moments, forces, and angles.

Wing reference dimension

Area	5.77 m^2
Aspect ratio	1.93
Mean aerodynamic chord	2.03 m
Spanwise location of M.A.C.	0.383 b/2 (0.64 m)
Span	3.34 m
Incidence	
Root	-1° 20'
0.80 b/2	-5° 31'

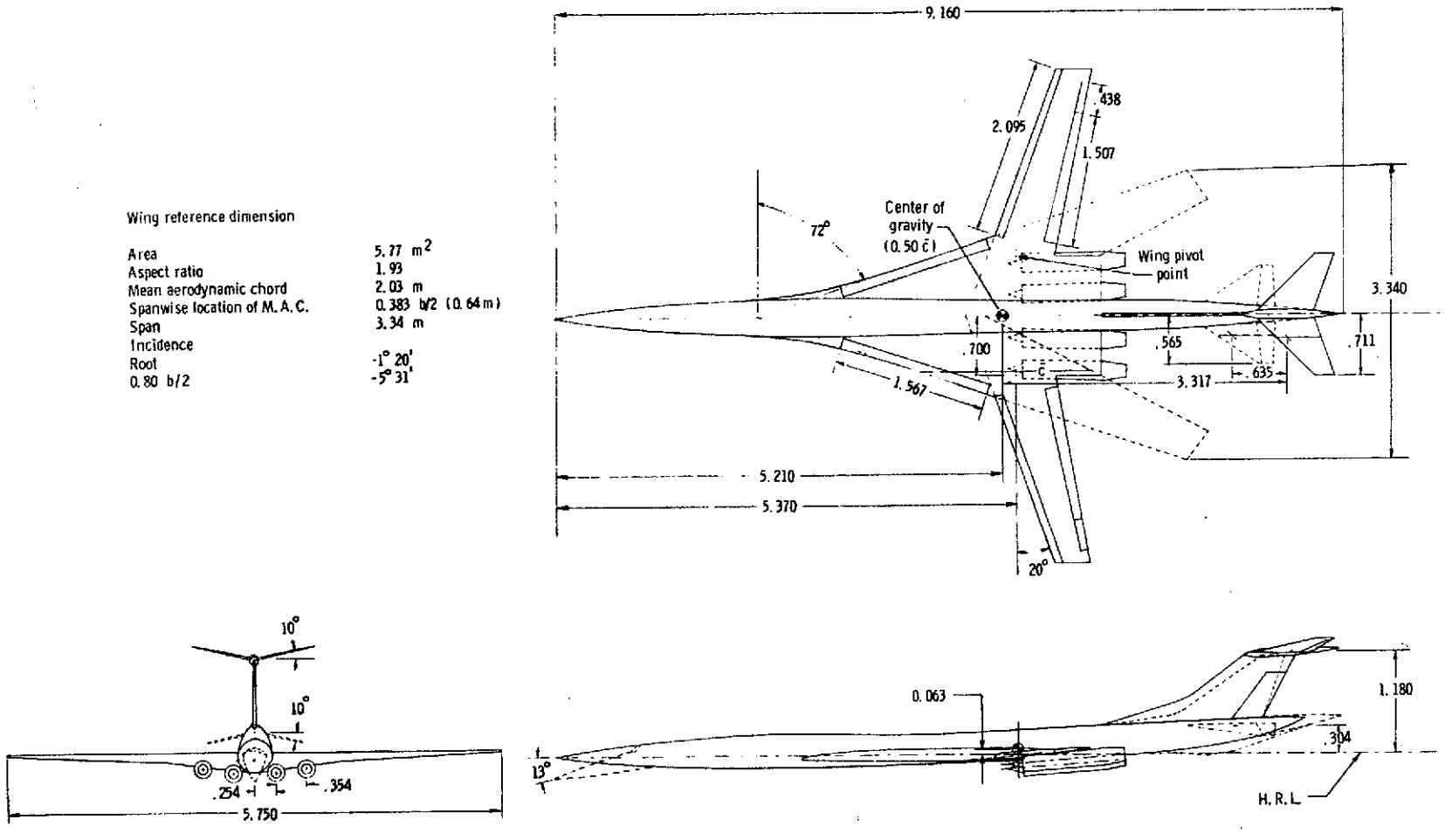

Figure 2. - Geometric characteristics of $\frac{1}{9}$ scale, variable sweep, advanced supersonic transport model.
All dimensions in meters.

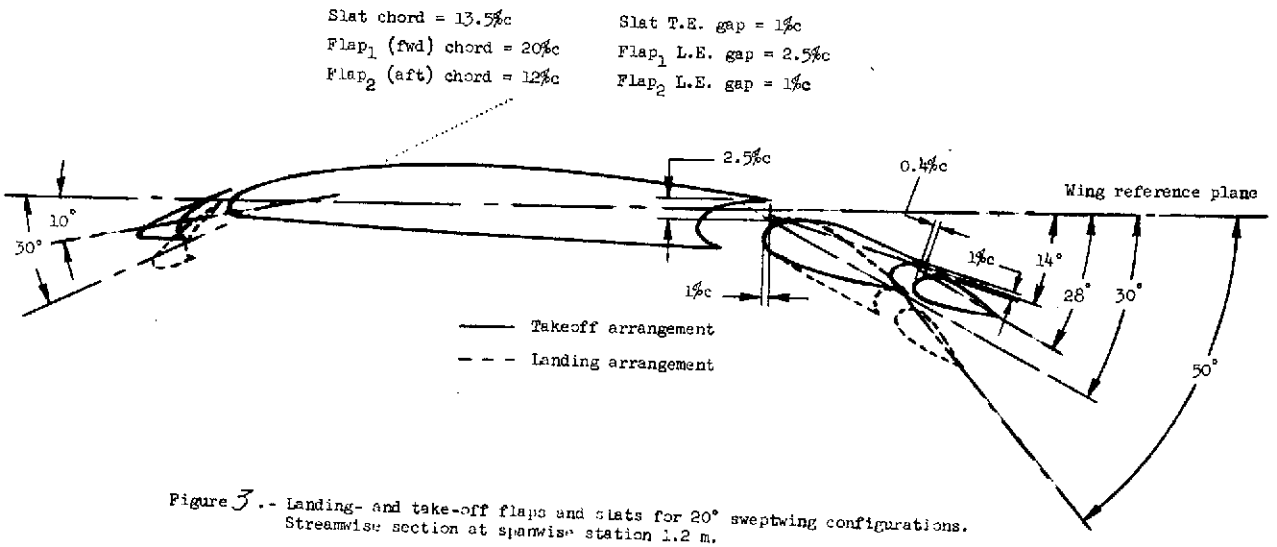

Figure 3.- Landing- and take-off flaps and slats for 20° sweptwing configurations. Streamwise section at spanwise station 1.2 m.

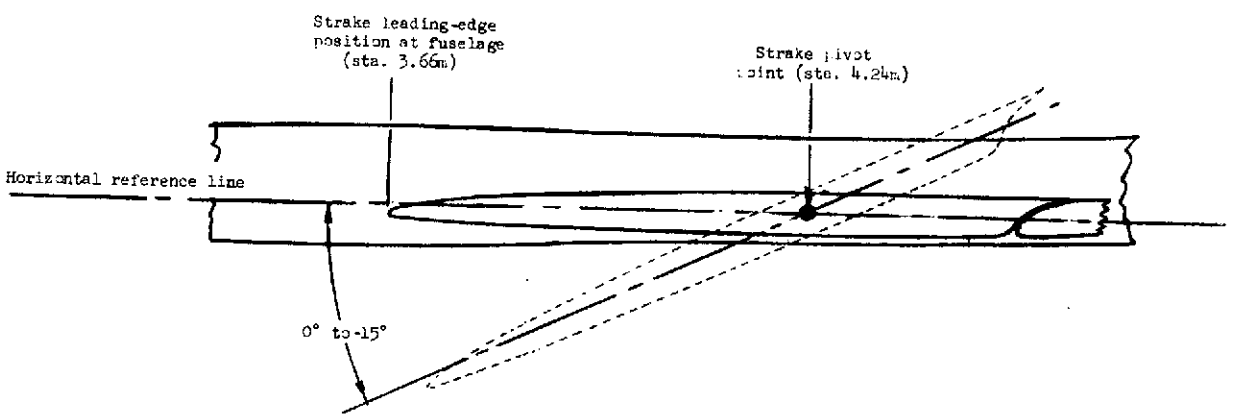

Figure 4.- Wing strake with pivot at station 4.24 m from undeflected nose of model. Streamwise section at spanwise station 0.44 m.

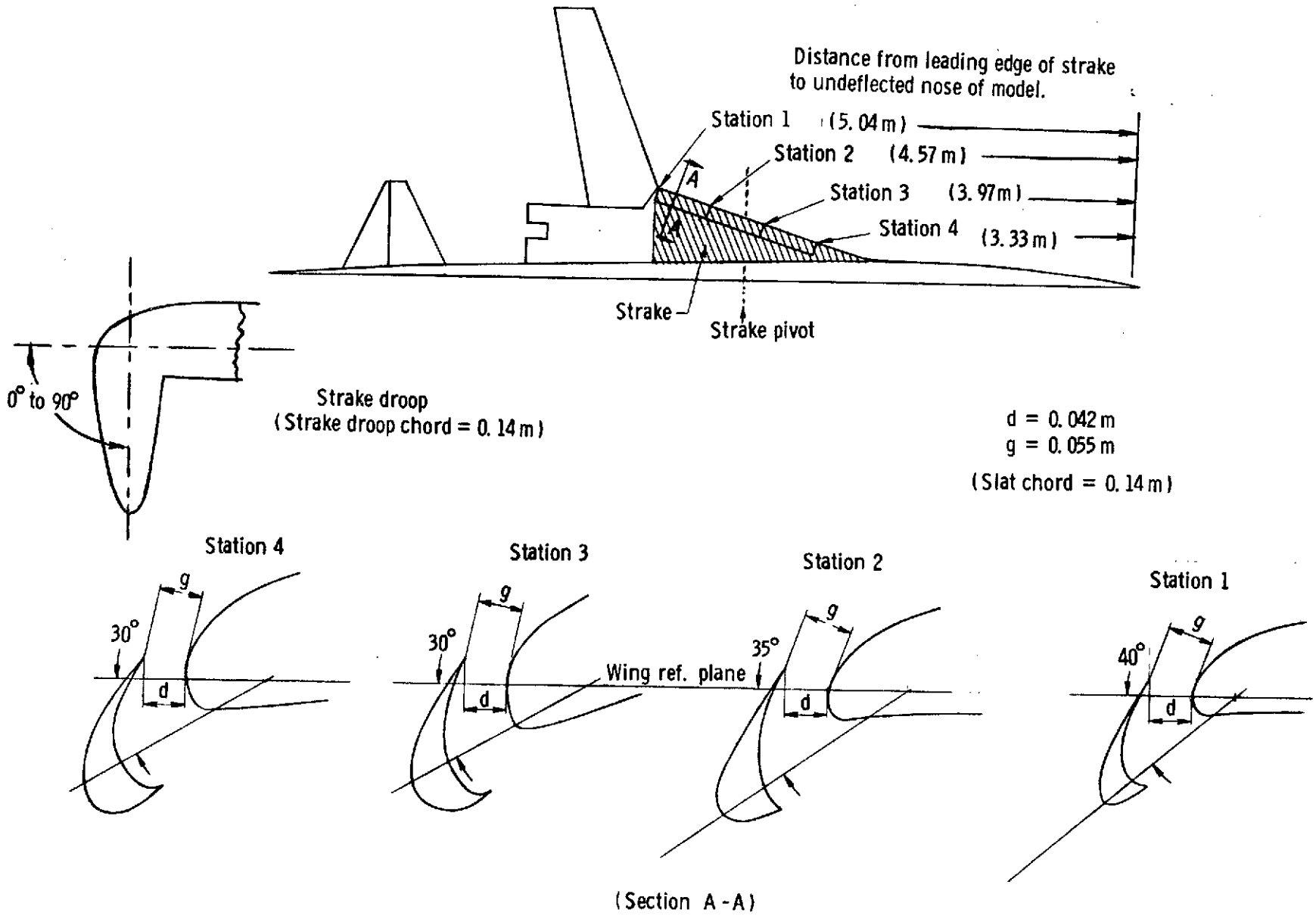

Figure 5 .- Wing strake slat and droop. Sectional views are normal to strake leading edge.

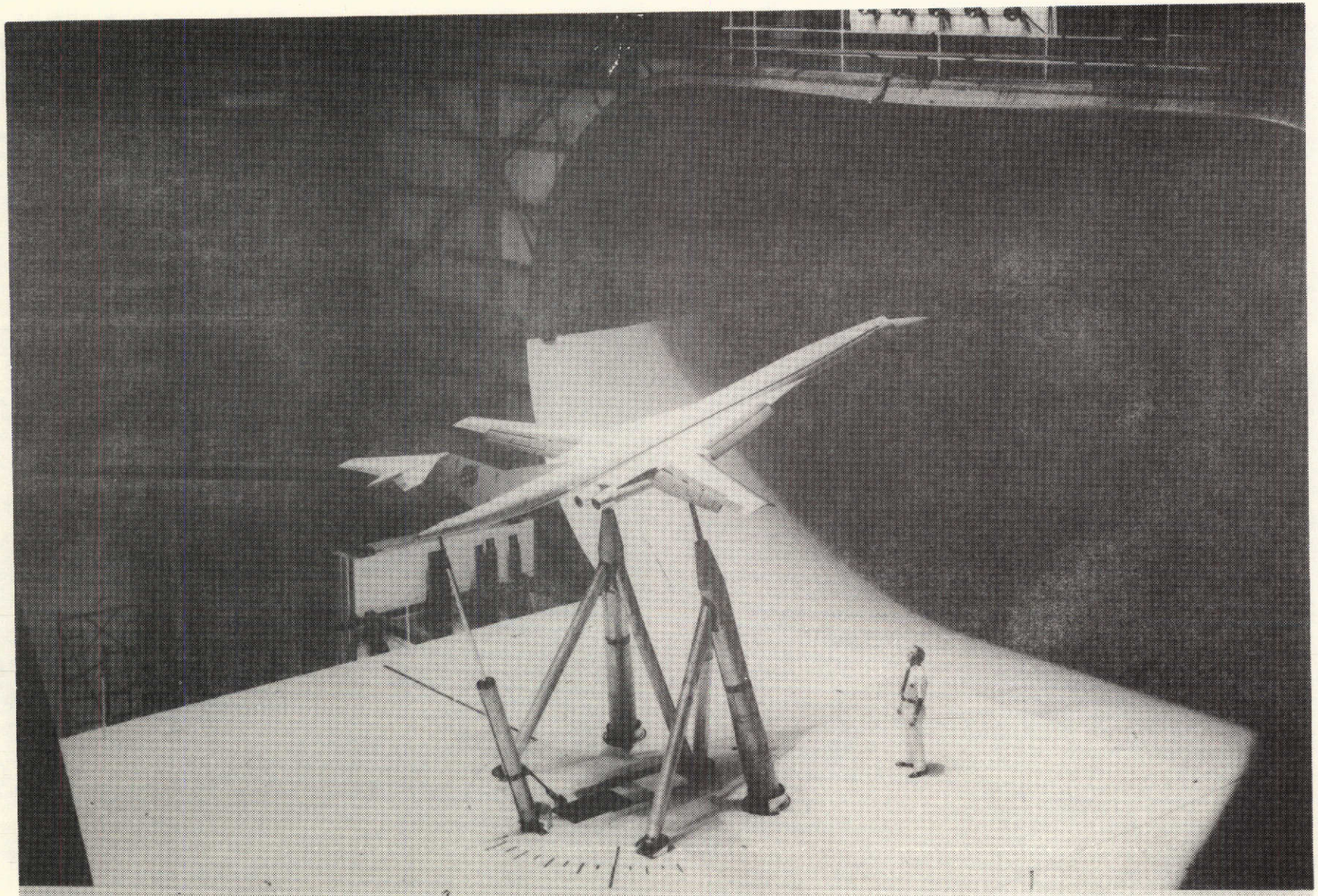

Figure 6.- 1/9-scale model mounted for tests in the Langley full-scale tunnel.

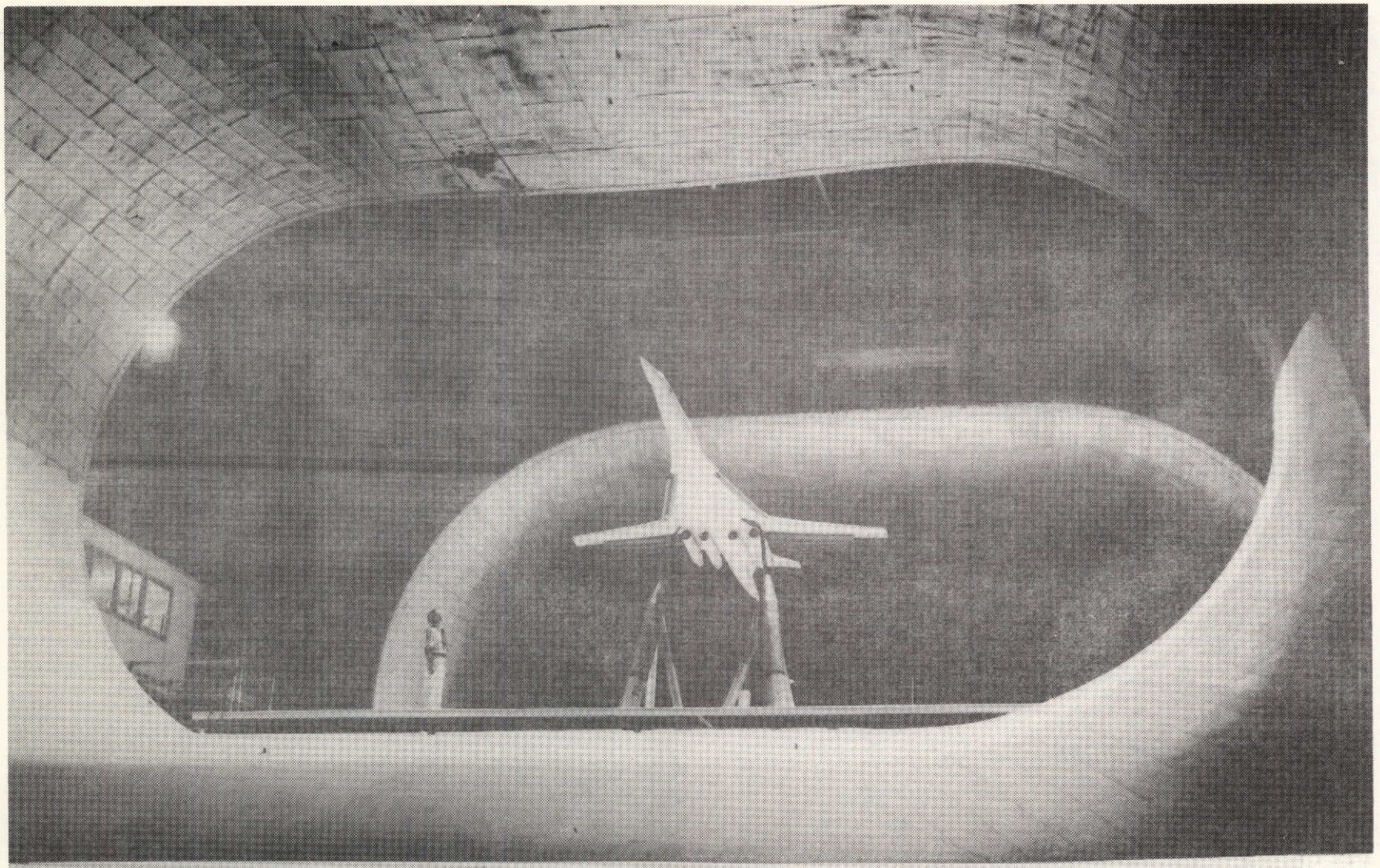

Figure 7. - 1/9-scale model mounted for tests in the Langley full-scale tunnel.

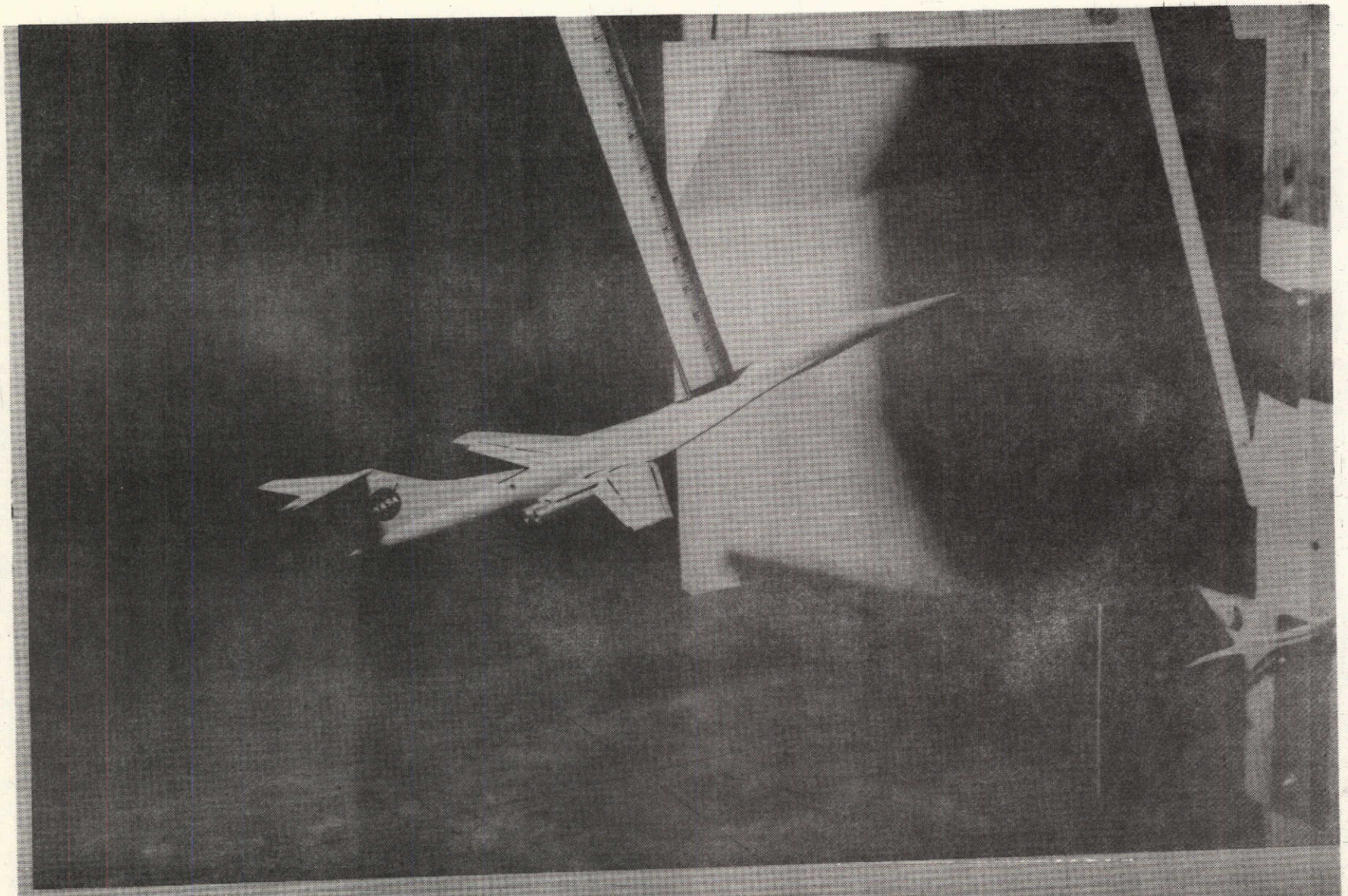

Figure 8. - 1/135-scale model mounted for tests in a 1/15-scale model of the Langley full-scale tunnel.

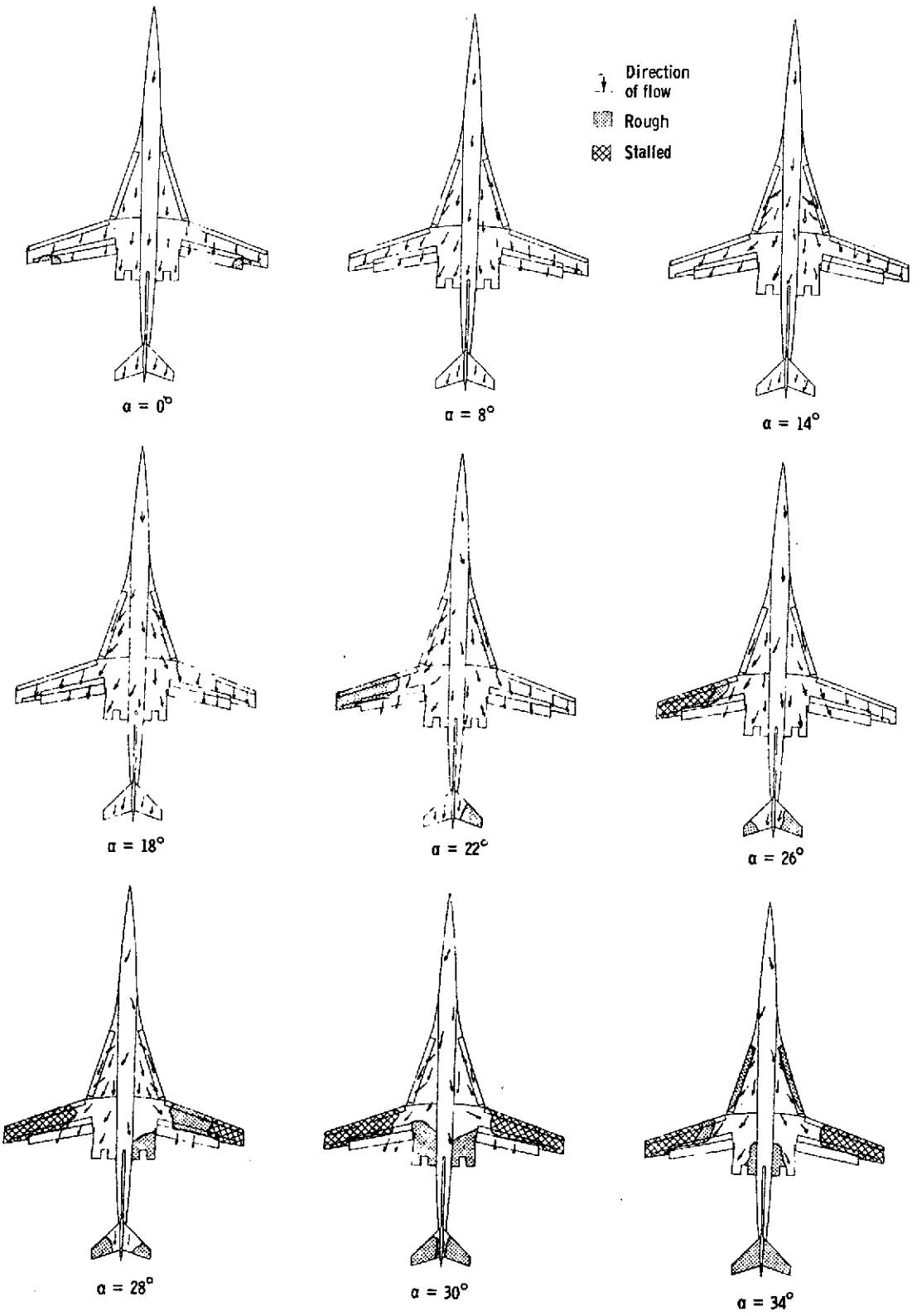

(a) $i_s = 0°$.

Figure 9.- Airflow patterns with strake incidence varied. $\delta_f = 30°/50°$, $\delta_n = 0°$, T-tail, $i_t = 0°$, $\Lambda = 20°$, $\beta = 0°$.

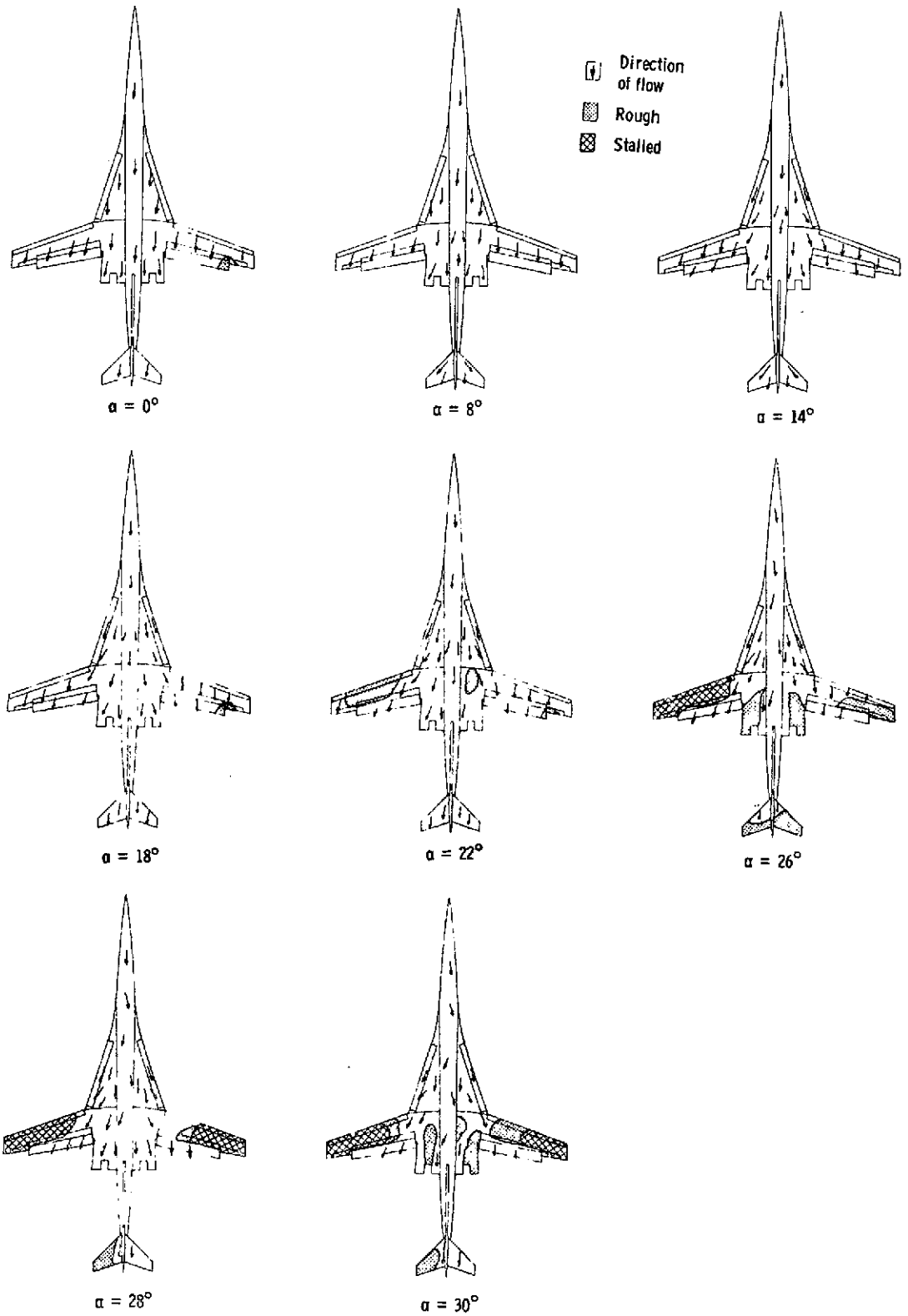

(b) $i_s = 5°$.

Figure 9. - Continued.

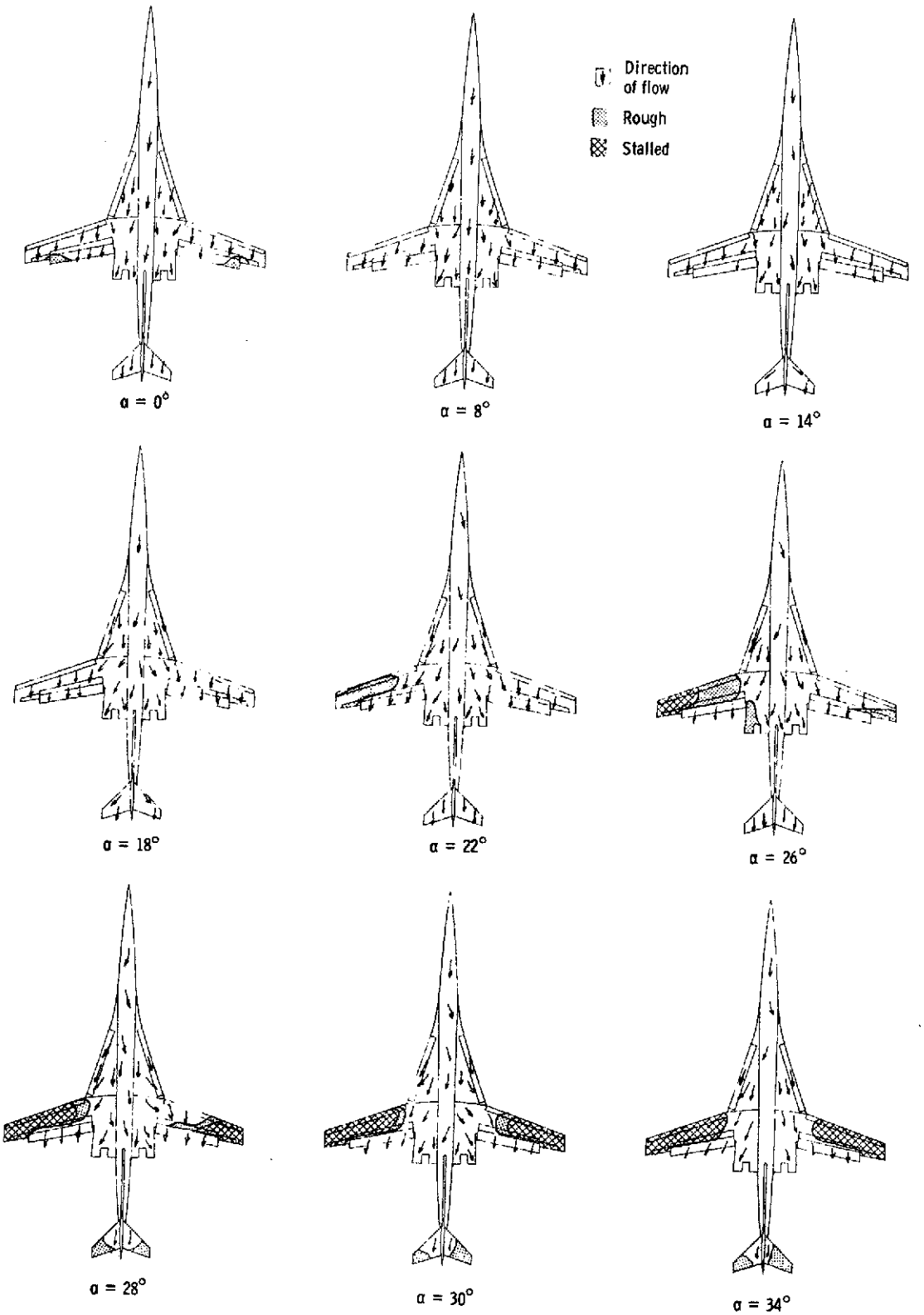

(c) $i_s = 10°$.

Figure 9. - Concluded.

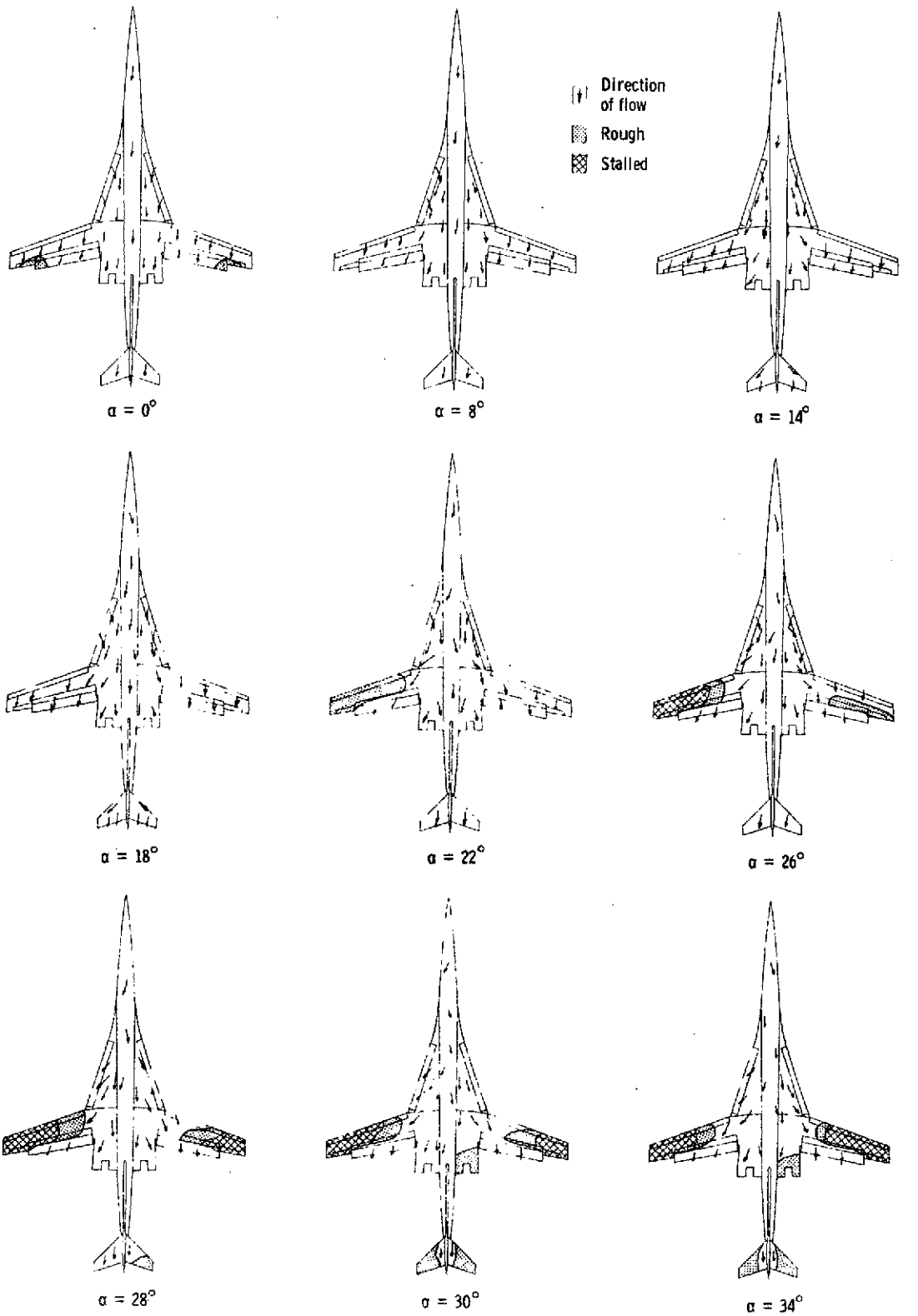

(a) $\delta_n = 30°$.

Figure 10. - Airflow patterns with strake leading edge drooped.
$\delta_f = 30°/50°$, $i_s = 0°$, T-tail, $i_t = 0°$, $\Lambda = 20°$, $\beta = 0°$.

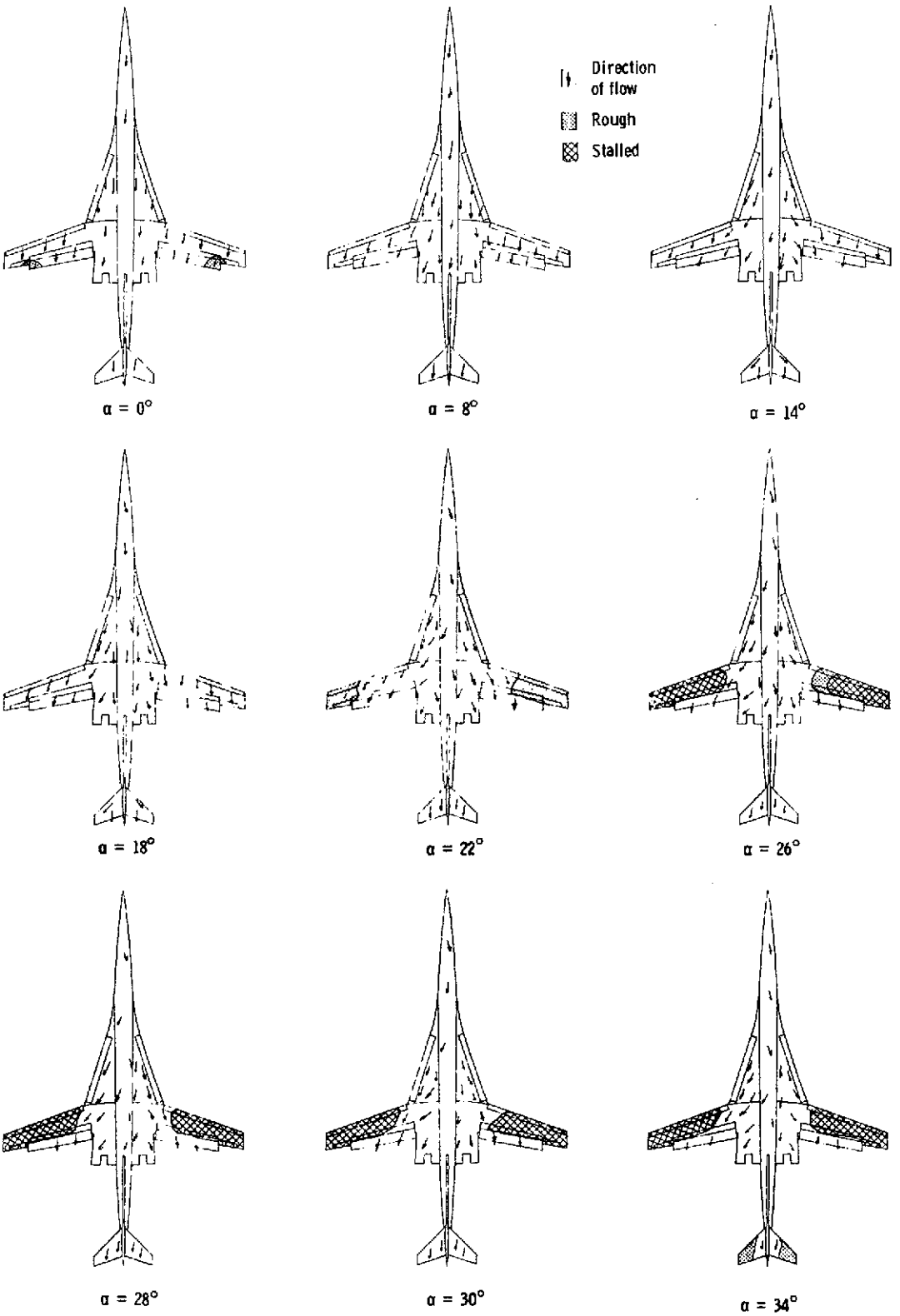

(b) $\delta_n = 60°$.

Figure 10. - Continued.

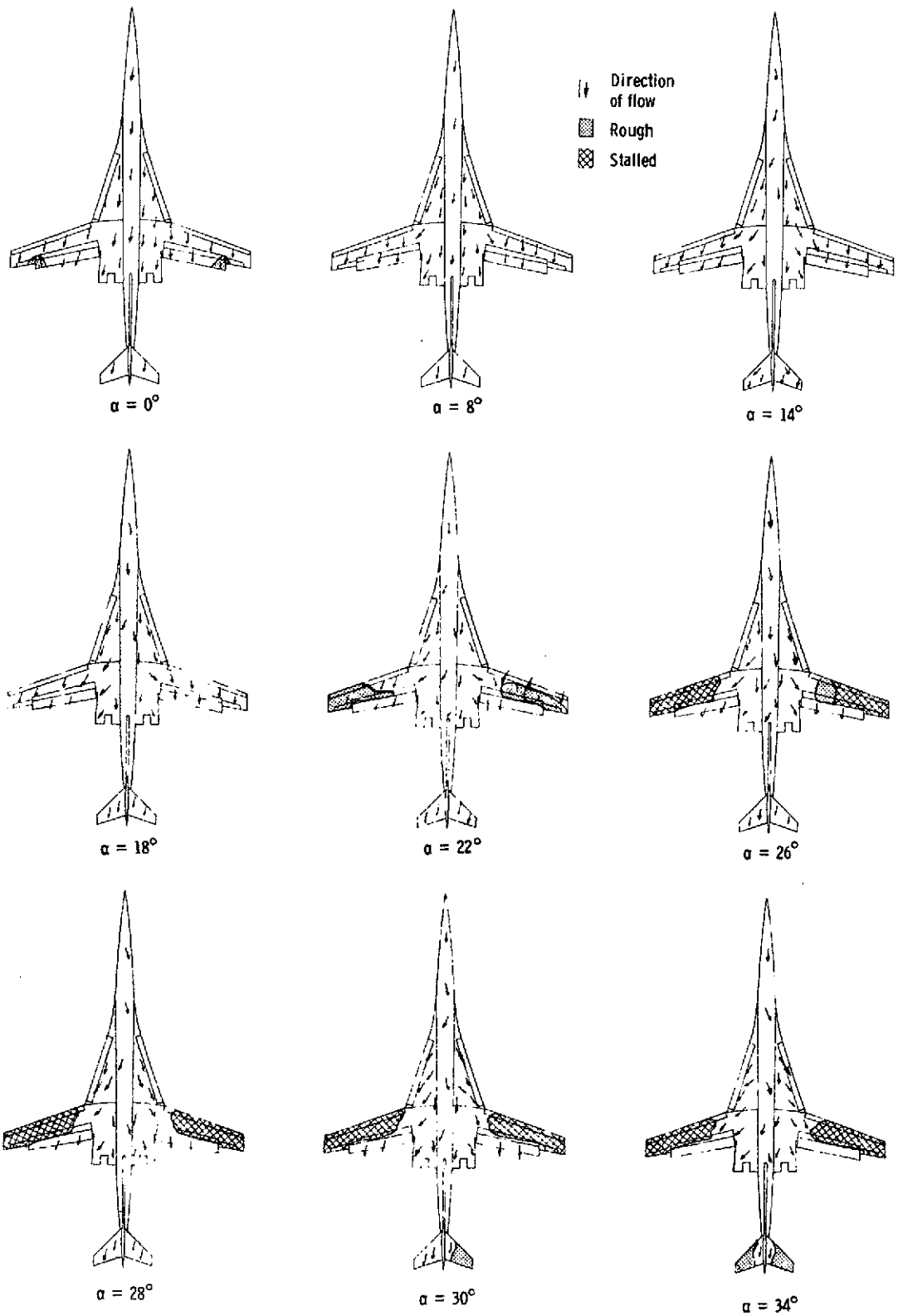

(c) δ_n = 90°.

Figure 10. - Concluded.

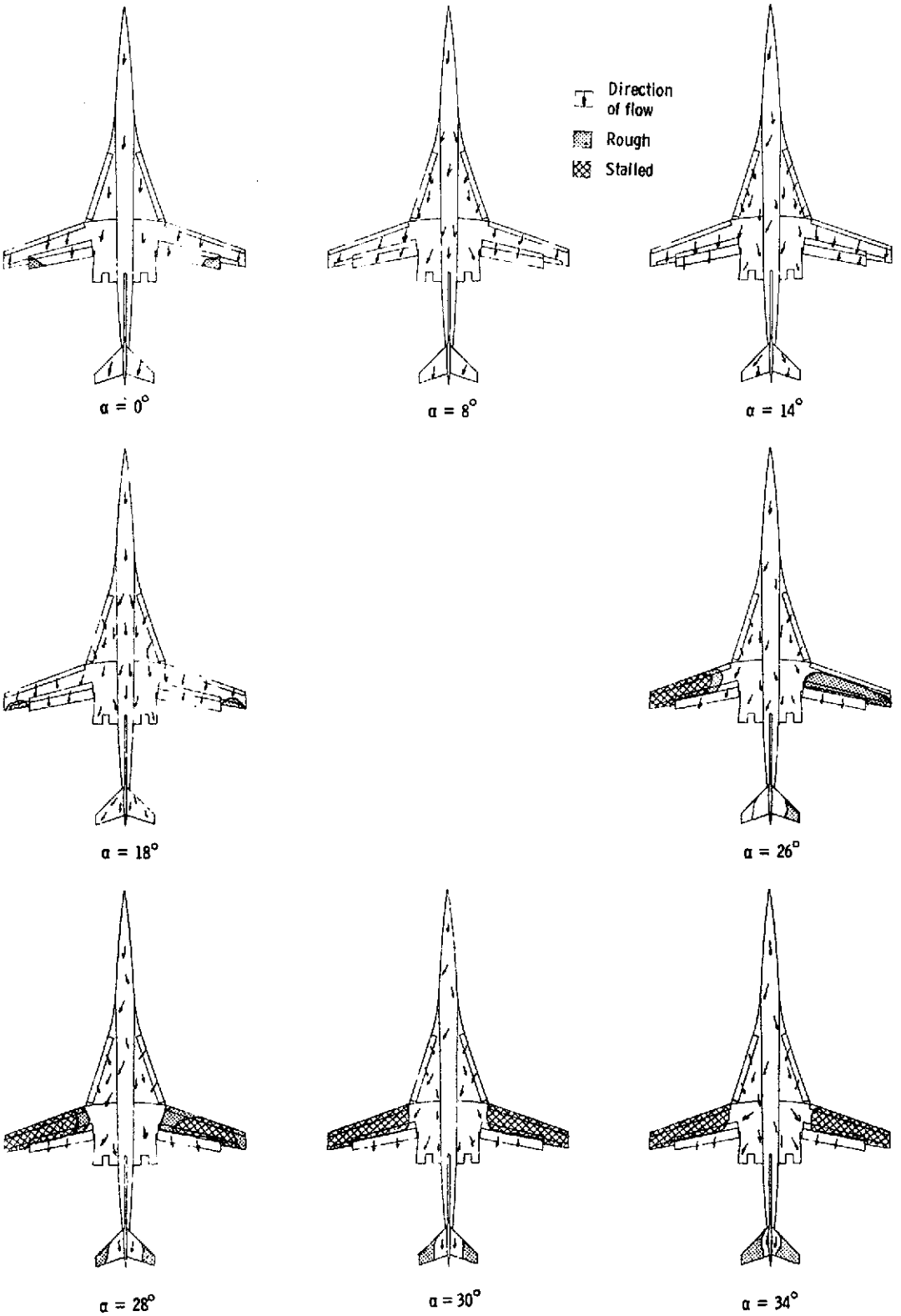

(a) $\beta = 0°$.

Figure 11. - Airflow patterns with sideslip. Slatted strake, $\delta_f = 30°/50°$, $i_s = 0°$, T-tail, $i_t = 0°$, $\Lambda = 20°$.

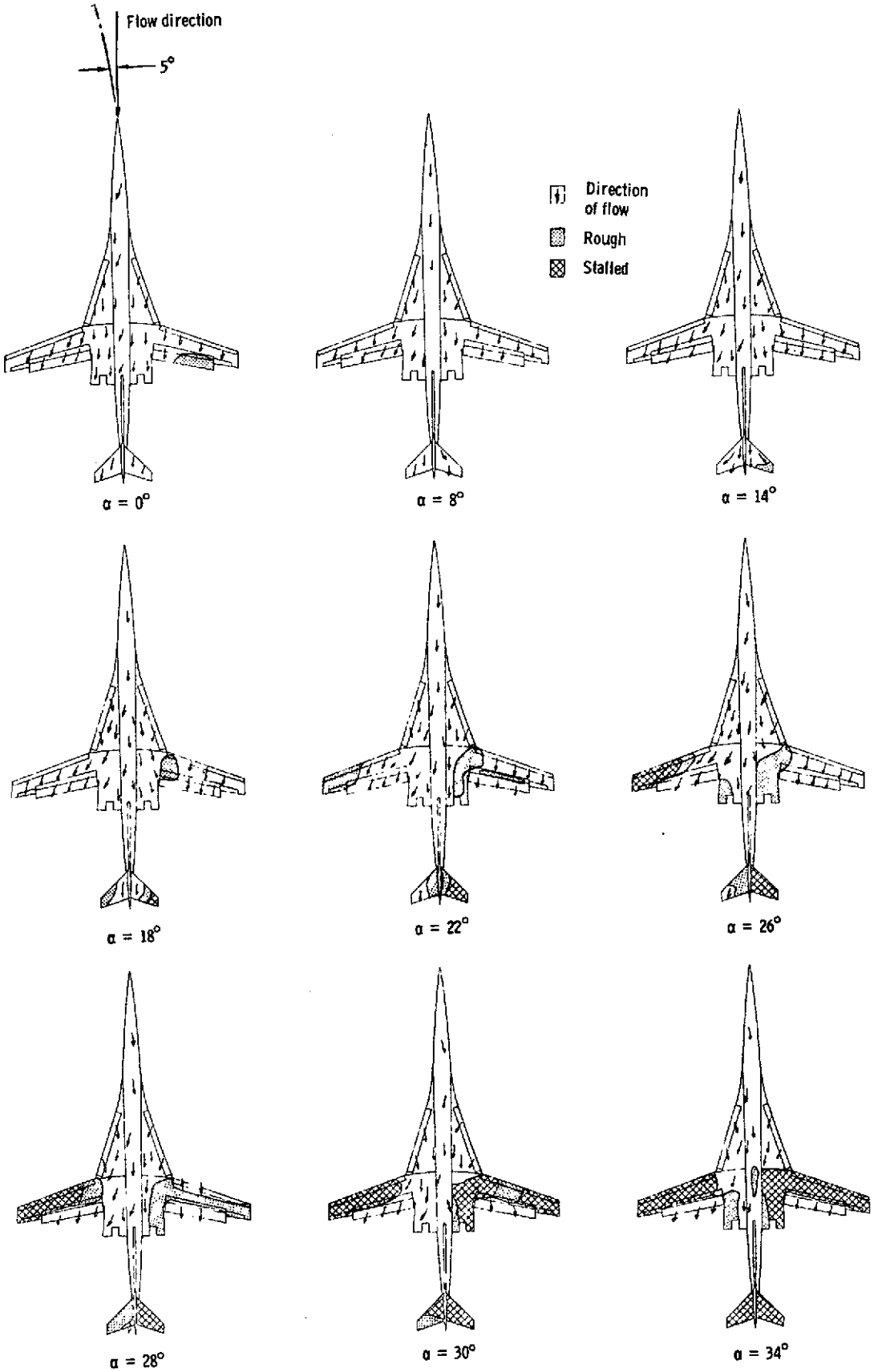

(b) $\beta = 5°$.

Figure 11. - Continued.

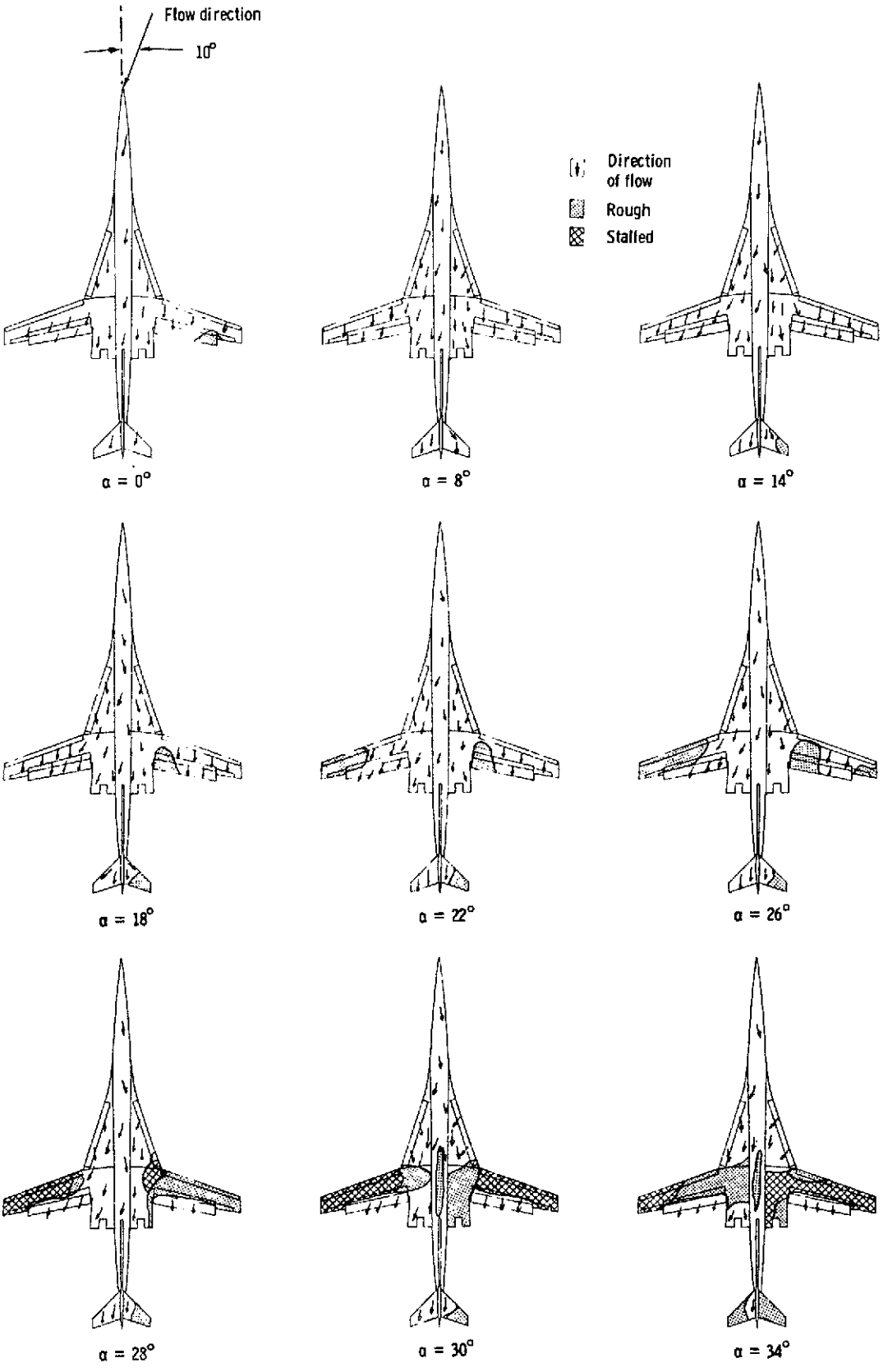

(c) $\beta = 10°$.

Figure 11. - Concluded.

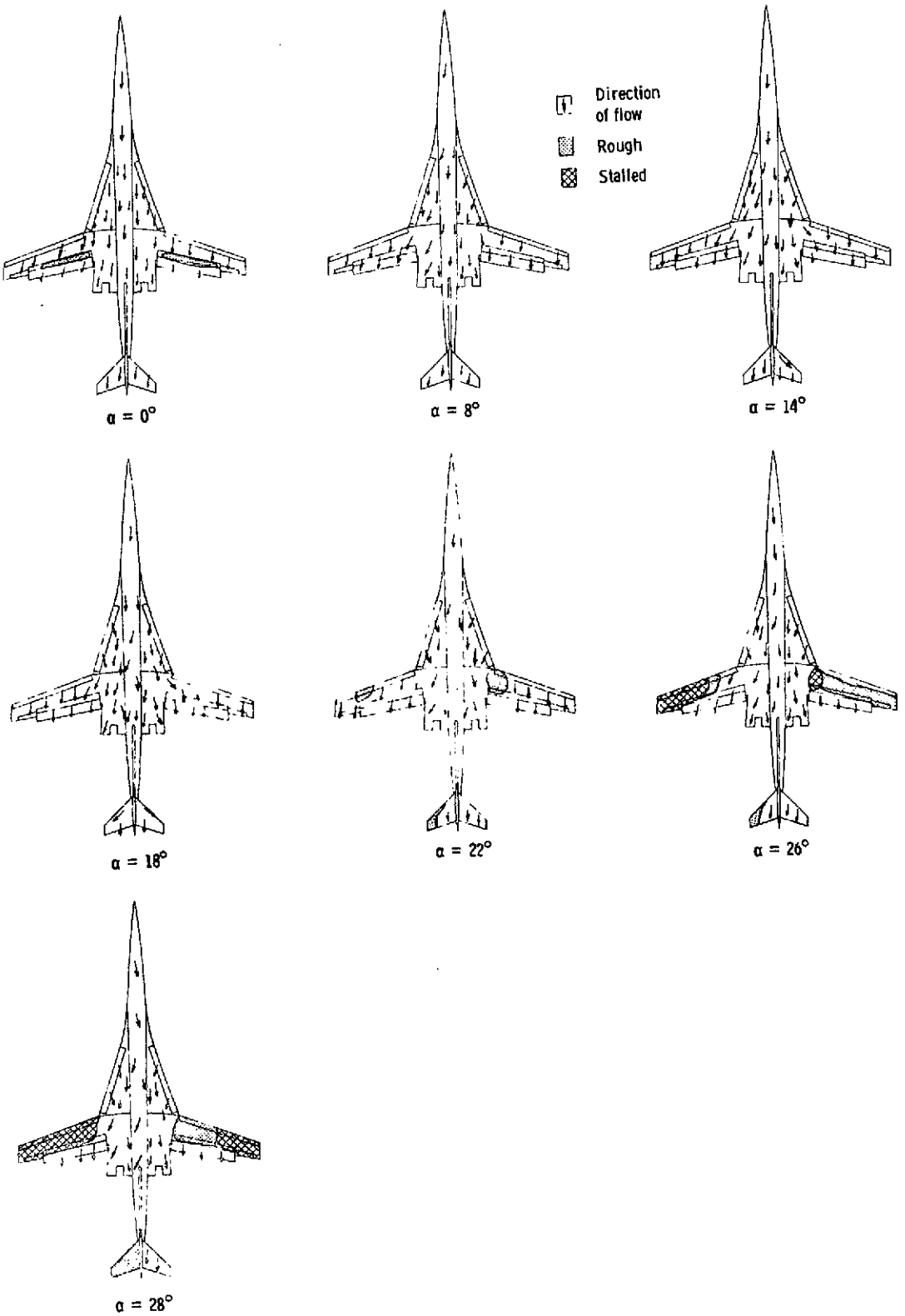

Figure 12.- Airflow patterns at increased speed (≈84 knots). Slatted strake, δ_f = 30°/50°, i_s = 0°, T-tail, i_t = 0°, Λ = 20°, β = 0°. Compare with patterns of figure 11(a) (≈54 knots).

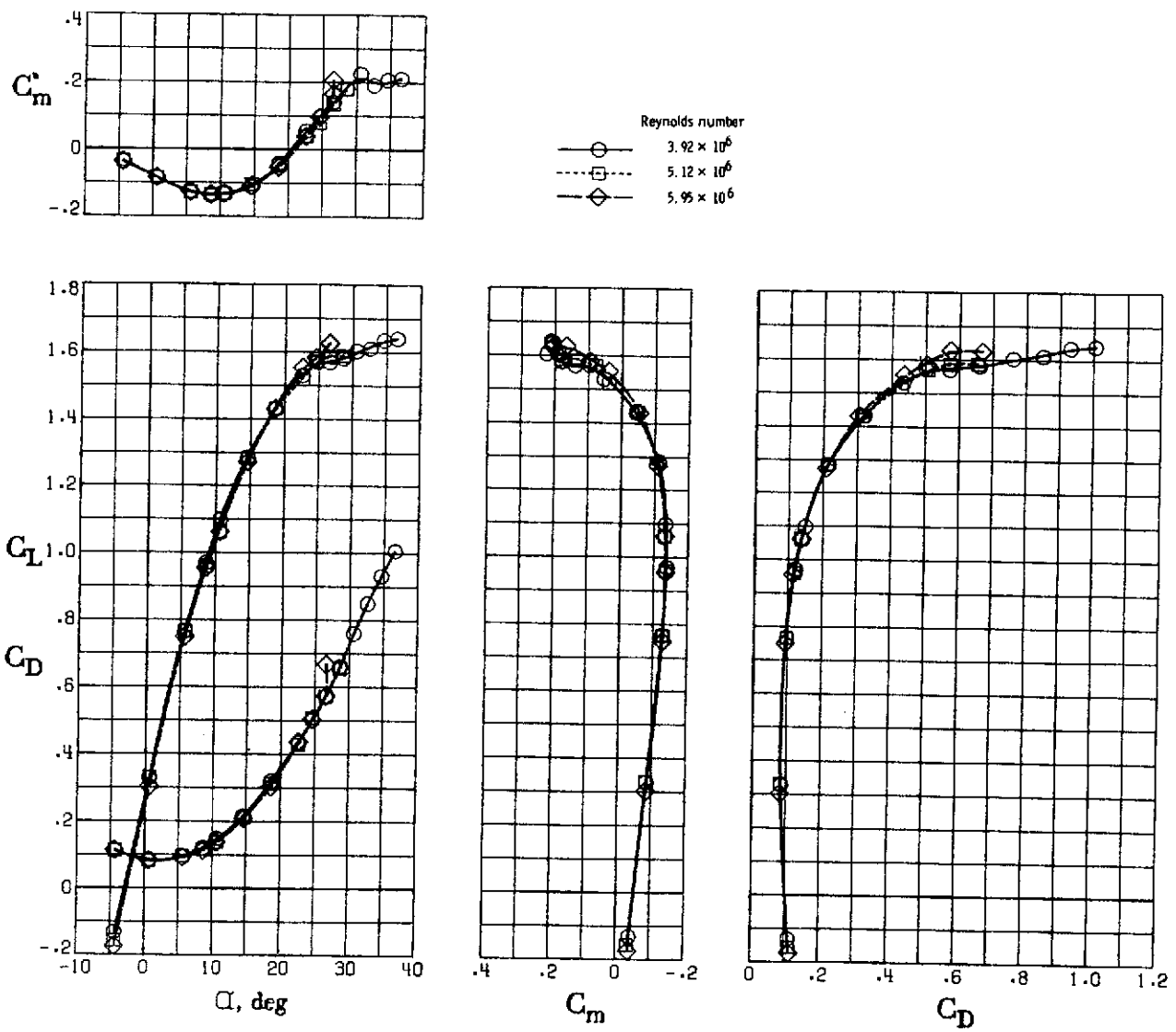

(a) Basic strake.

Figure 13. - Effect of Reynolds number for two strake arrangements. $\delta_f = 30°/50°$, $i_s = 0°$, T-tail, $i_t = 0°$, $\Lambda = 20°$, $\beta = 0°$.

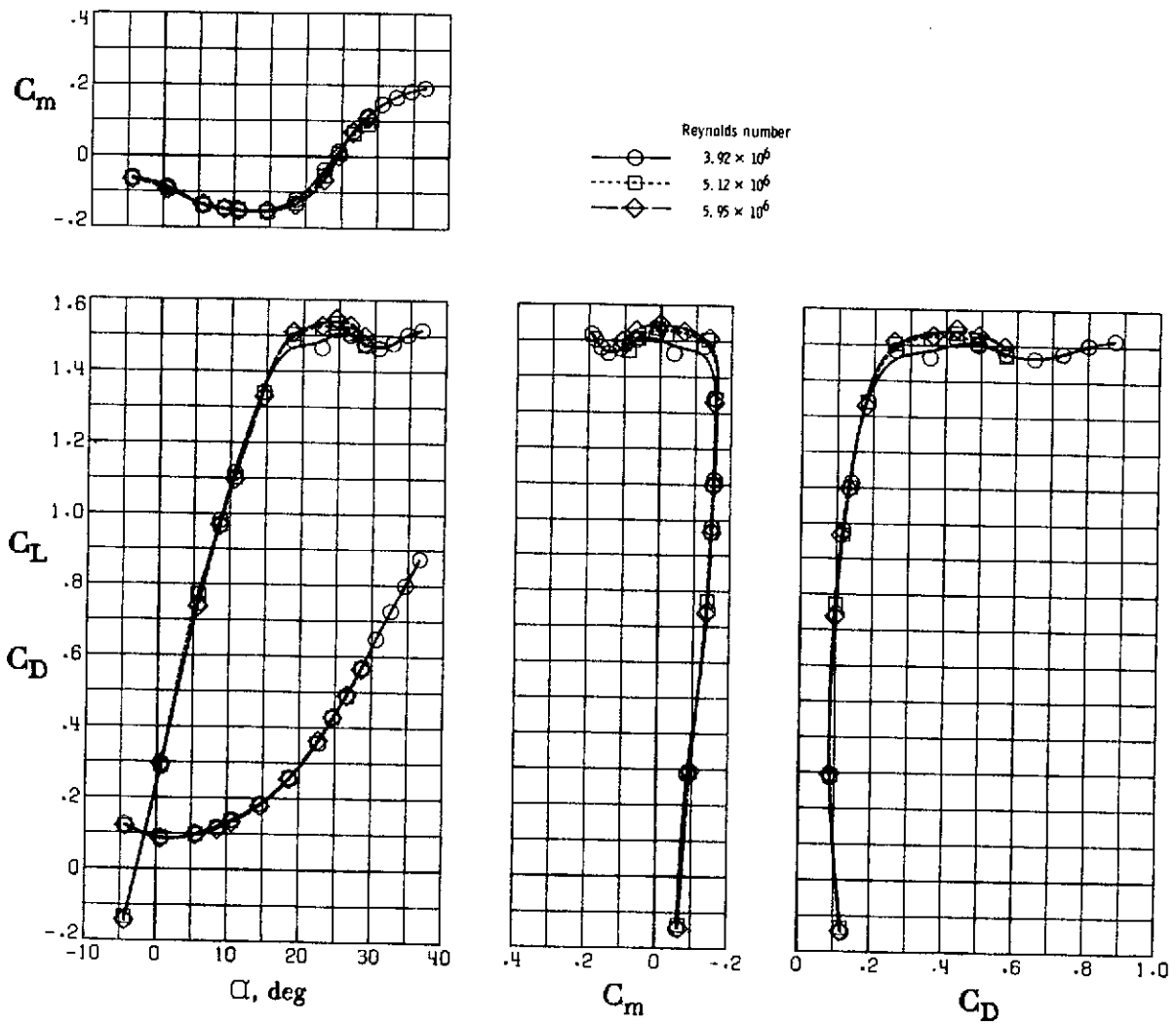

(b) Slatted strake.

Figure 13. - Concluded.

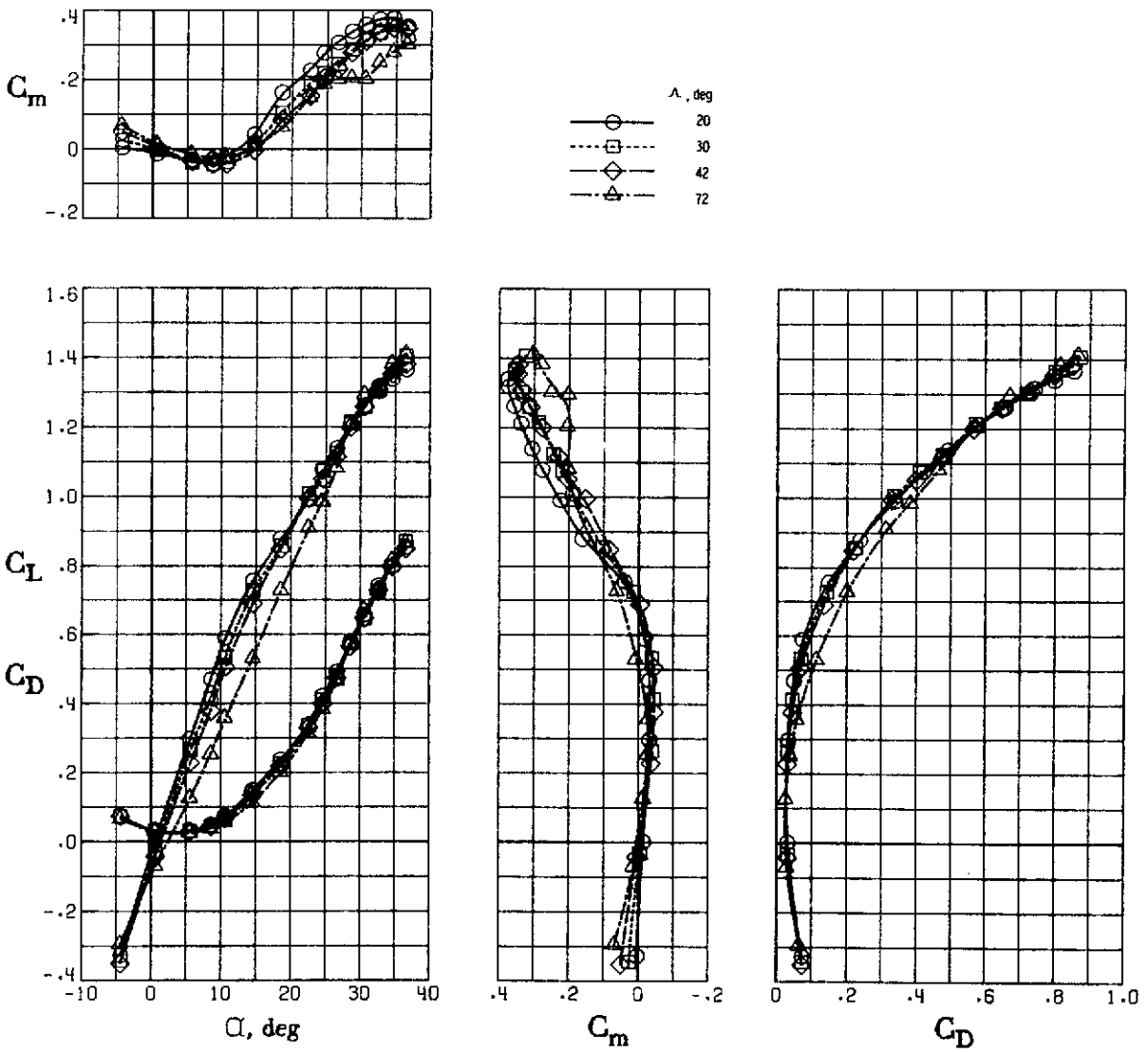

(a) T-tail.

Figure 14.- Effect of wing leading-edge sweep for two tail arrangements. Clean wing, i_t = 0°, β = 0°. Undrooped fuselage nose.

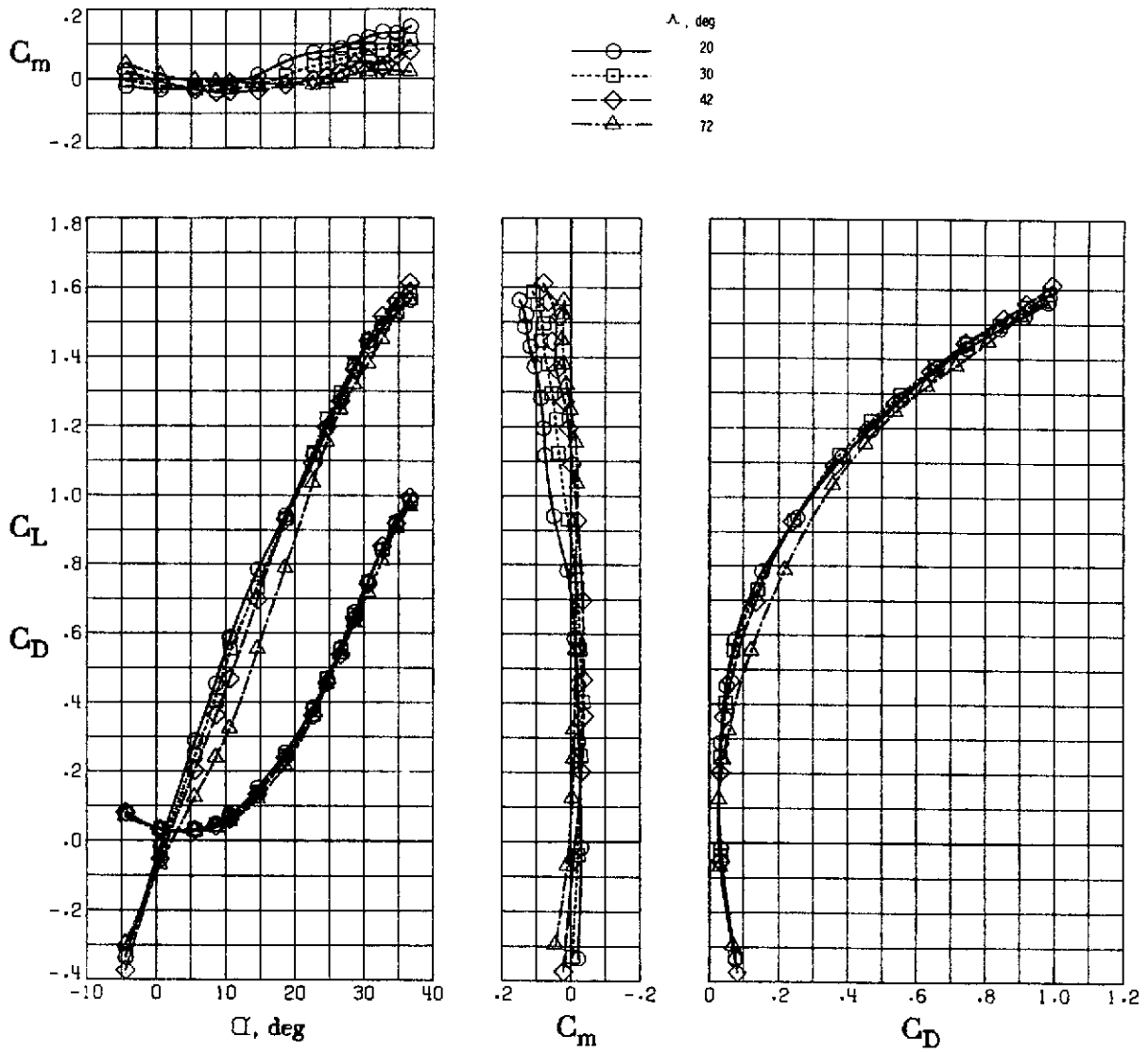

(b) Low-tail

Figure 14. - Concluded.

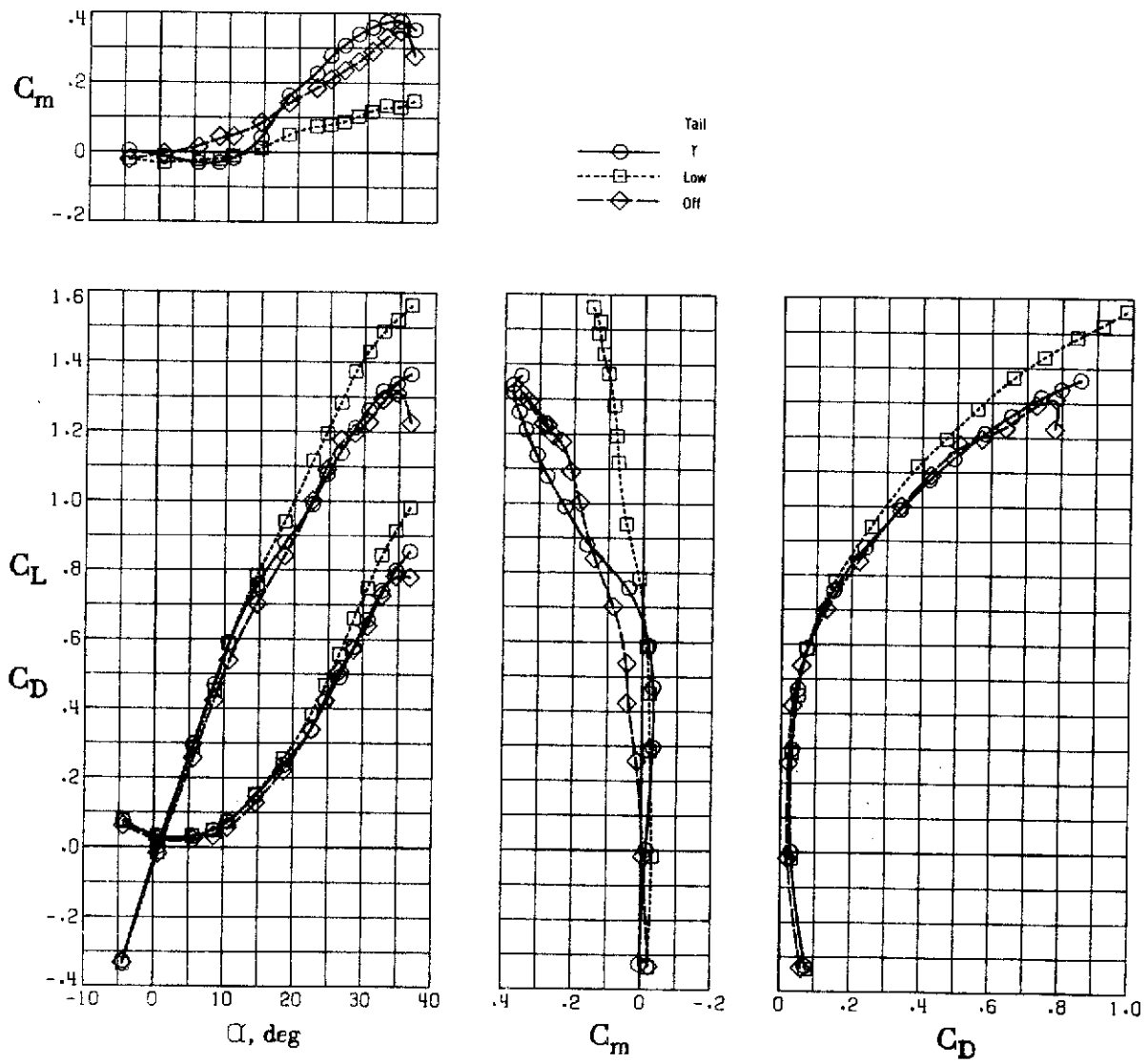

(a) $\Lambda = 20°$.

Figure 15. - Effect of tail position for various wing sweep angles. $\delta_f = 0°$, $i_t = 0°$, $\beta = 0°$.

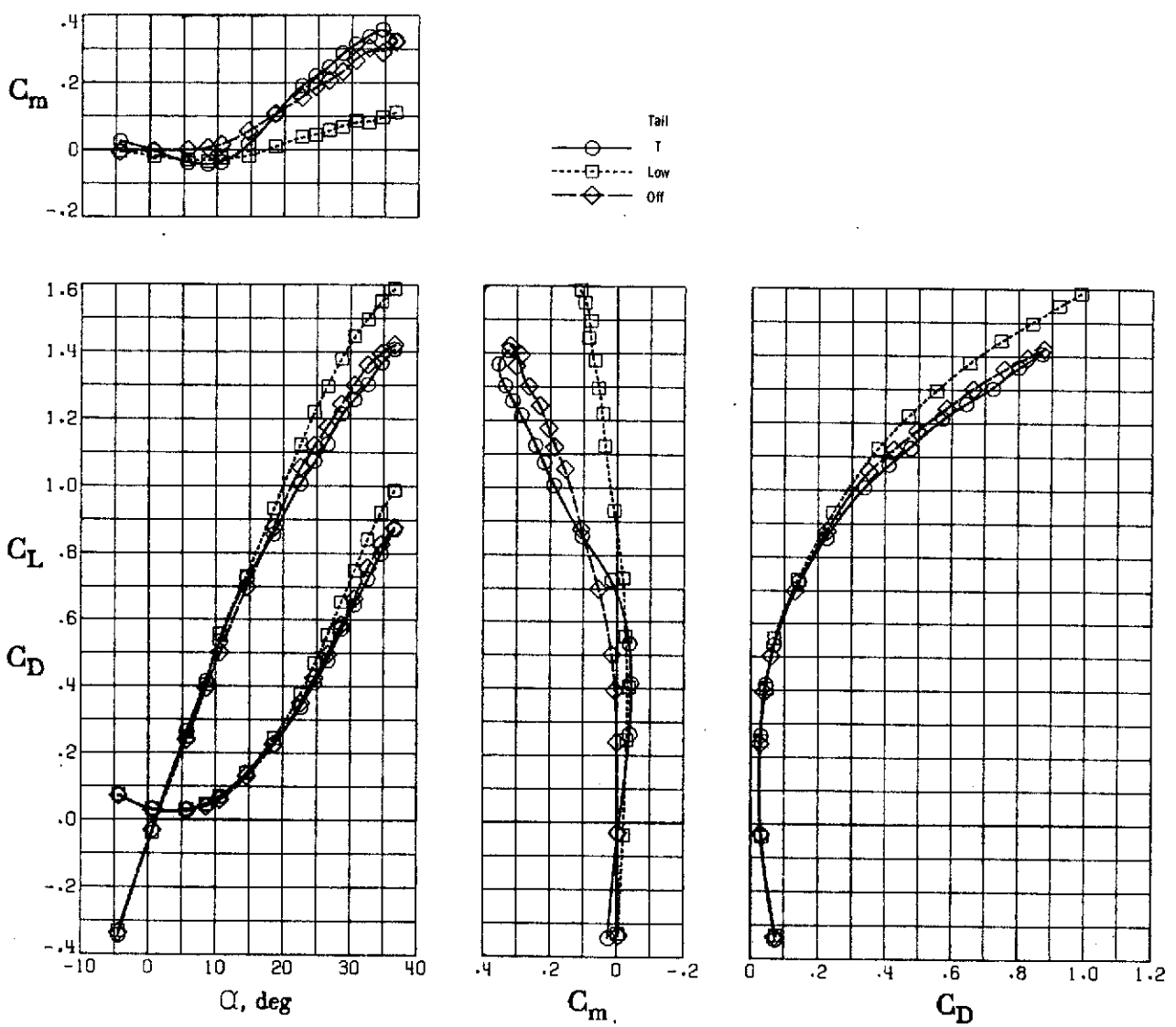

(b) Λ = 30°.

Figure 15. - Continued.

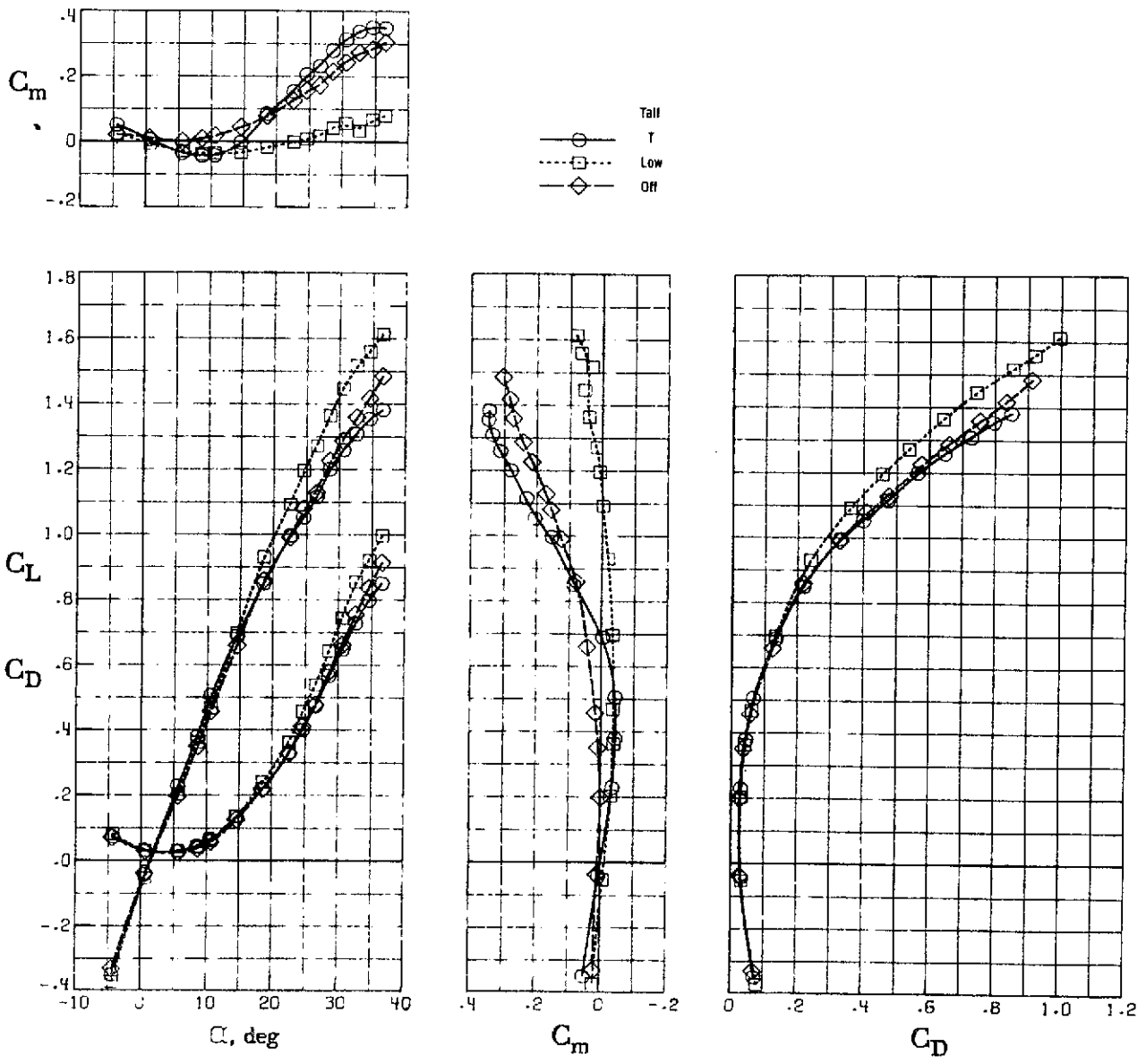

(c) Λ = 42°.

Figure 15. - Continued.

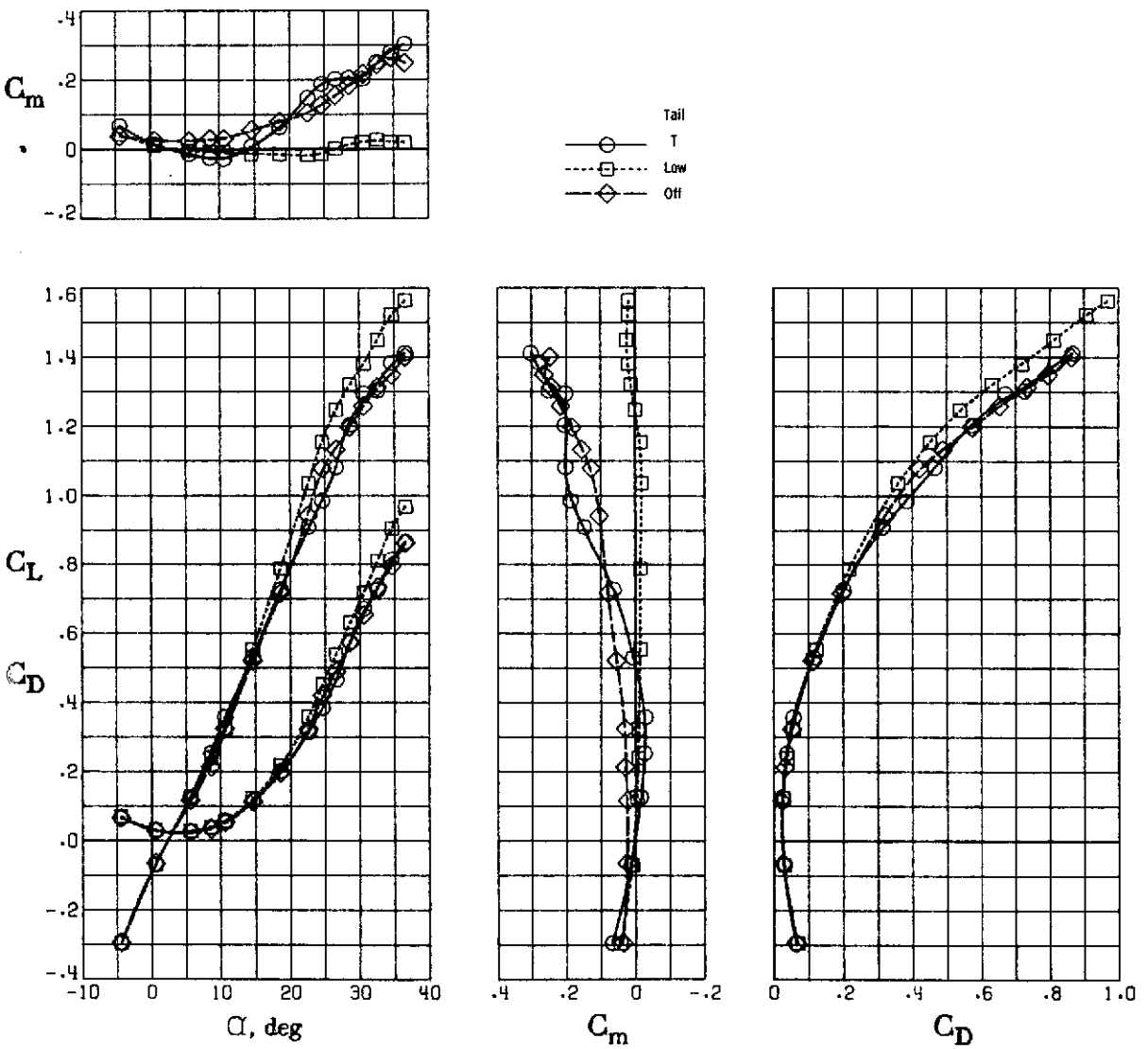

(d) $\Lambda = 72°$.

Figure 15. - Concluded.

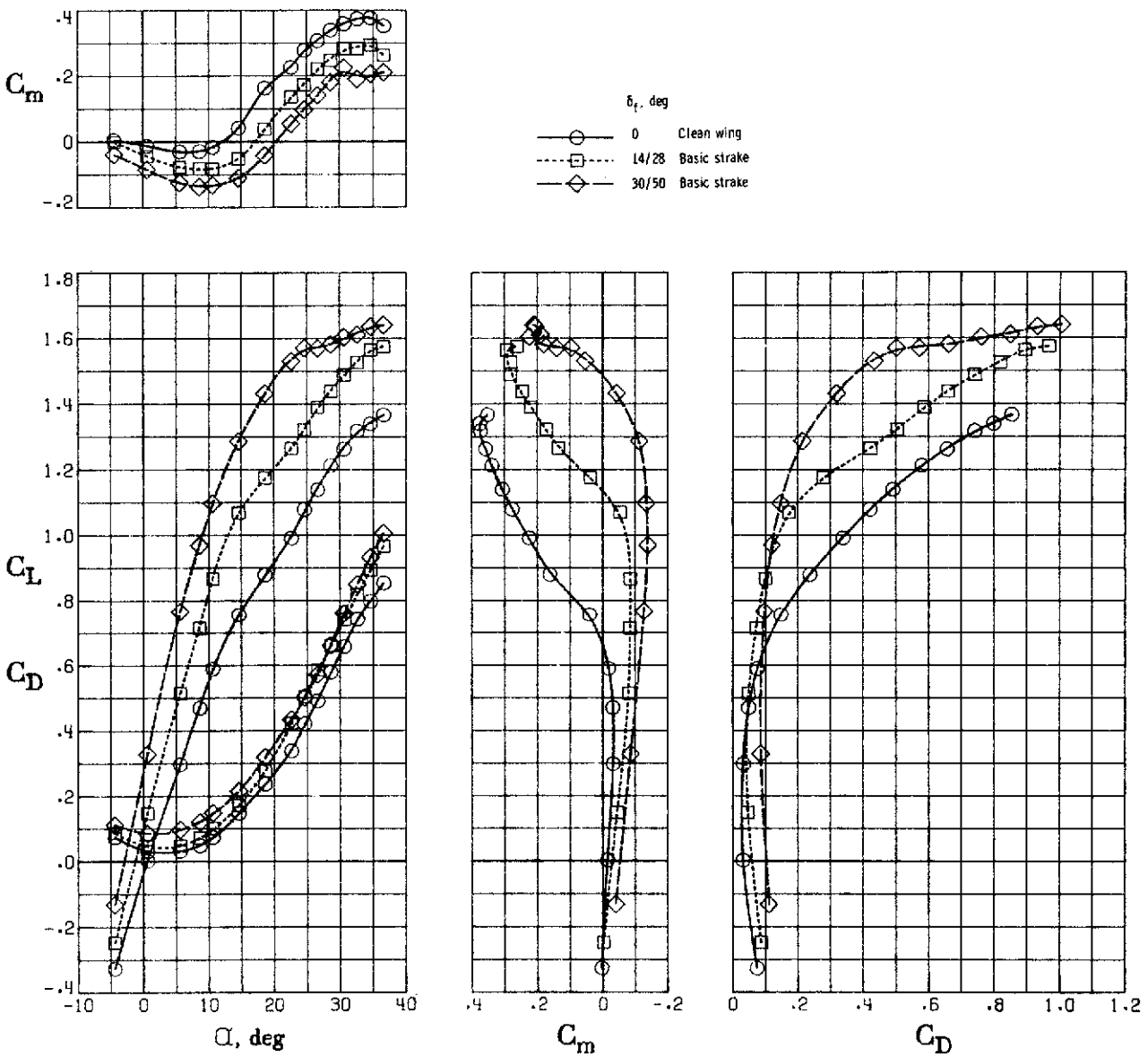

(a) T-tail.

Figure 16. - Effect of high - lift devices for two strake configurations.
$i_t = 0°$, $\Lambda = 20°$, $\beta = 0°$.

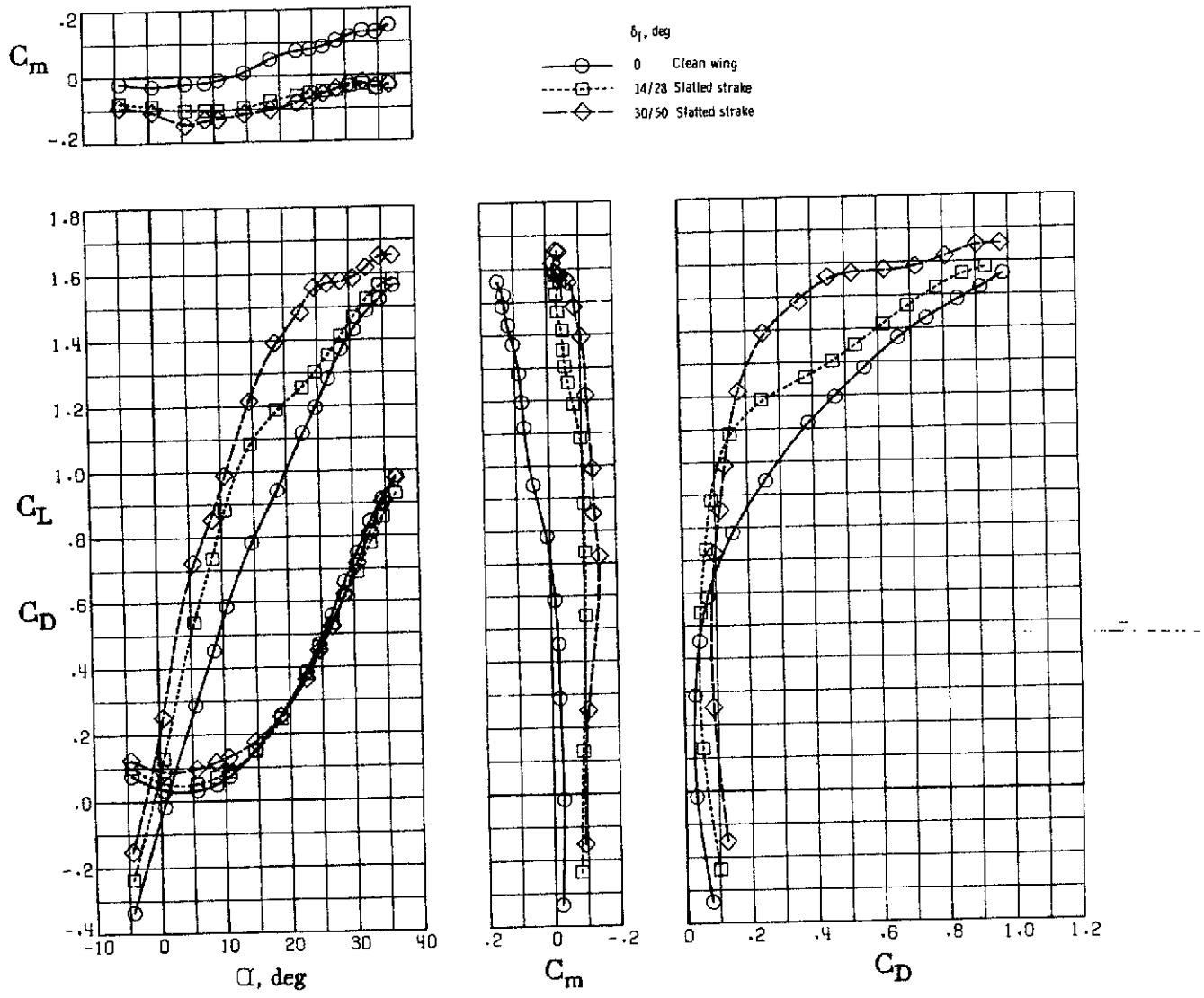

(b) Low-tail.

Figure 16.- Concluded.

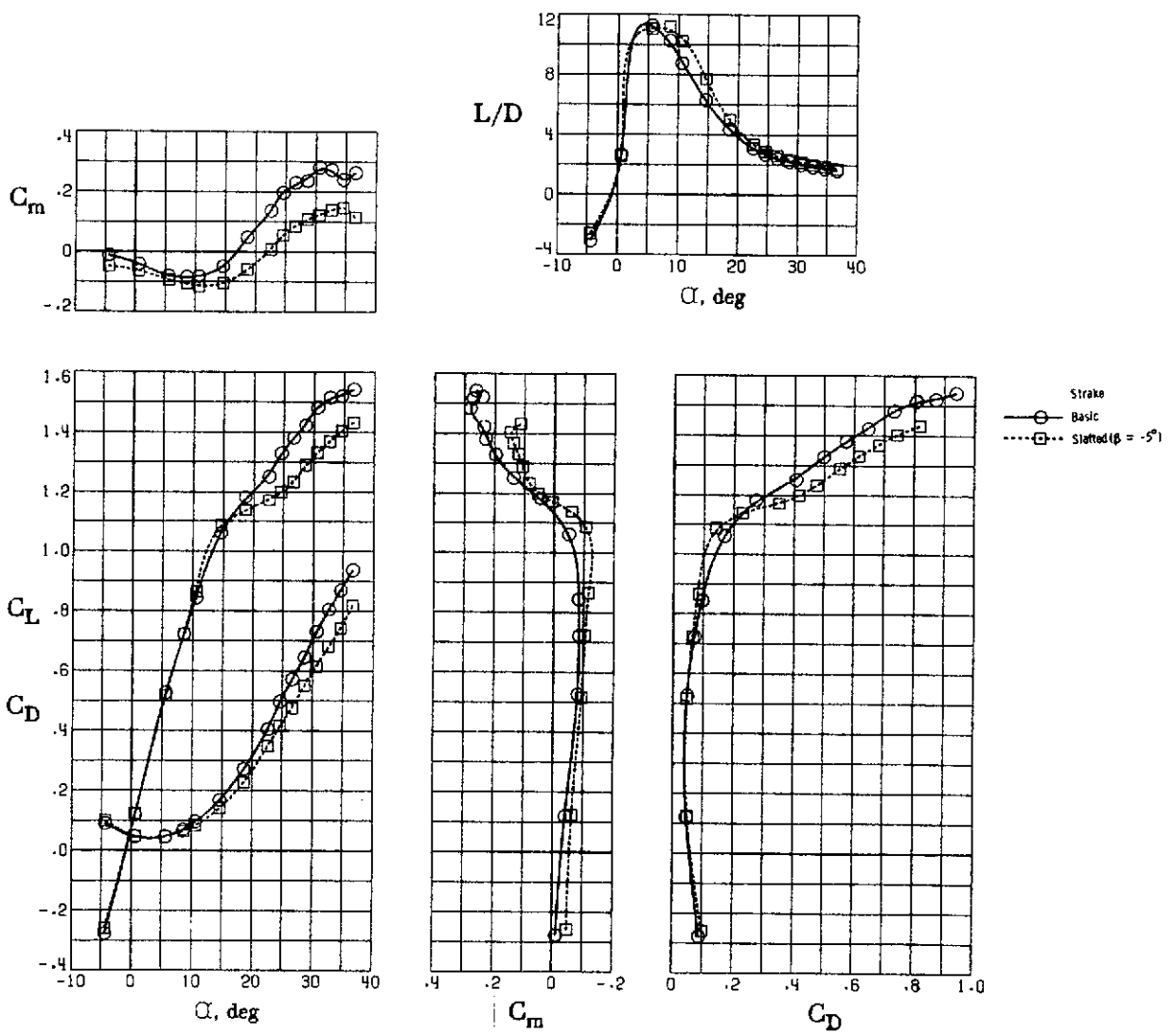

(a) T-tail, $\delta_f = 14°/28°$.

Figure 17. - Effect of strake slat, $\Lambda = 20°$, $\delta = 0°$.

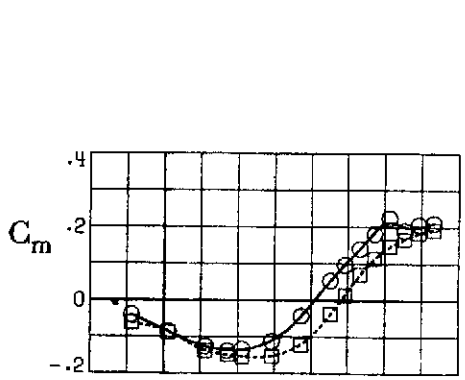

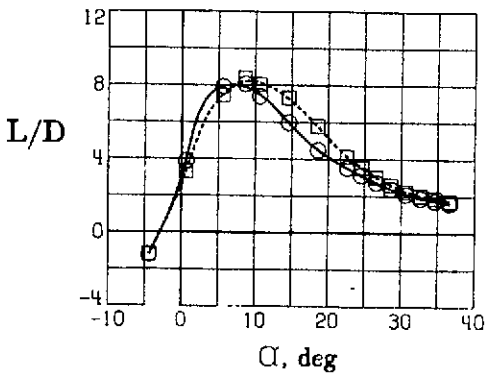

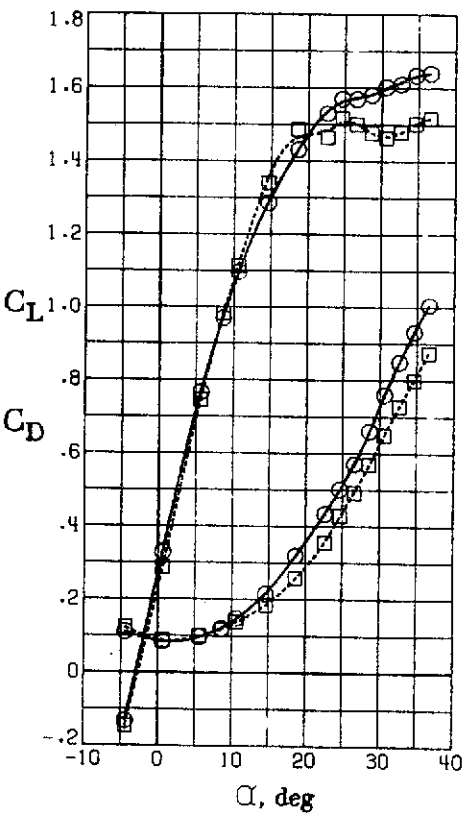

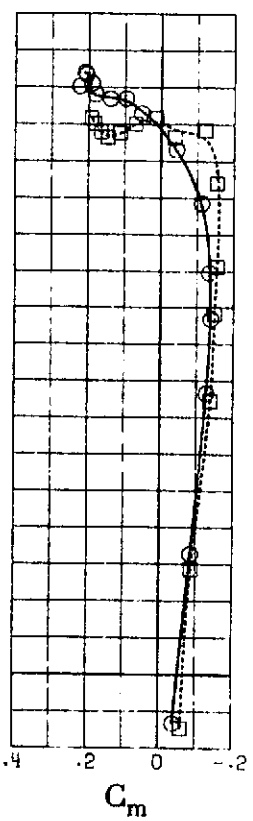

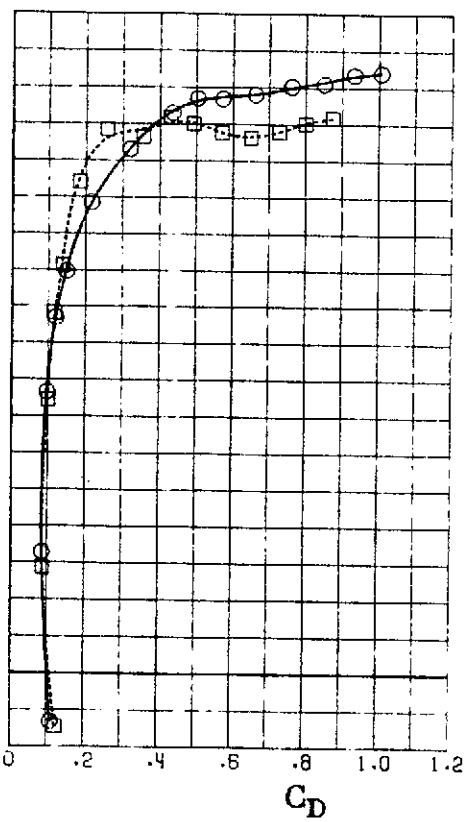

(b) T-tail, $\delta_f = 30°/50°$.

Figure 17. - Concluded.

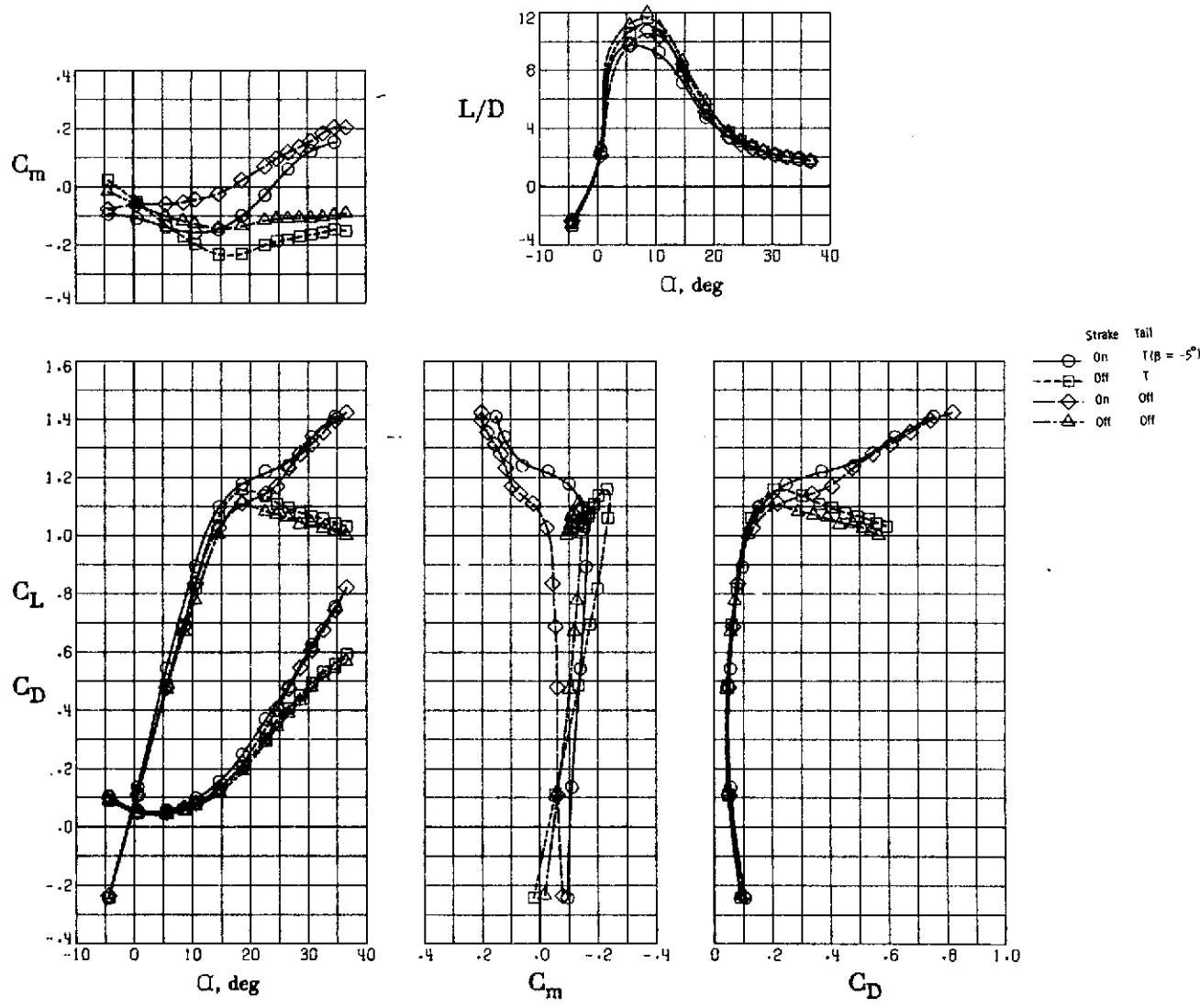

(a) $\delta_f = 14°/28°$.

Figure 18. - Effect of removing strake (slatted strake).
$i_t = 0°, \Lambda = 20°, \beta = 0°$.

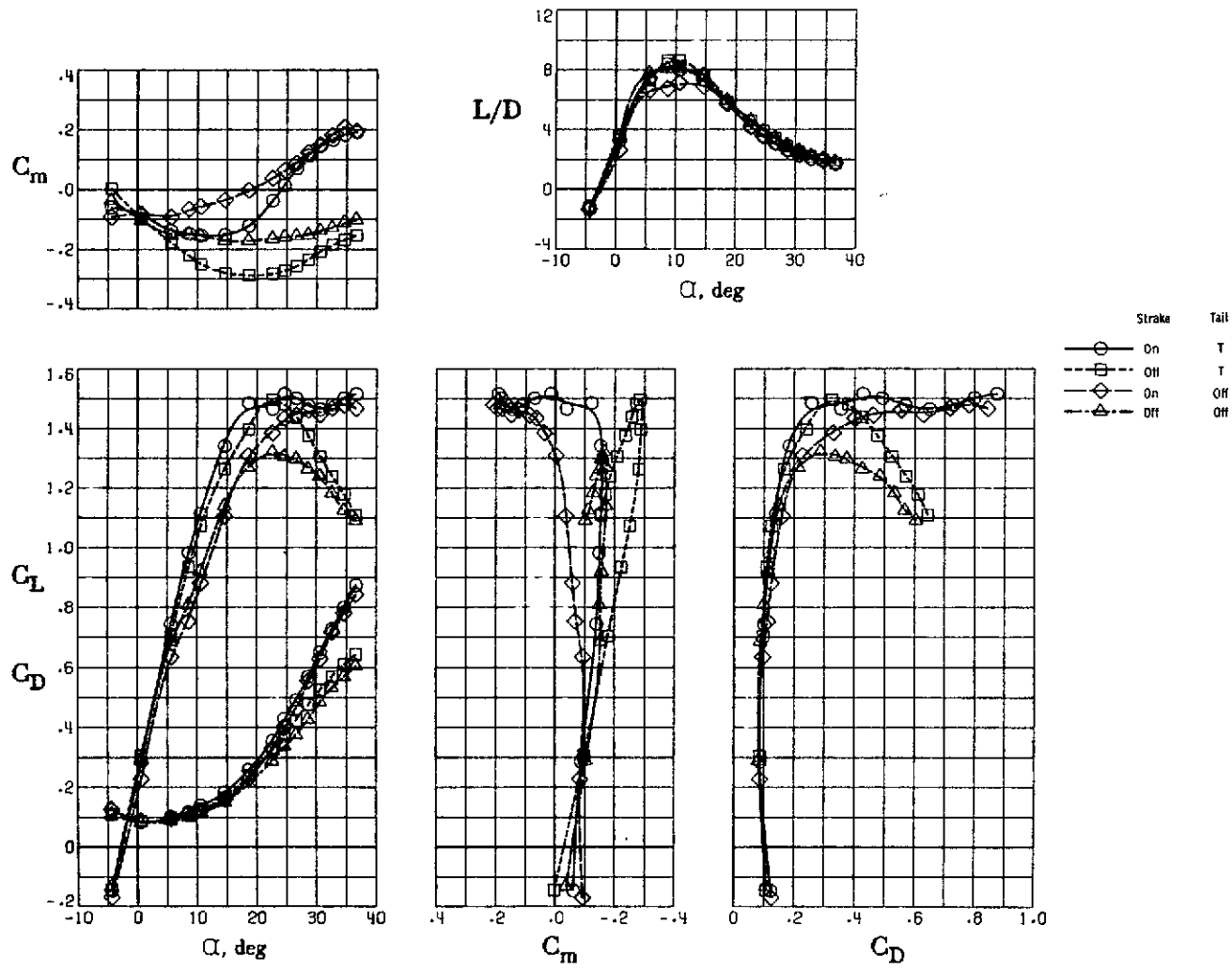

$(b/2)_f = 30°/50°$

Figure 18. - Concluded.

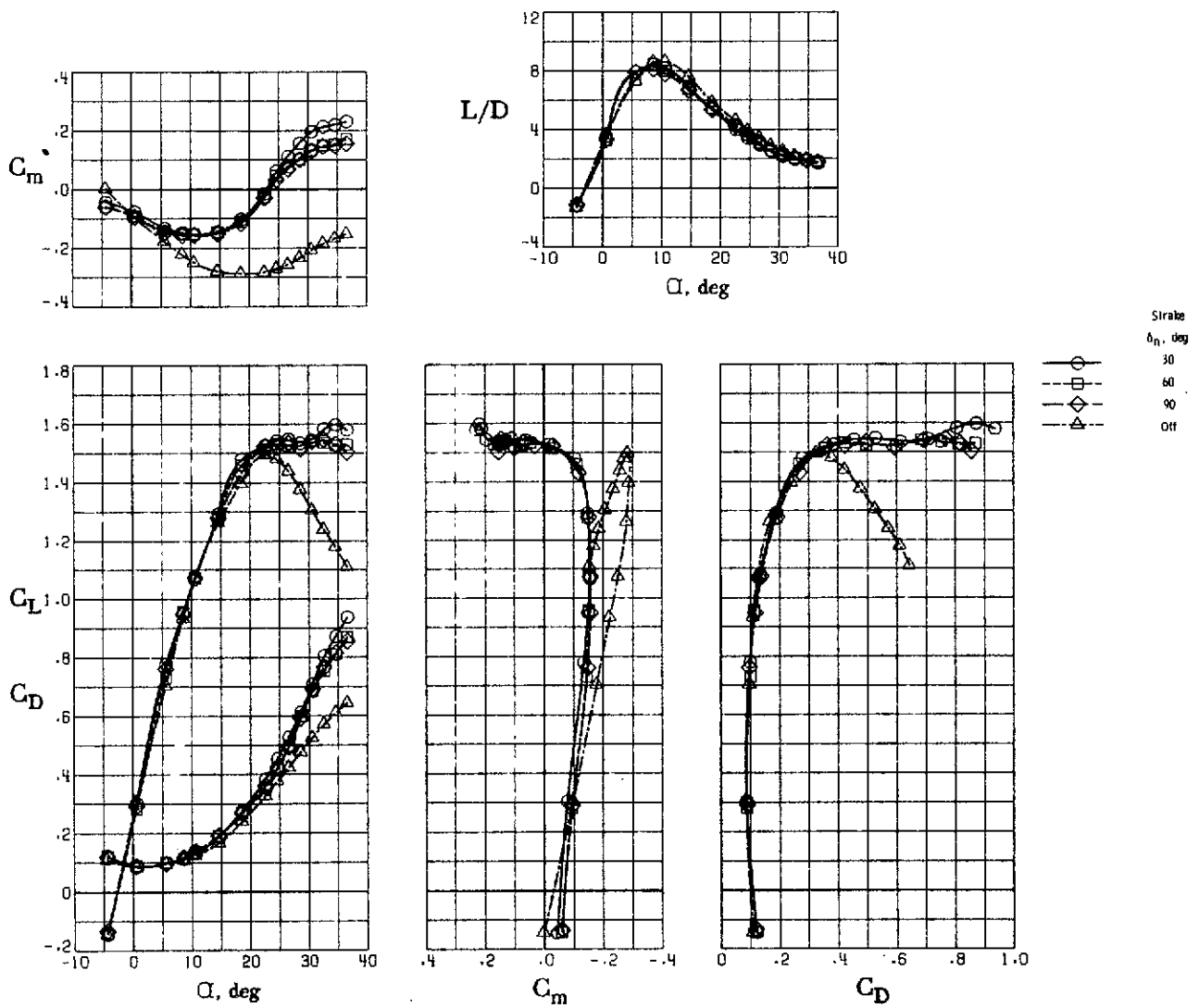

Figure 19: - Effect of strake leading - edge droop.
δ_f = 30°/50°, T - tail, i_t = 0°, Λ = 20° $\phi \rightarrow c^0$.

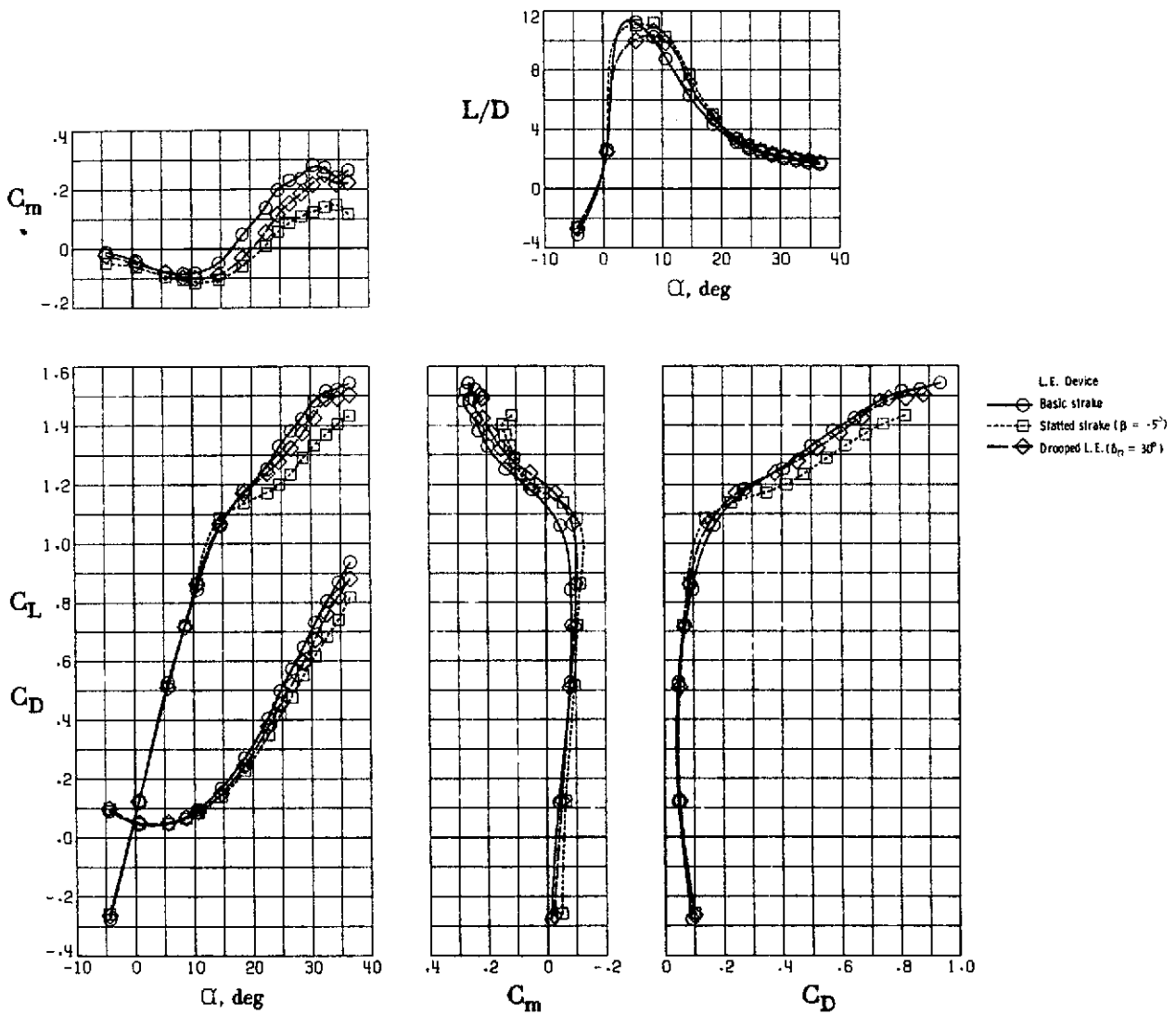

(a) δ_f = 14°/28°.

Figure 20. - Effect of strake leading edge device. T - tail, i_t = 0°, Λ = 20°, β = 0°.

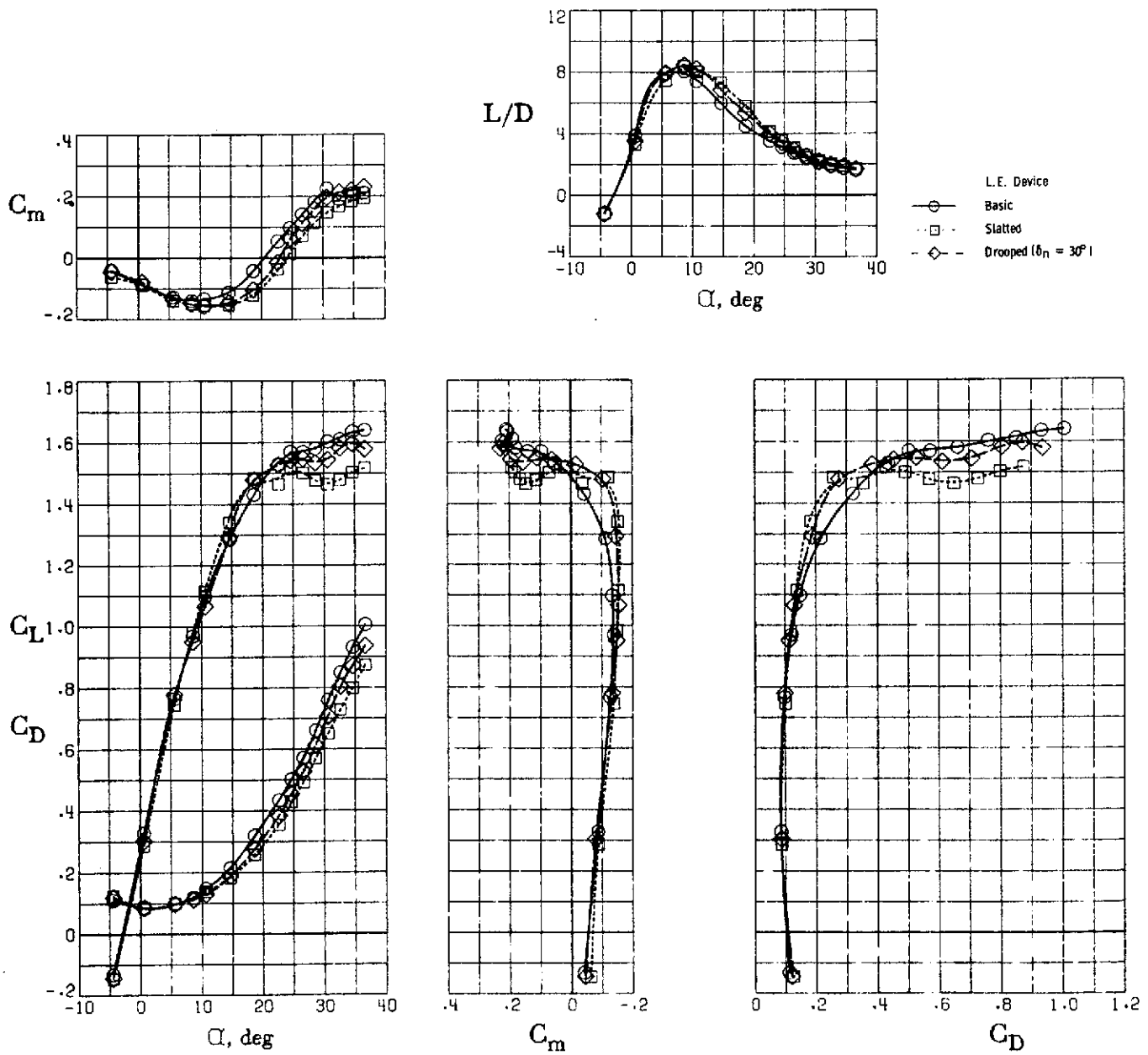

(b) δ_f = 30°/50°.

Figure 20. - Concluded.

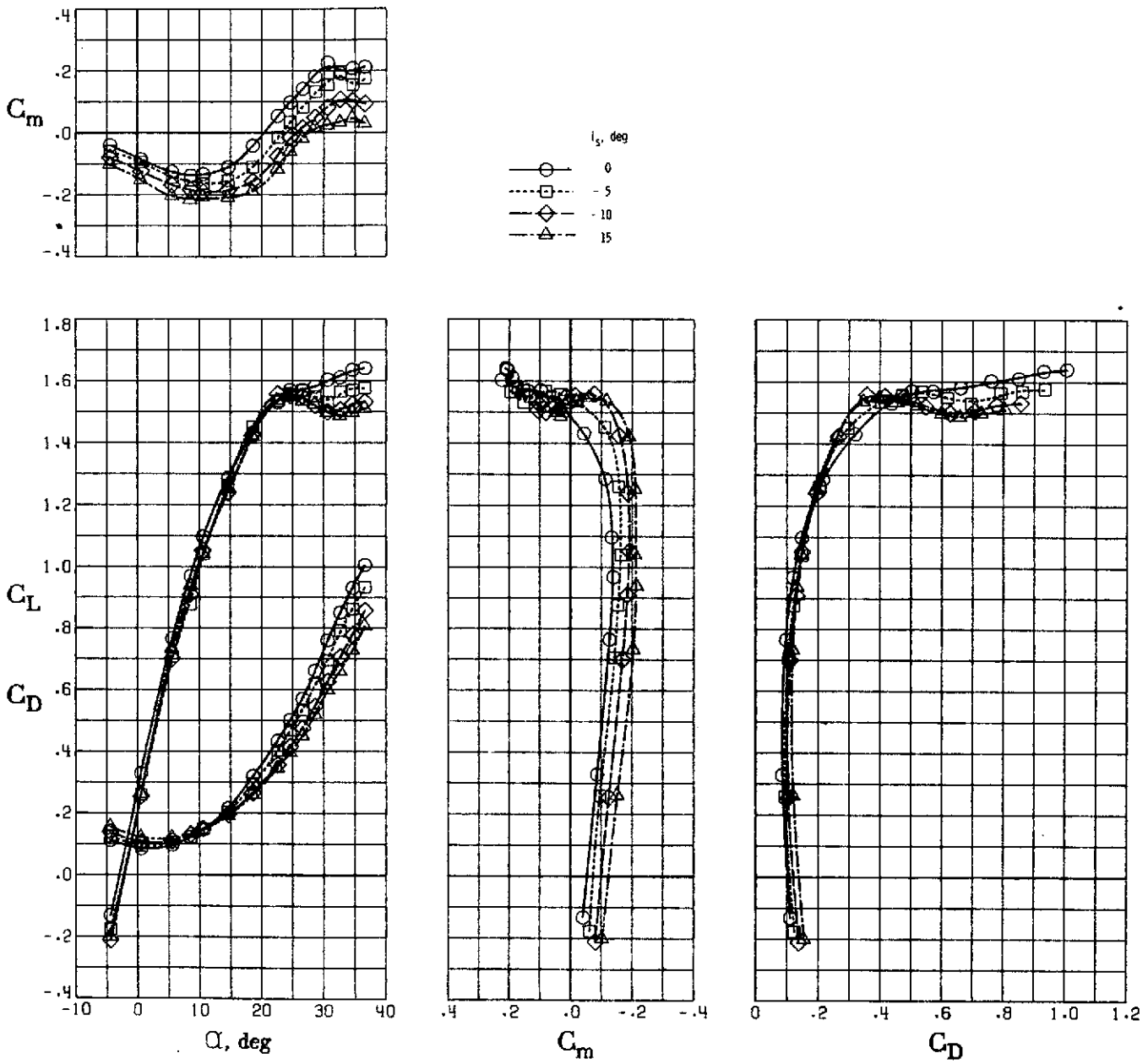

Figure 21. - Effect of strake incidence. δ_f = 30°/50°, T-tail, i_f = 0°, Λ = 20°, β = 0°.

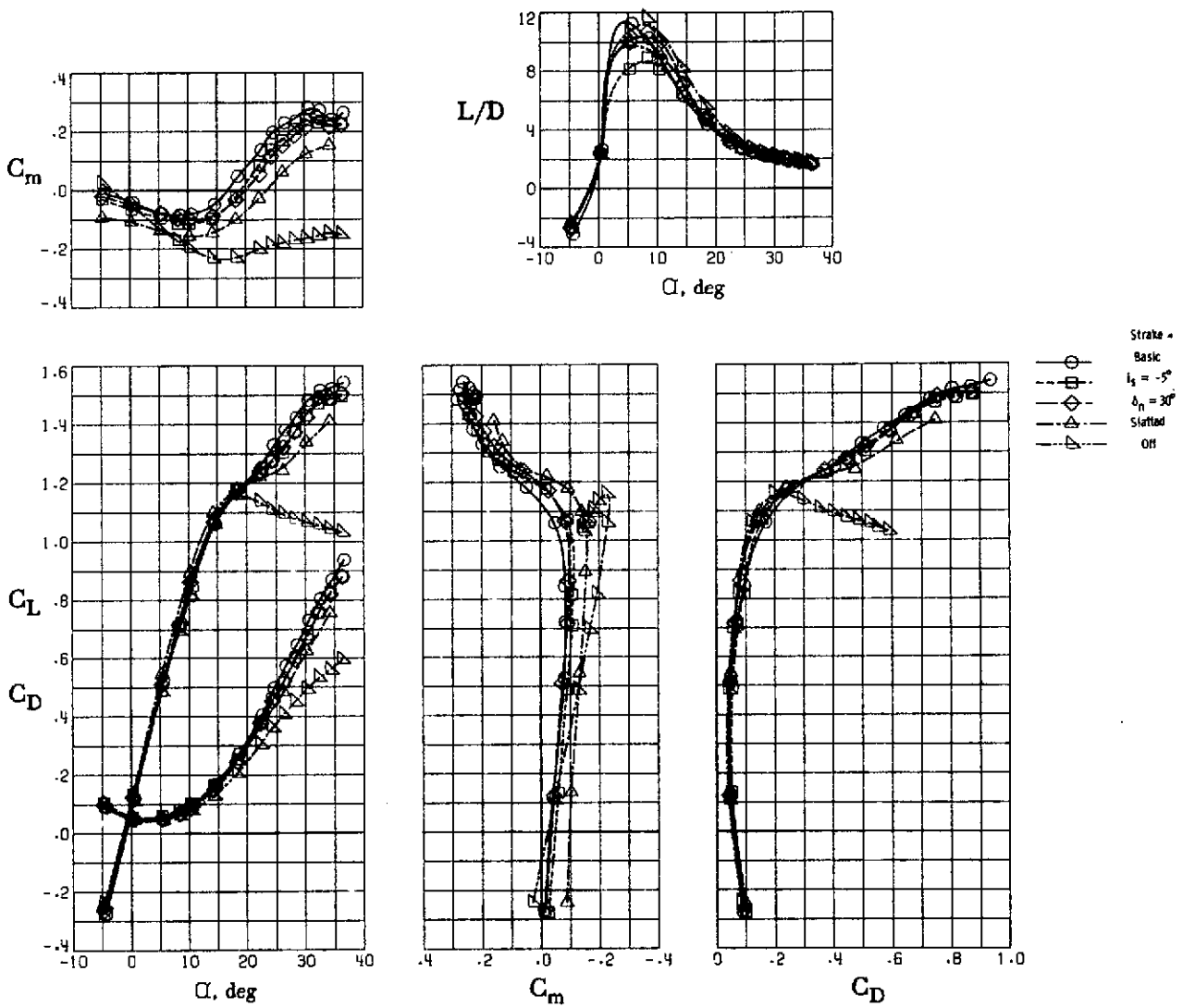

Figure 22.- Effect of strake leading-edge arrangement.
δ_f = 14°/28°, T-tail, i_t = 0°, Λ = 20°, β = 0°.

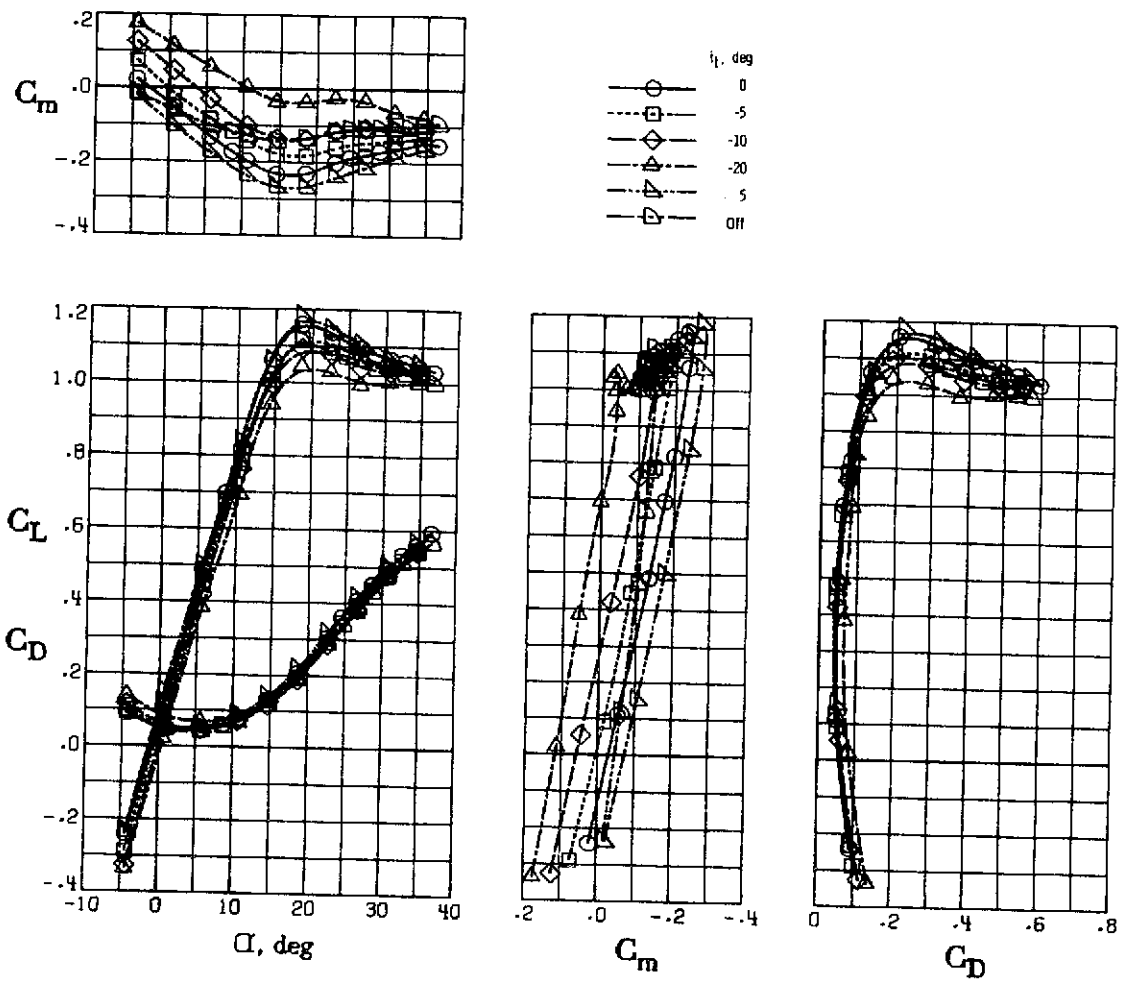

(a) δ_f = 14°/28°.

Figure 23. - Effect of tail deflection with strake removed. T-tail, Λ = 20°, β = 0°.

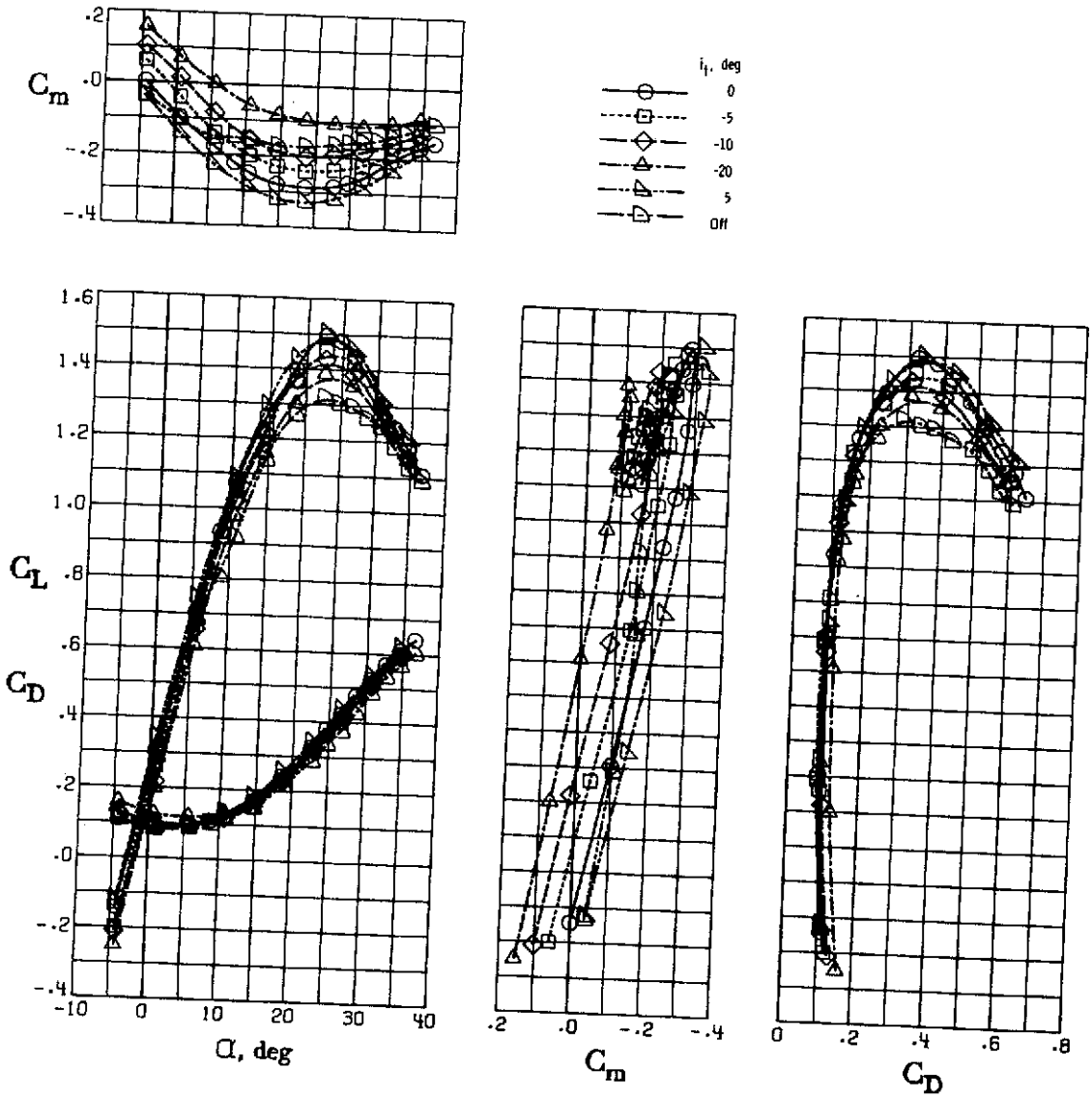

(b) δ_f = 30°/50°.

Figure 23. - Concluded.

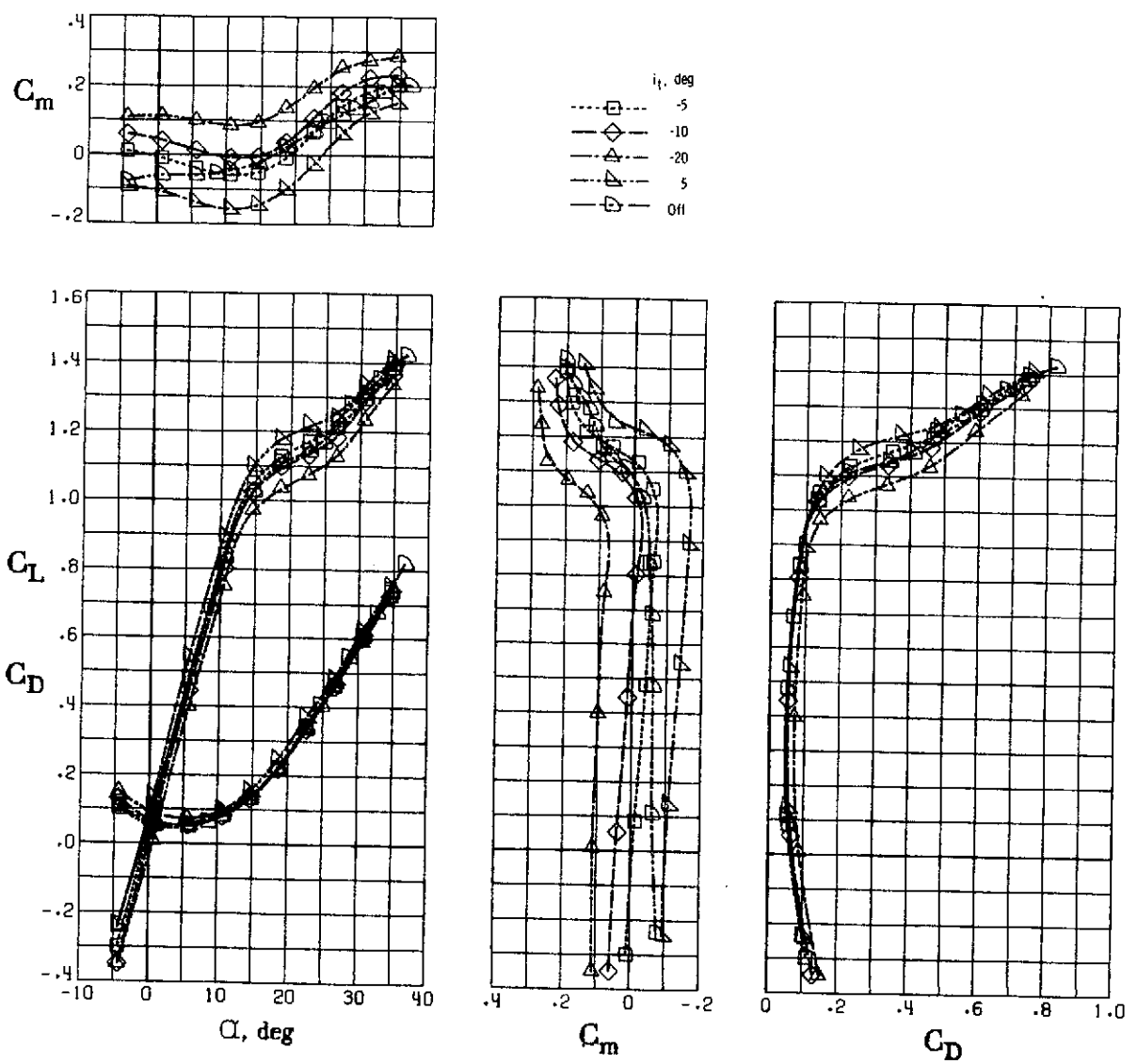

(a) δ_f = 14°/28°.

Figure 24.- Effect of tail deflection with slatted strake on. T-tail, Λ = 20°, β = 0°.

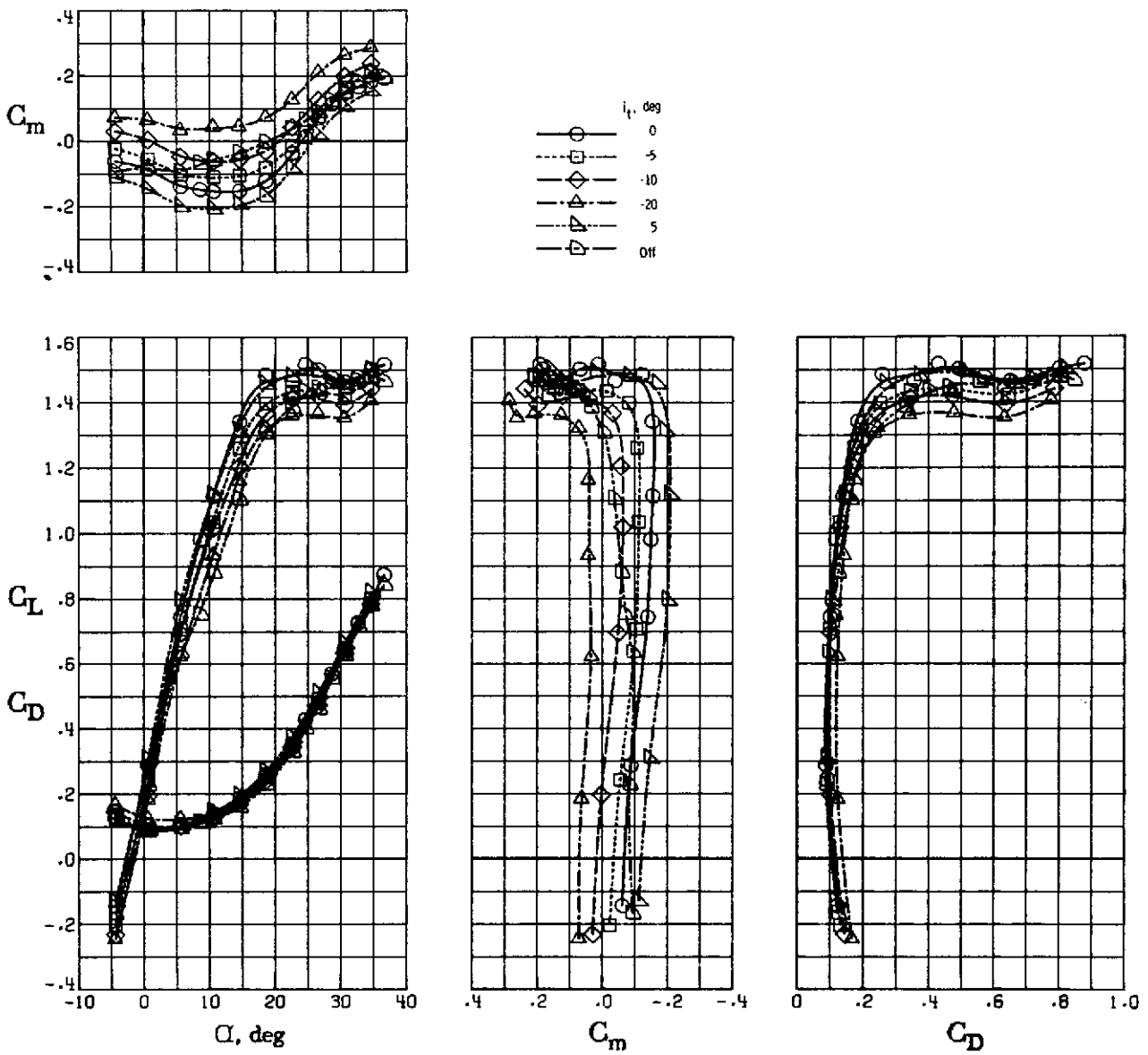

(b) δ_f = 30°/50°.

Figure 24.- Concluded.

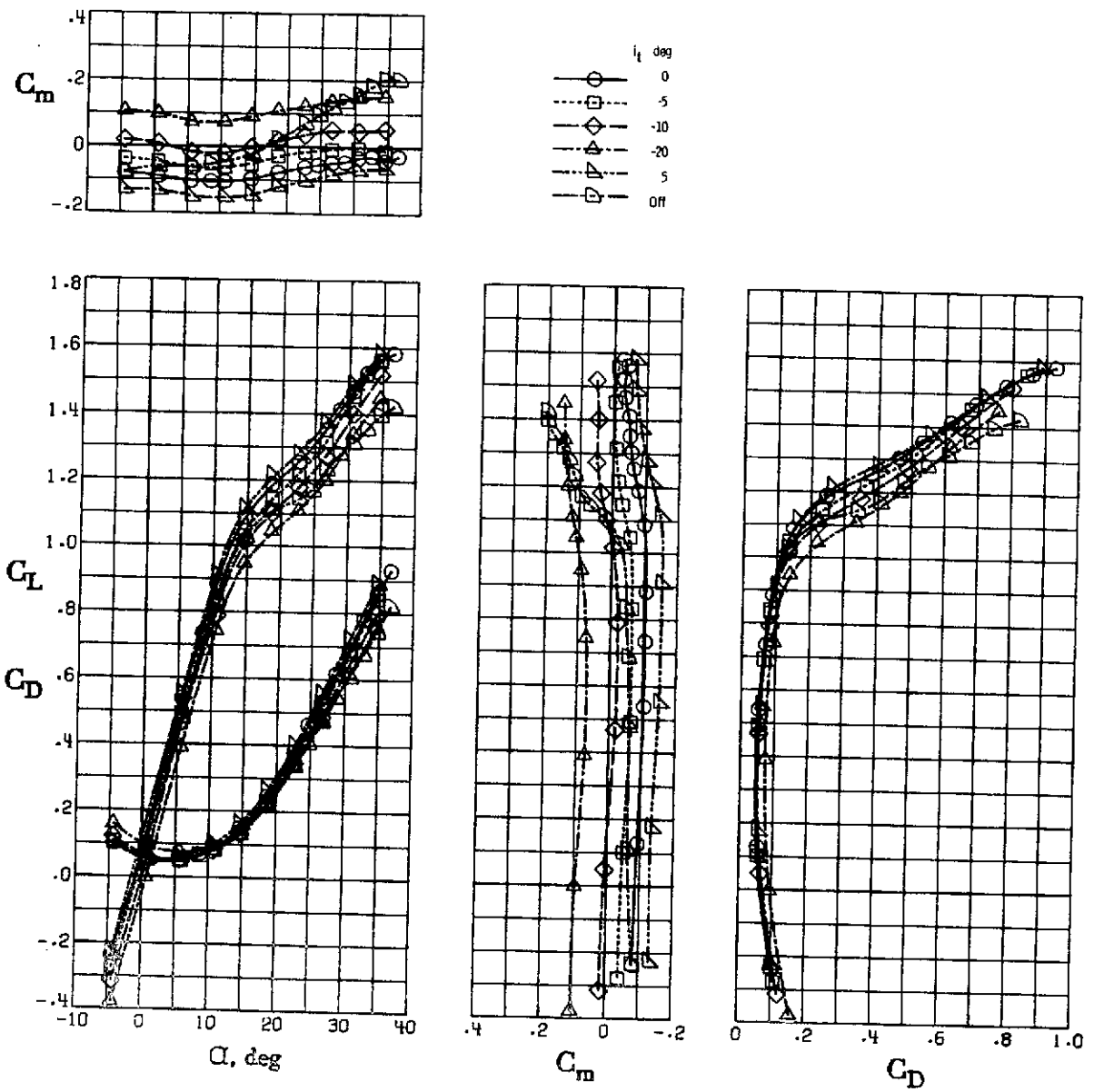

(a) δ_f = 14°/28°.

Figure 25.- Effect of tail deflection with slatted strake on. Low-tail, Λ = 20°, β = 0°.

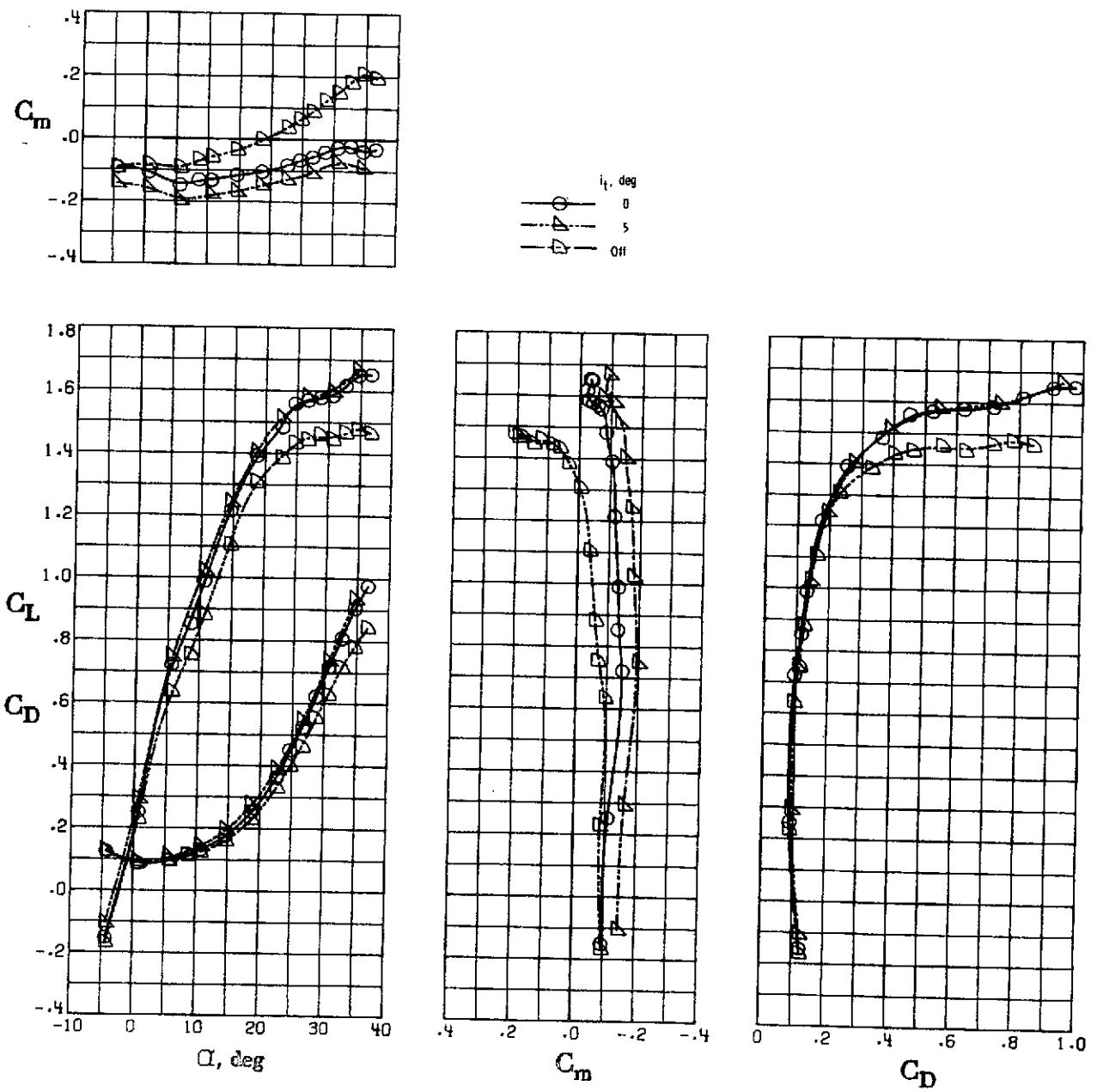

(b) δ_f = 30°/50°.

Figure 25. - Concluded.

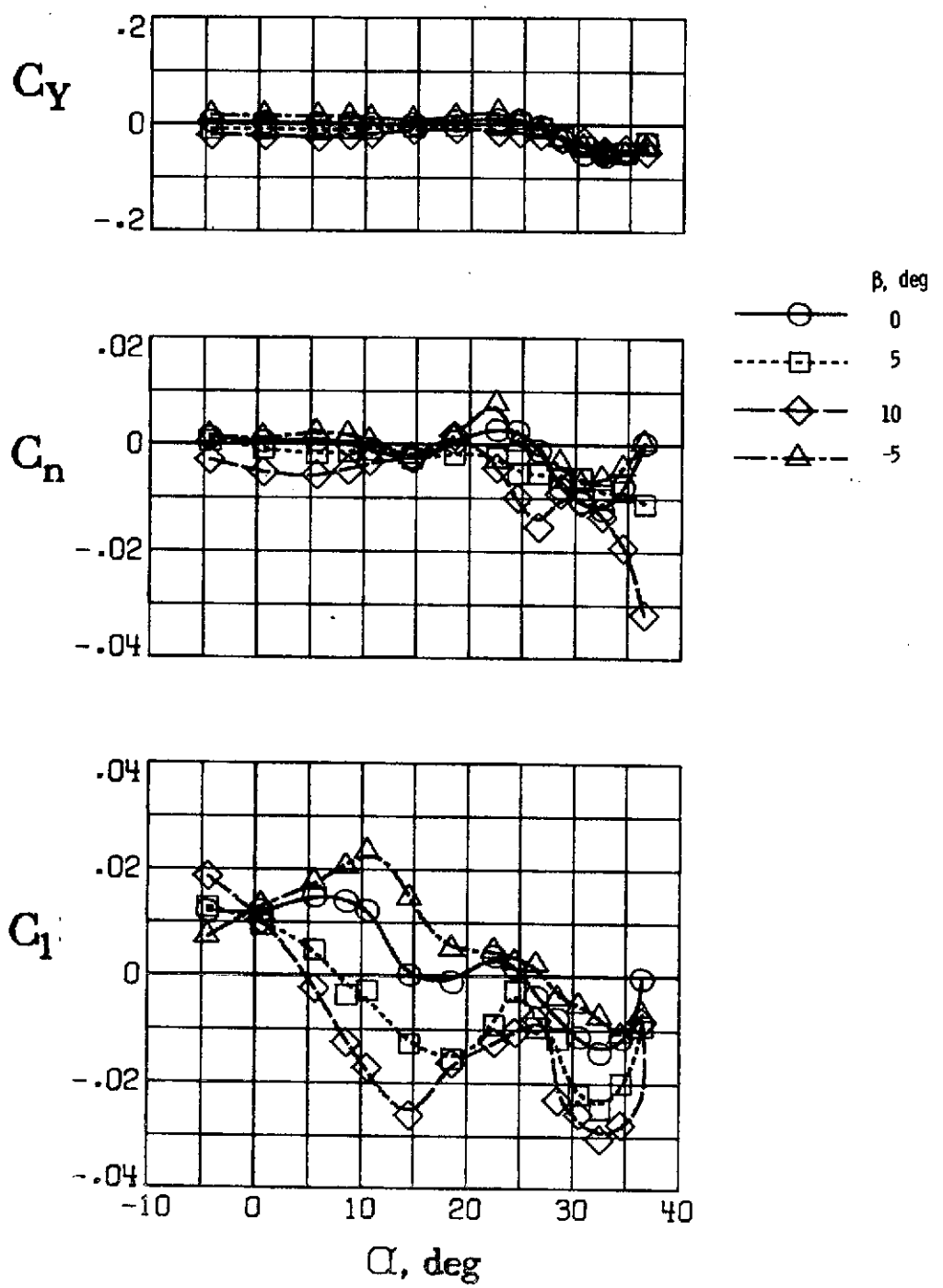

(a) $\Lambda = 20°$.

Figure 26. - Lateral-directional characteristics of clean wing configuration. Tail removed.

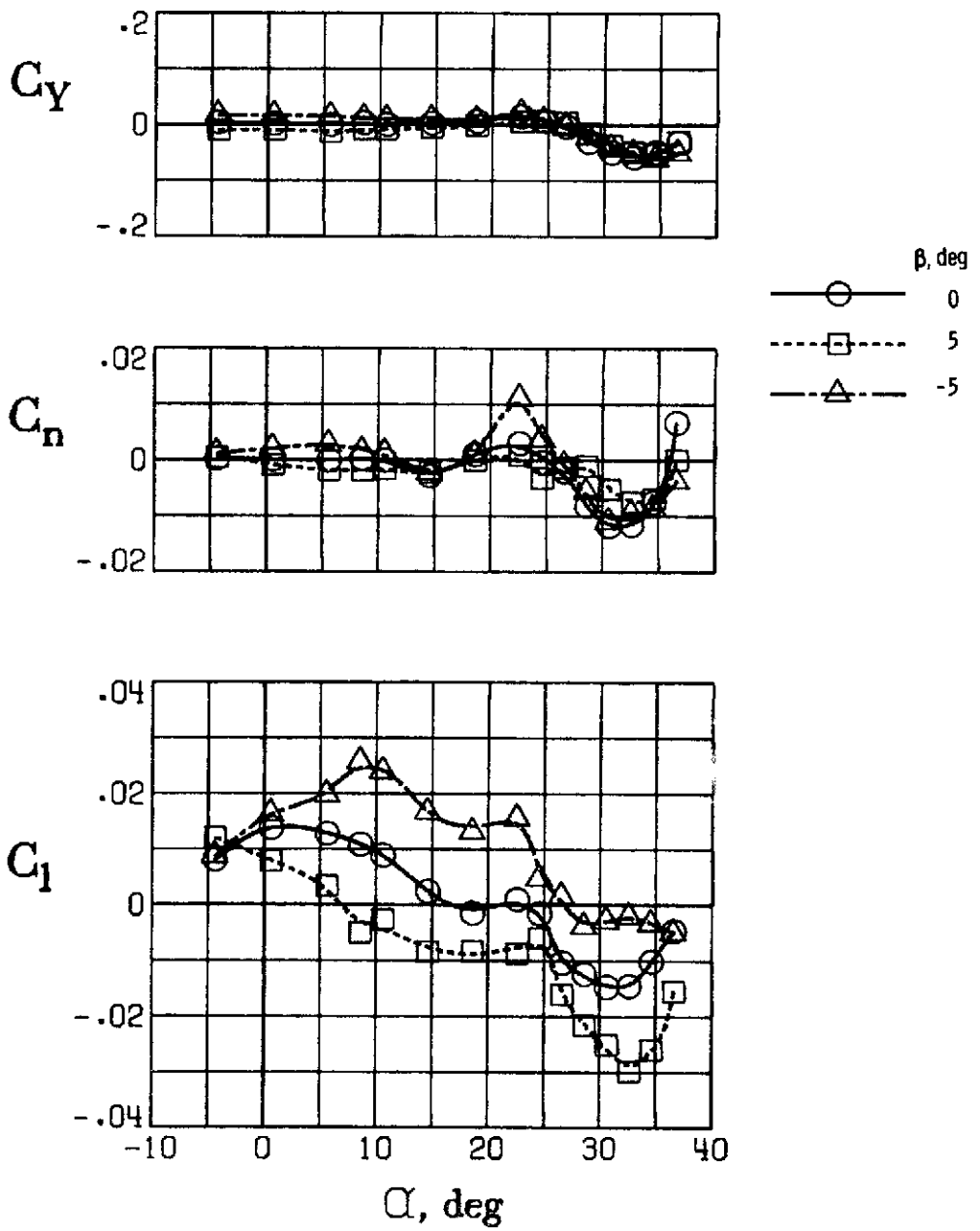

(b) $\Lambda_{\cdot} = 30°$.

Figure 26. - Continued.

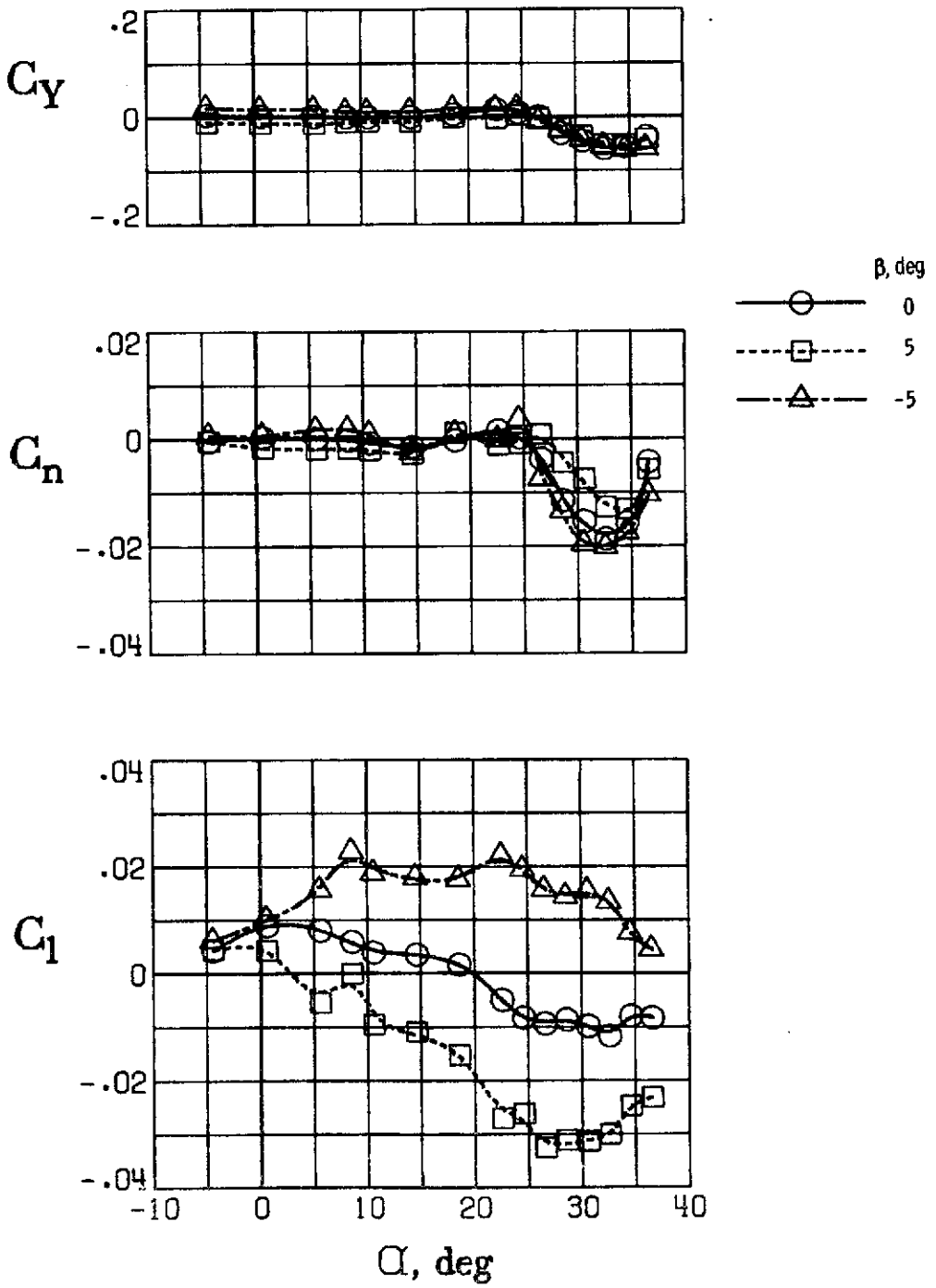

(c) $\Lambda = 42°$.

Figure 26'. - Continued.

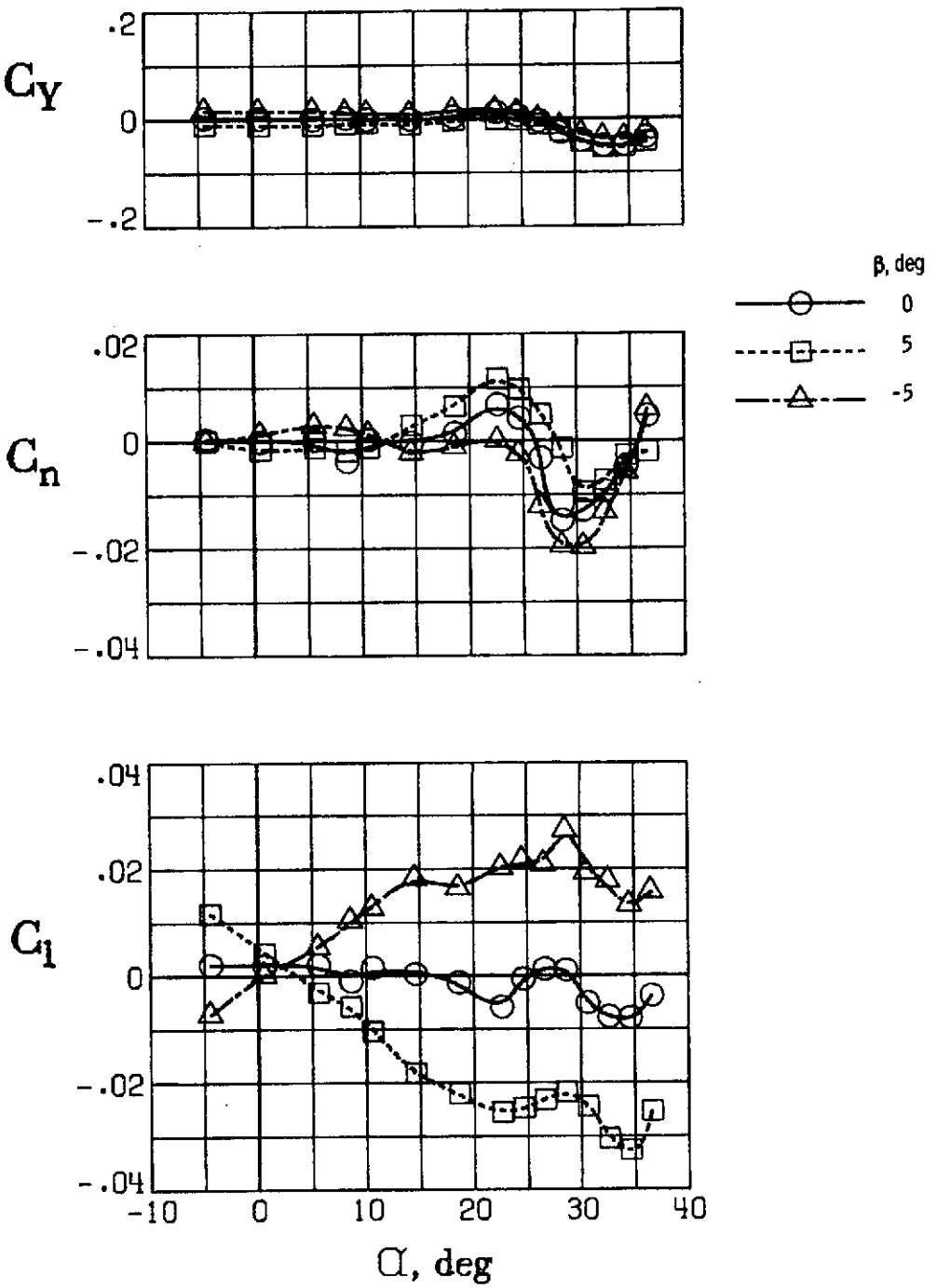

(d) $\Lambda = 72°$.

Figure 26. - Concluded.

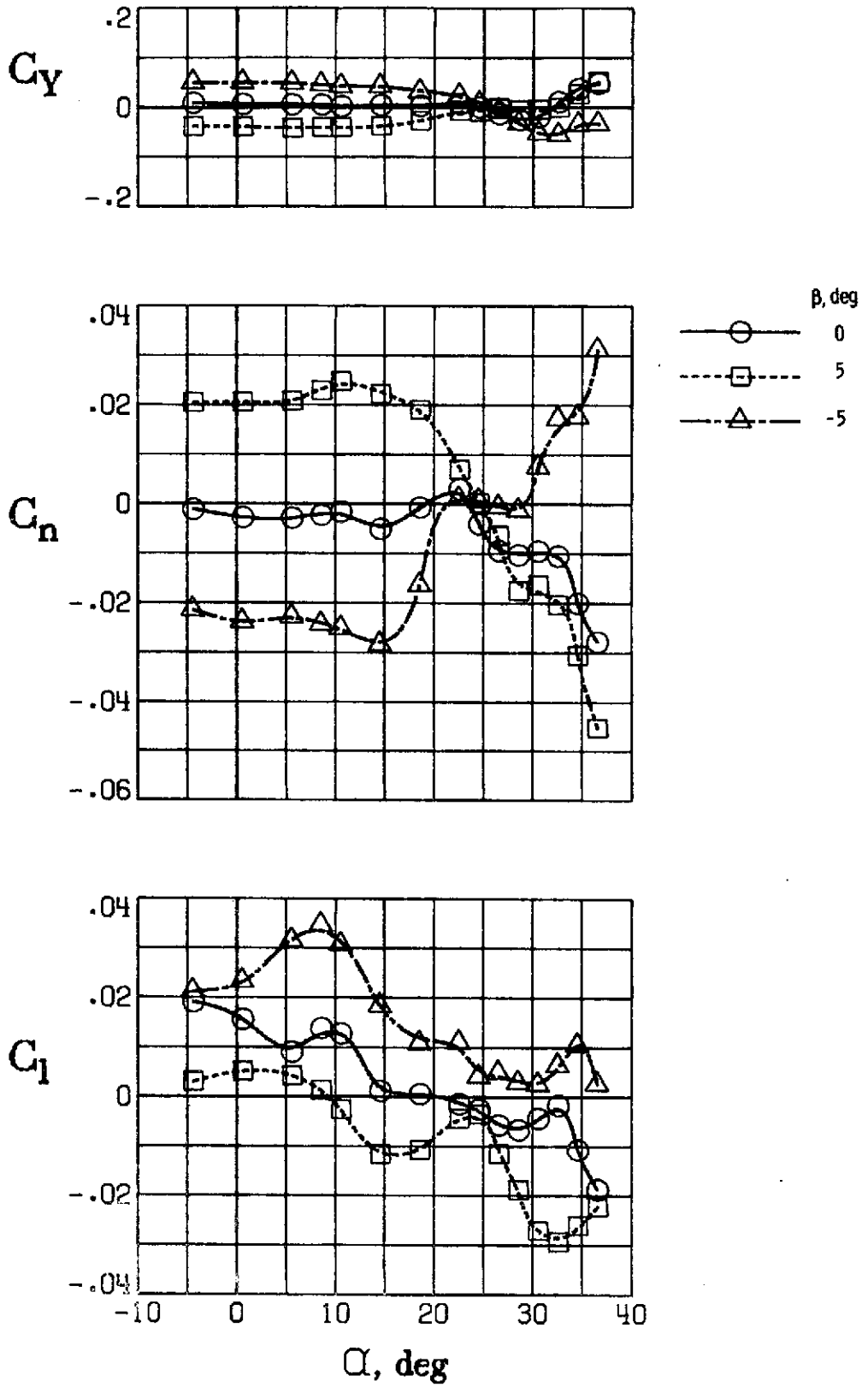

(a) Λ = 20°.

Figure 27. - Lateral-directional characteristics of clean wing configuration. T-tail, $i_t = 0°$.

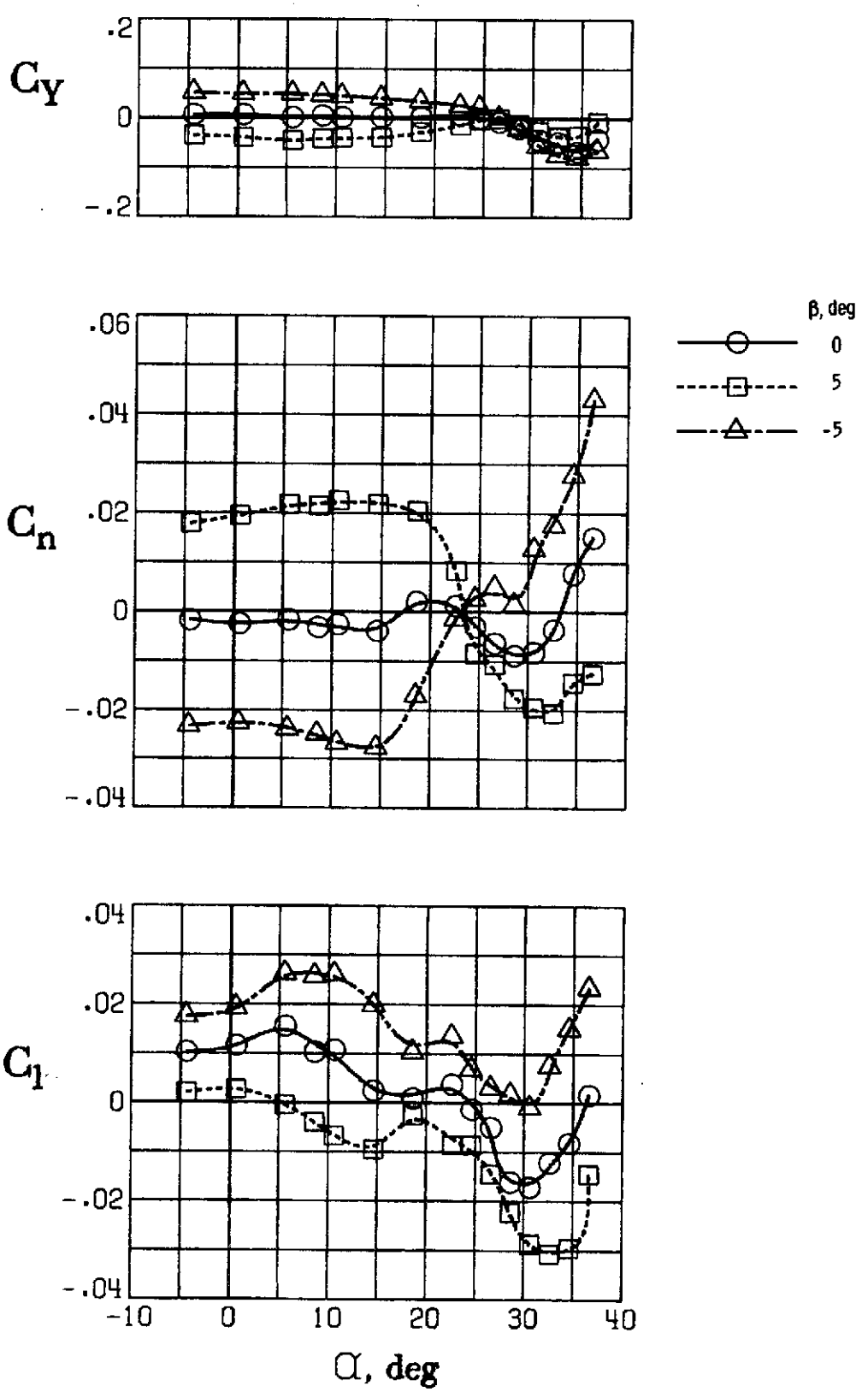

(b) $\Lambda = 30°$.

Figure 27 . - Continued.

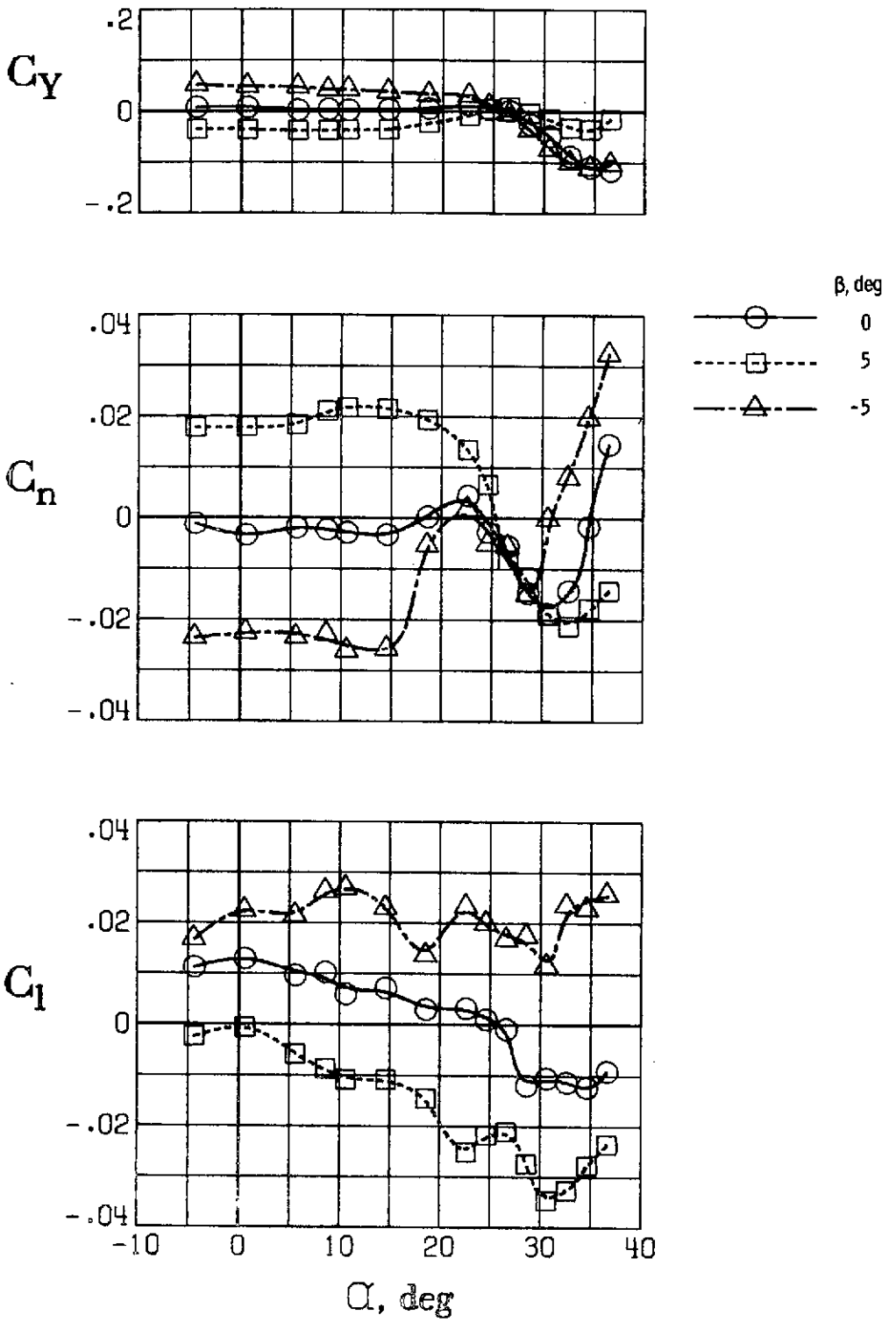

(c) $\Lambda = 42°$.

Figure 27. - Continued.

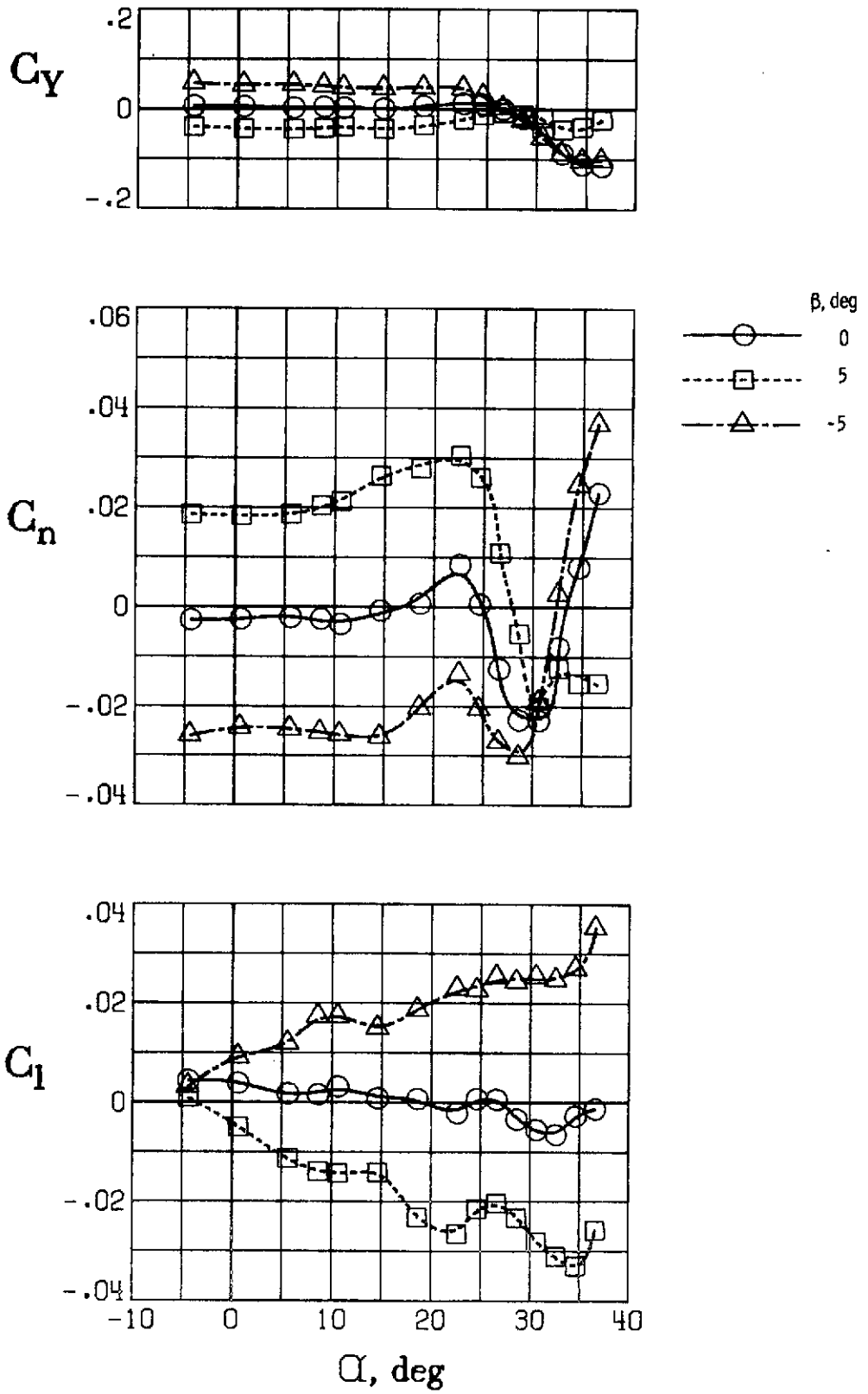

(d) $\Lambda = 72°$.

Figure 27. - Concluded.

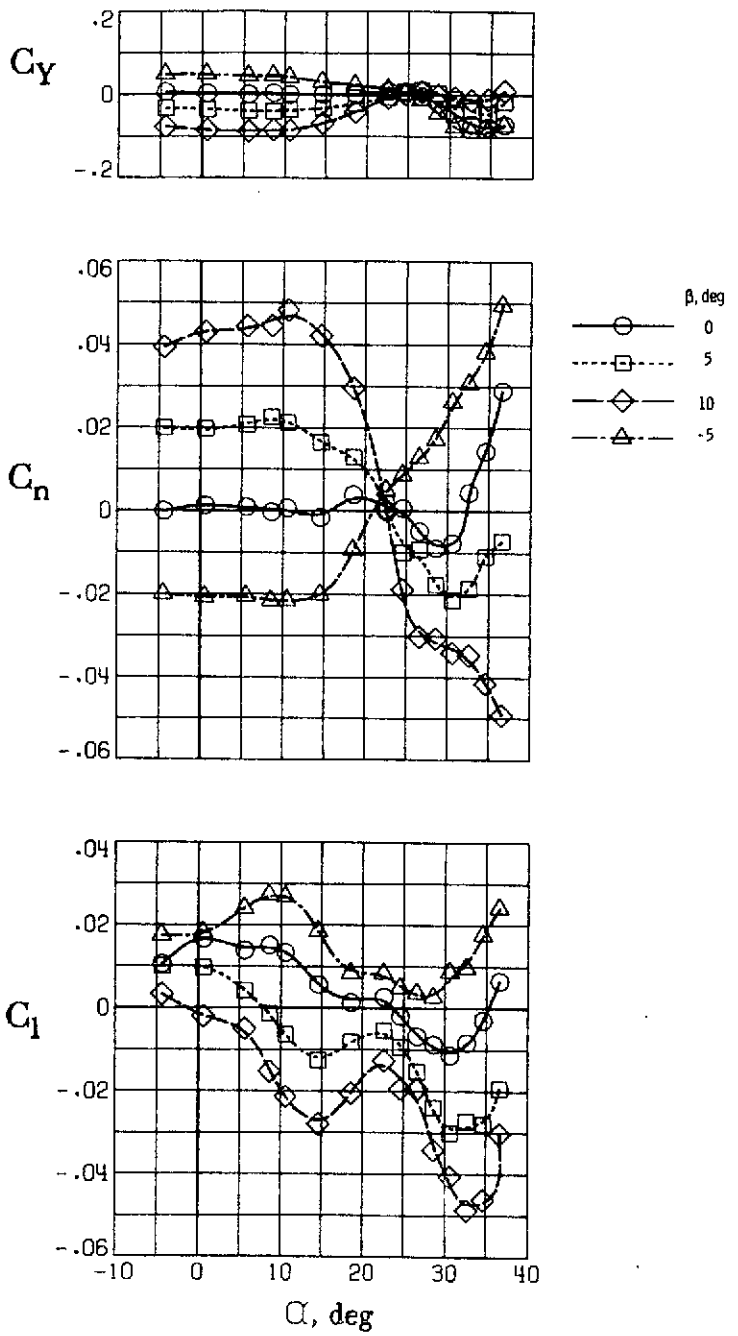

(a) $\Lambda_{.25} = 20°$.

Figure 28. - Lateral-directional characteristics of clean wing configuration. Low-tail; $i_t = 0°$.

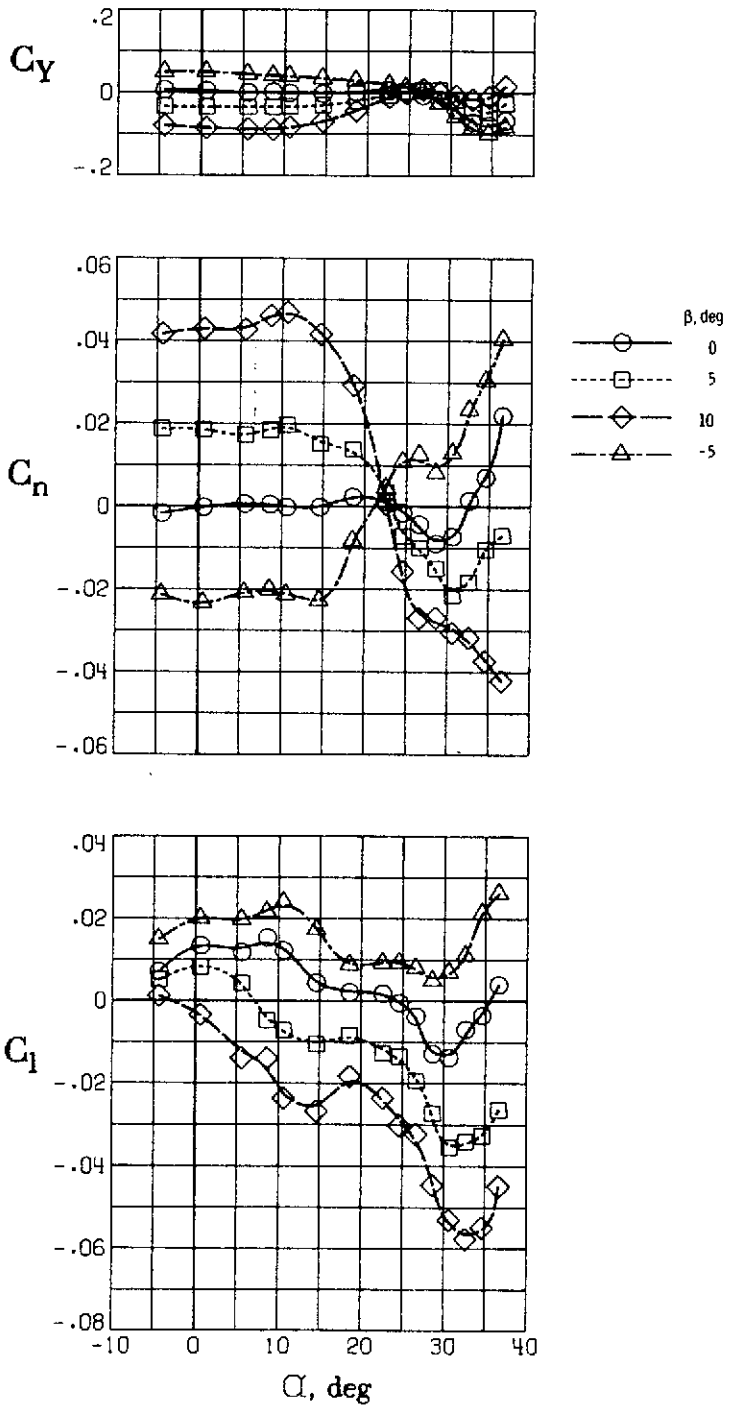

(b) $\Lambda = 30°$.

Figure 28.- Continued.

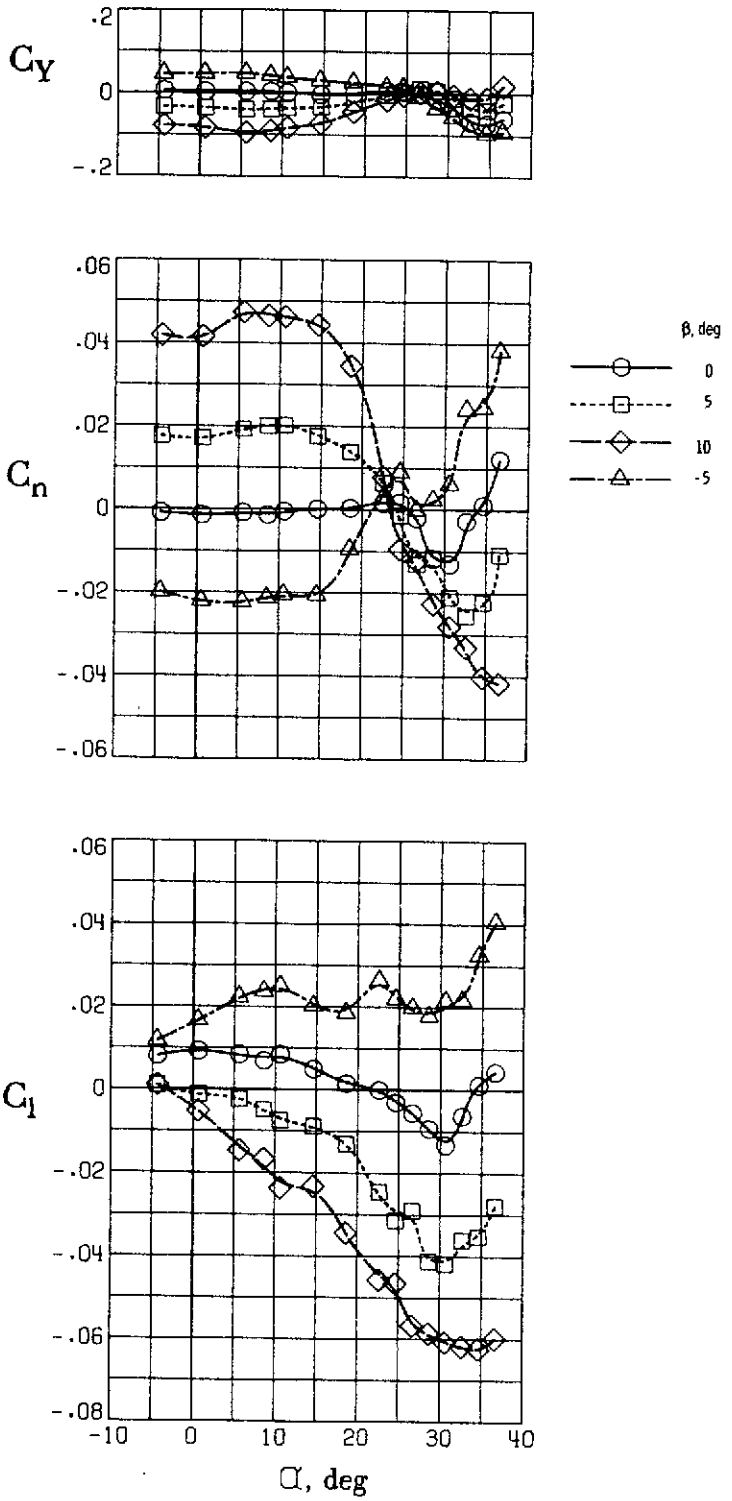

(c) Λ_L = 42°.

Figure 28. - Continued.

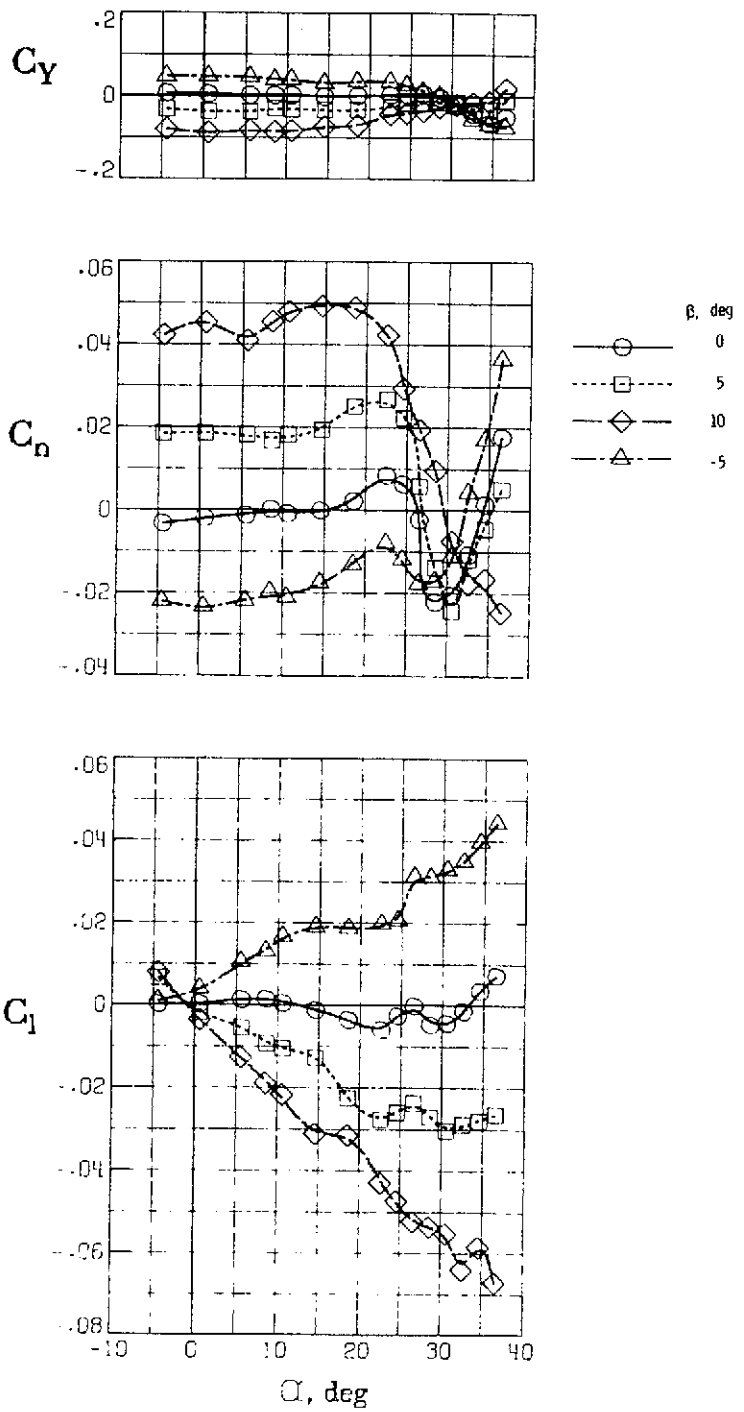

(d) $\Lambda = 72°$.

Figure 28. - Concluded.

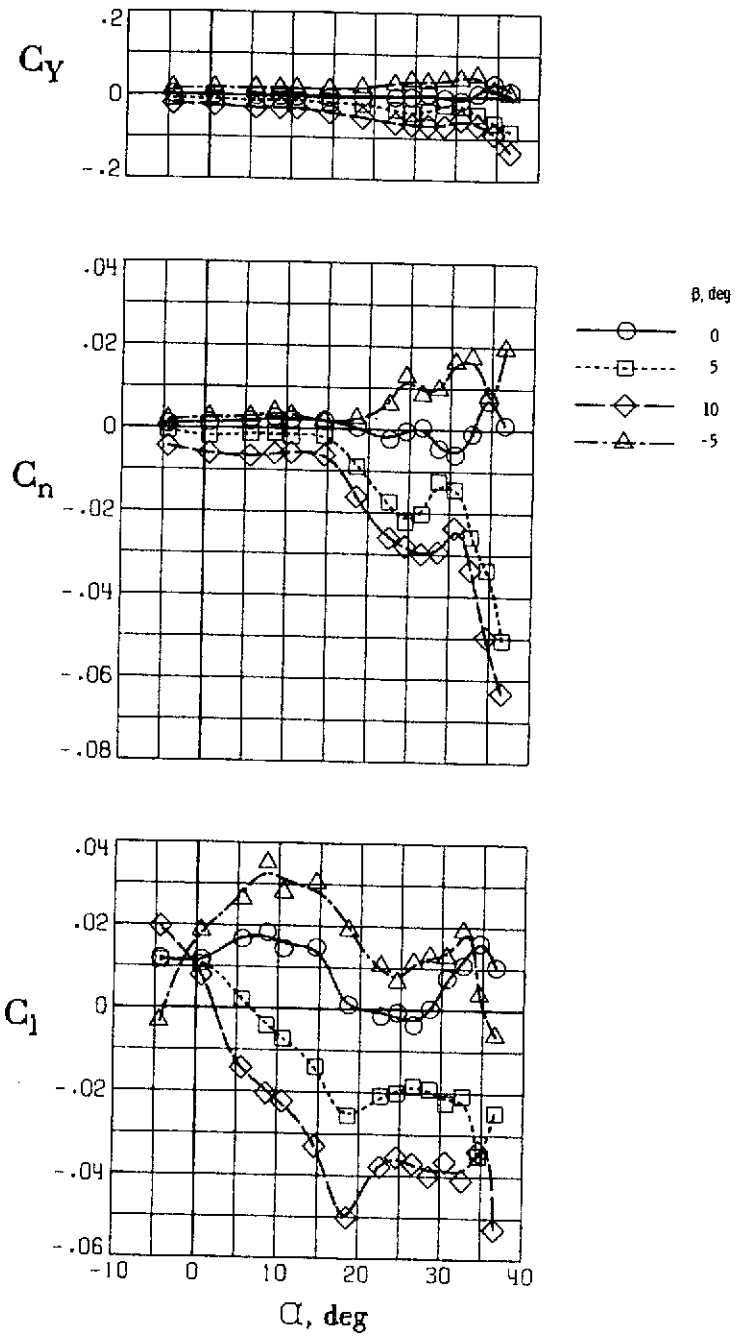

Figure 29. - Lateral-directional characteristics of basic-strake configuration. δ_f = 14°/28°, tail removed, Λ = 20°.

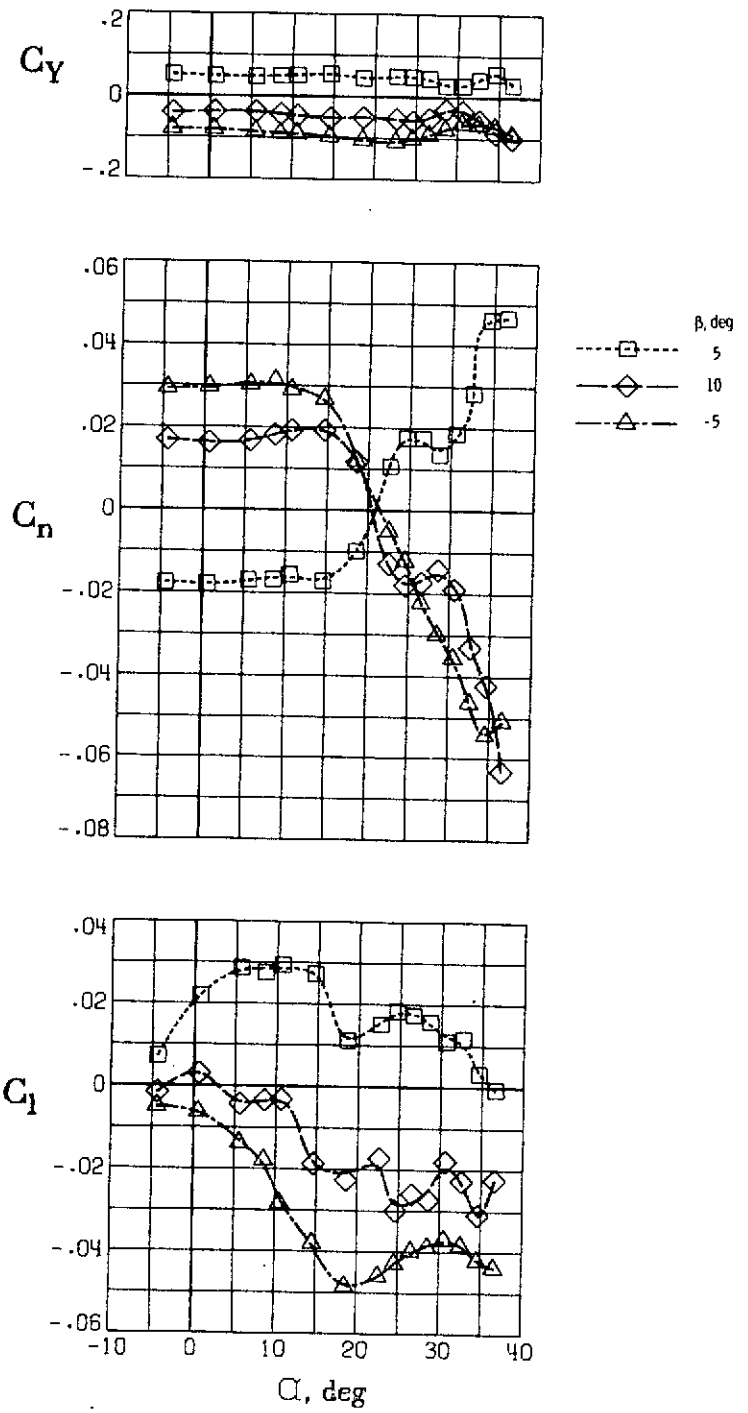

(a) $\Lambda_{\perp} = 20°$.

Figure 30.- Lateral-directional chracteristics of slatted strake configuration. $\delta_f = 14°/28°$, T-tail, $i_t = 0°$.

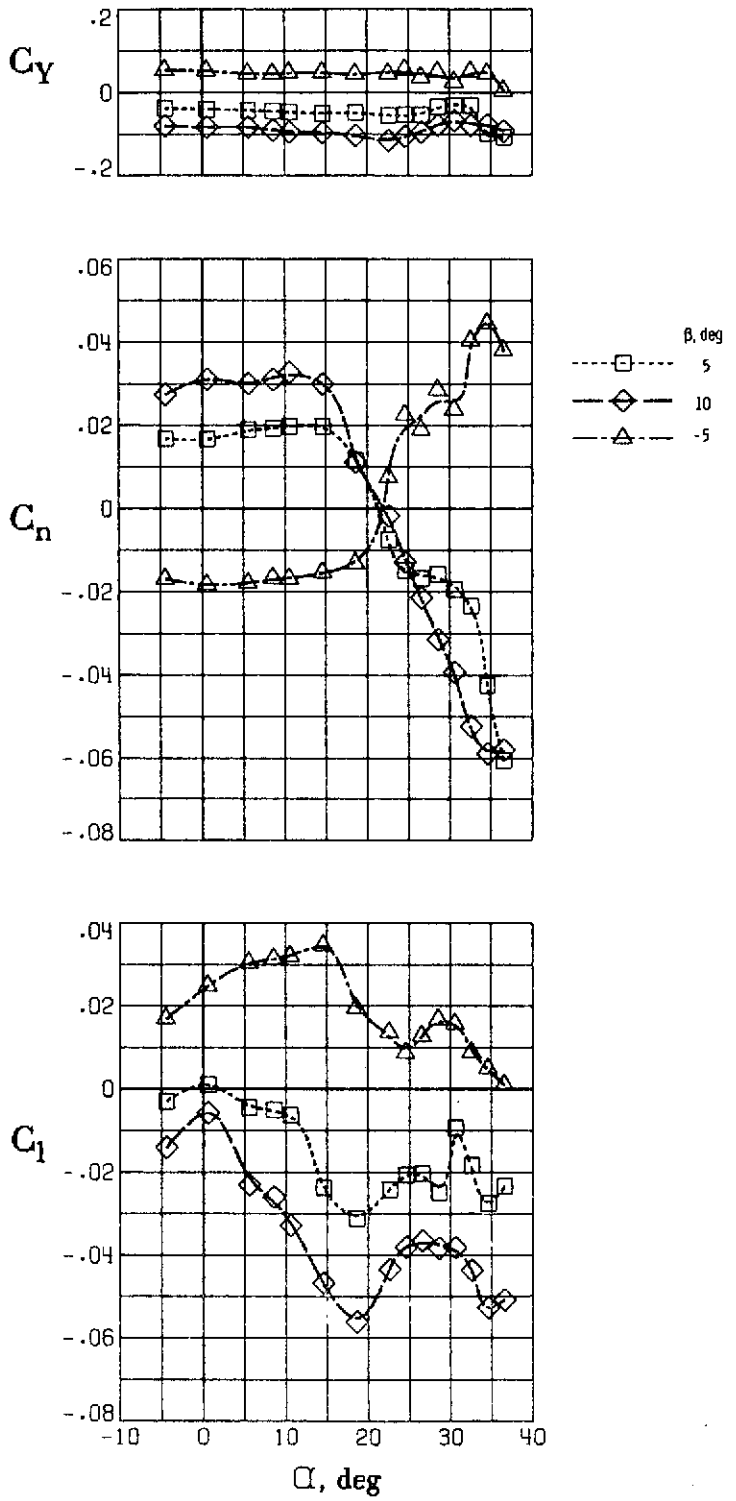

(b) Λ_c = 30°.

Figure 30. - Concluded.

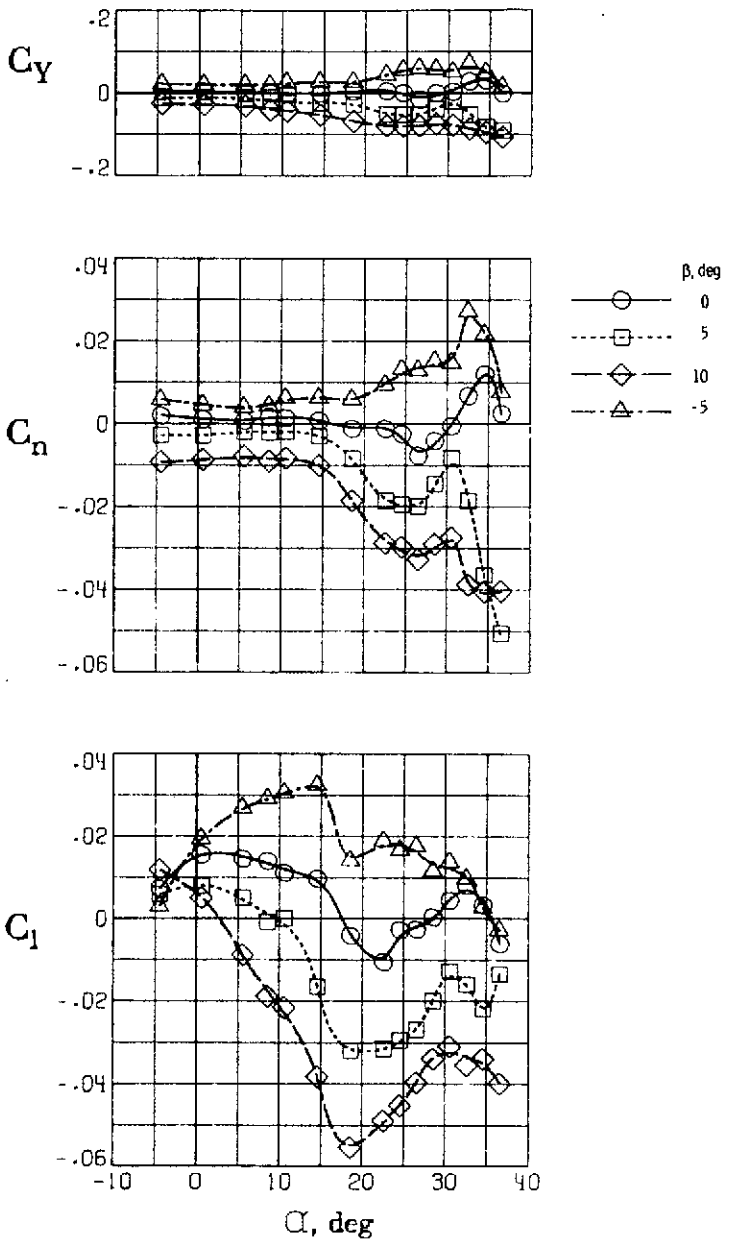

(a) Tail off.

Figure 31.- Lateral-directional characteristics for three tail arrangements. Slatted strake, δ_f = 14°/28°, Λ_{LE} = 20°.

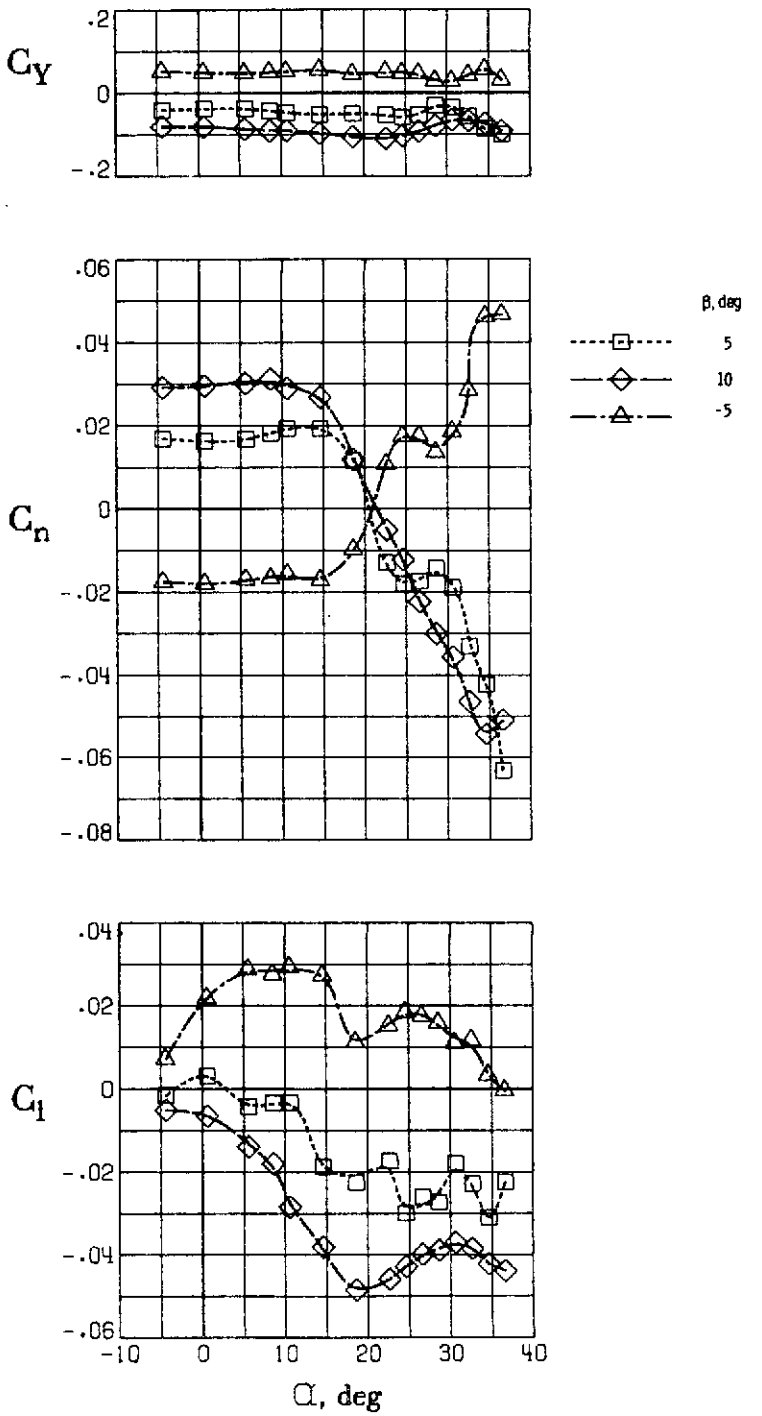

(b) T-tail.

Figure 31. - Continued.

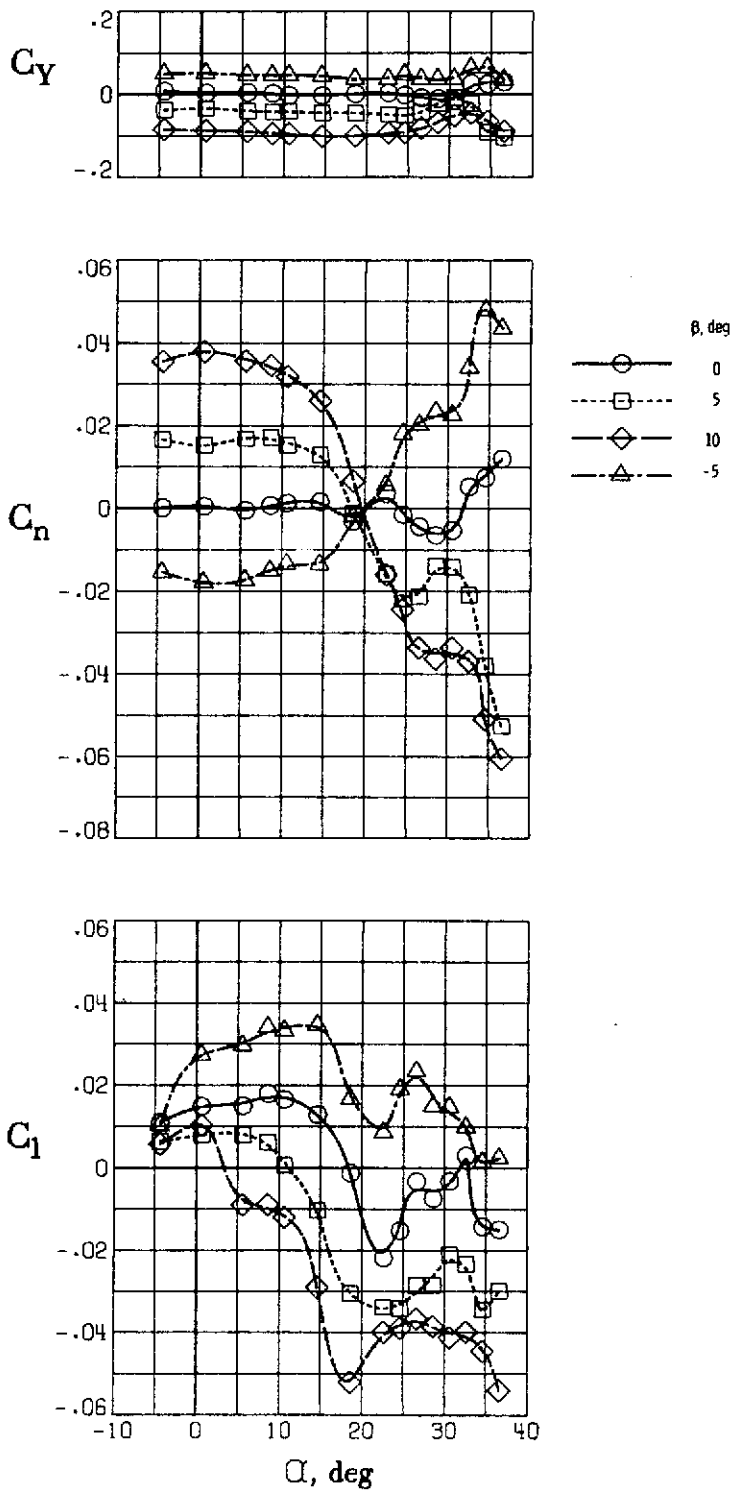

(c) Low-tail.

Figure 31. - Concluded.

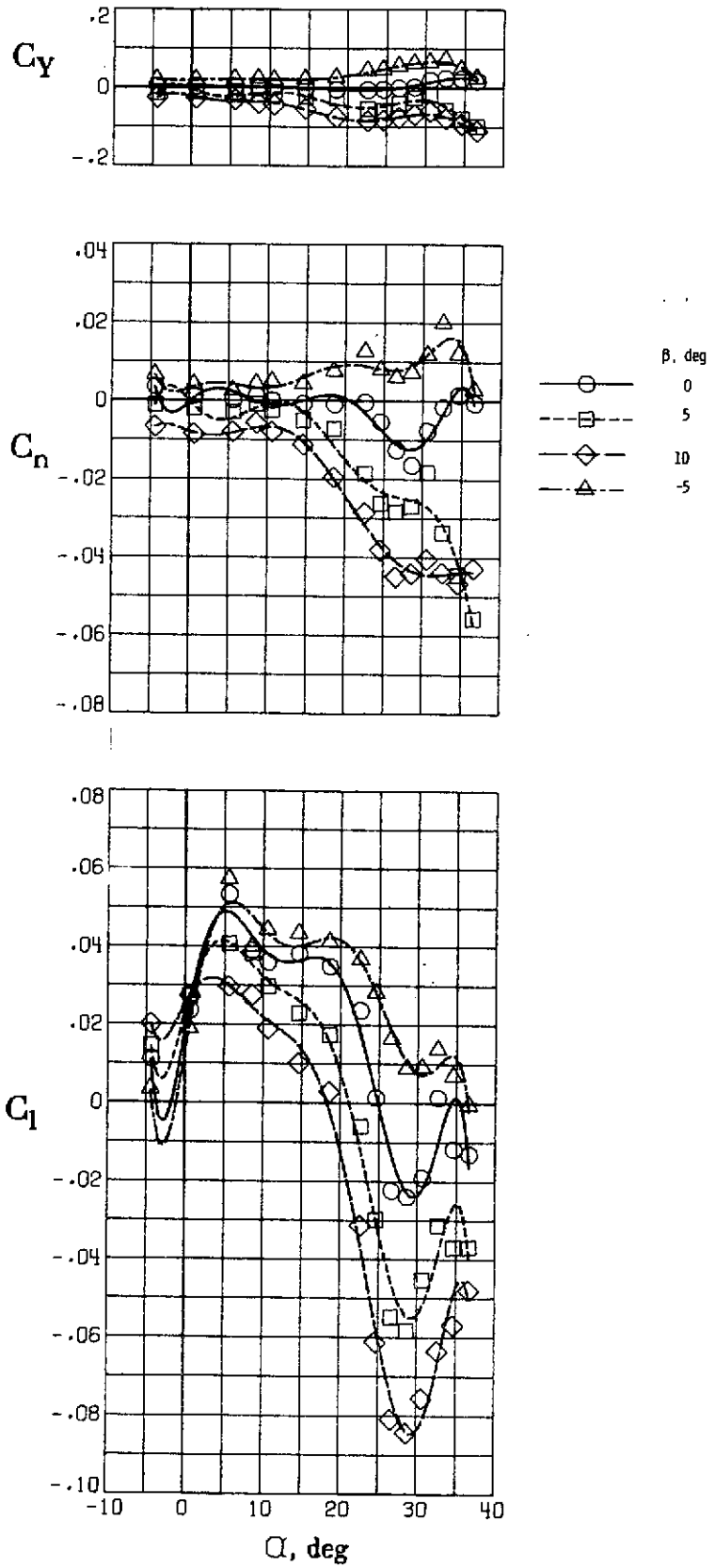

(a) Tail off.

Figure 32.- Lateral-directional characteristics for three tail arrangements. Slatted strake, δ_f = 30°/50°. Λ_c = 20°

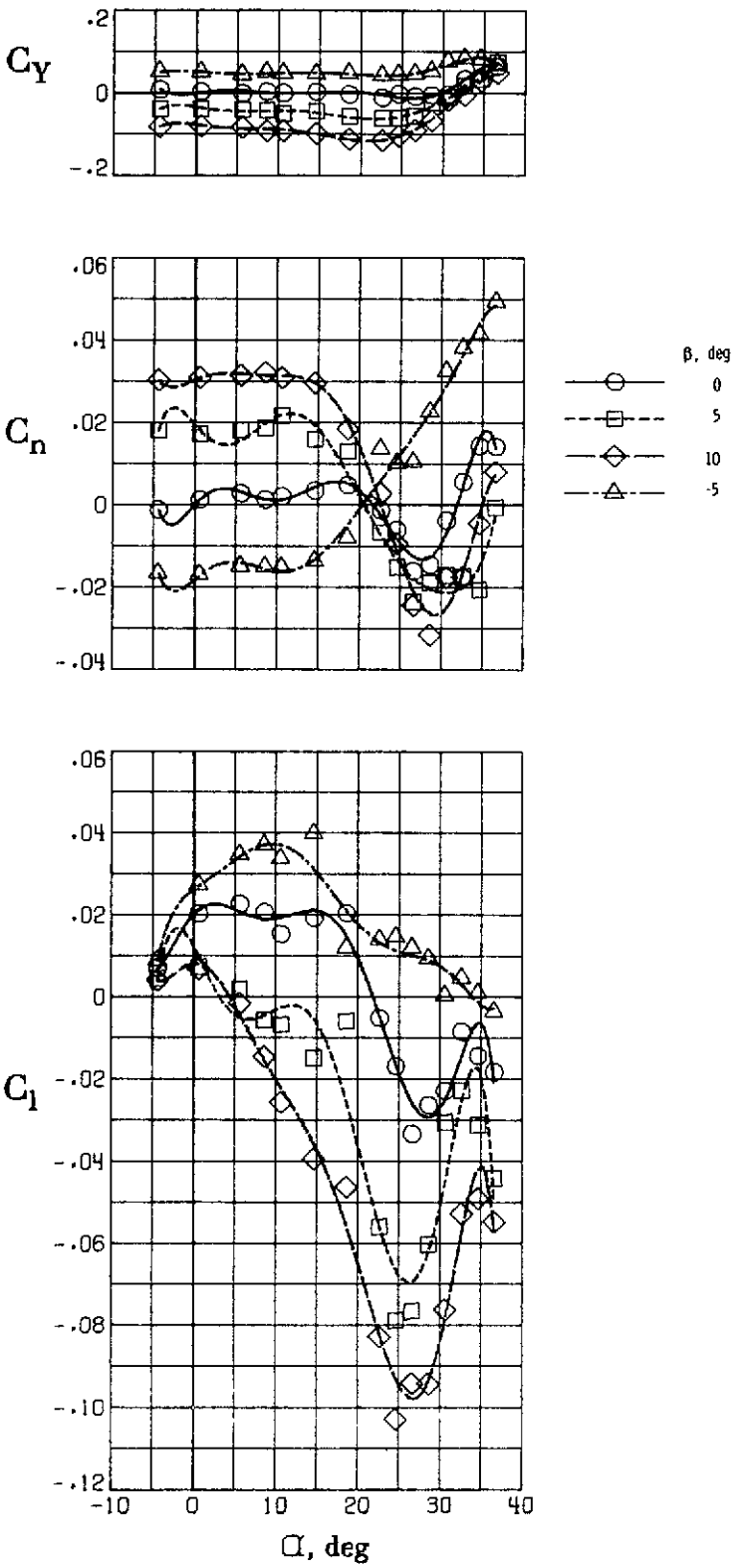

(b) T-tail.

Figure 32. - Continued.

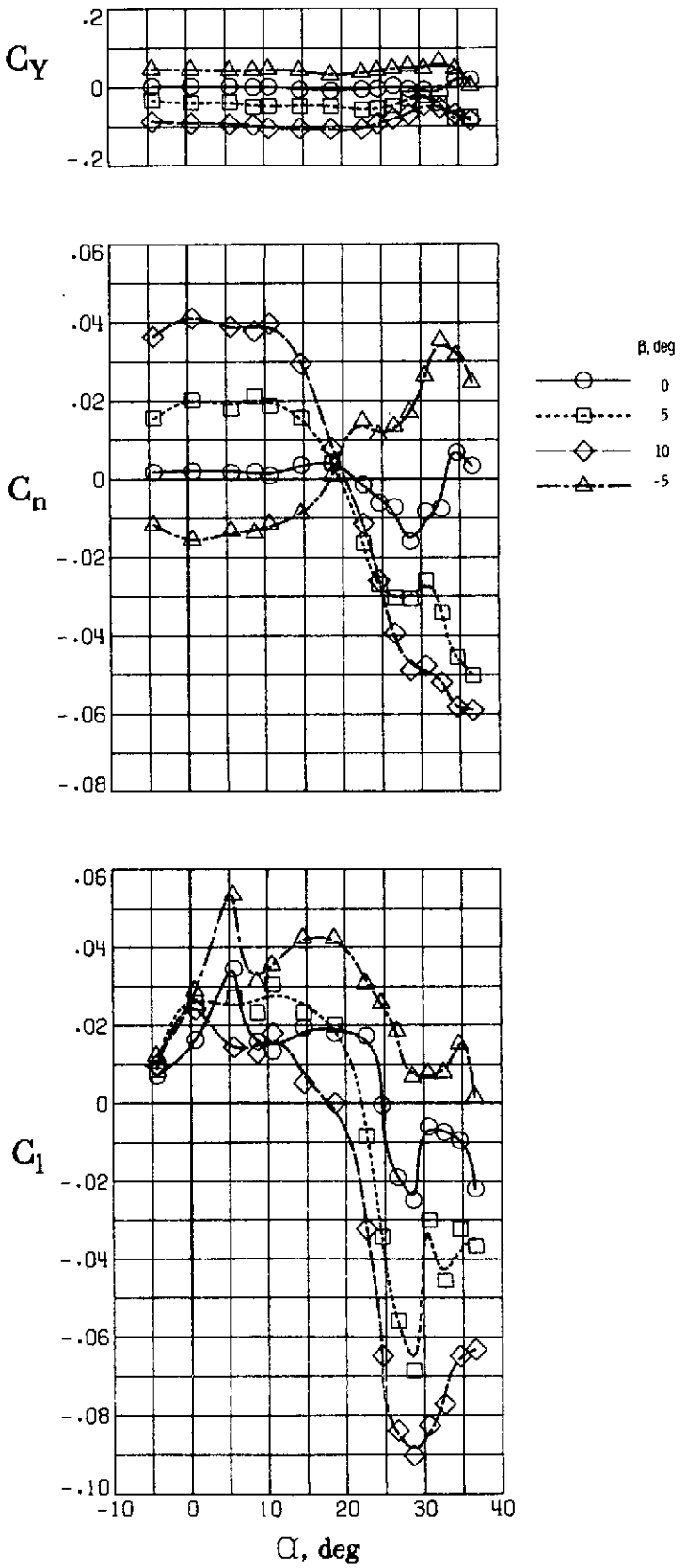

(c) Low-tail.

Figure 32. - Concluded.

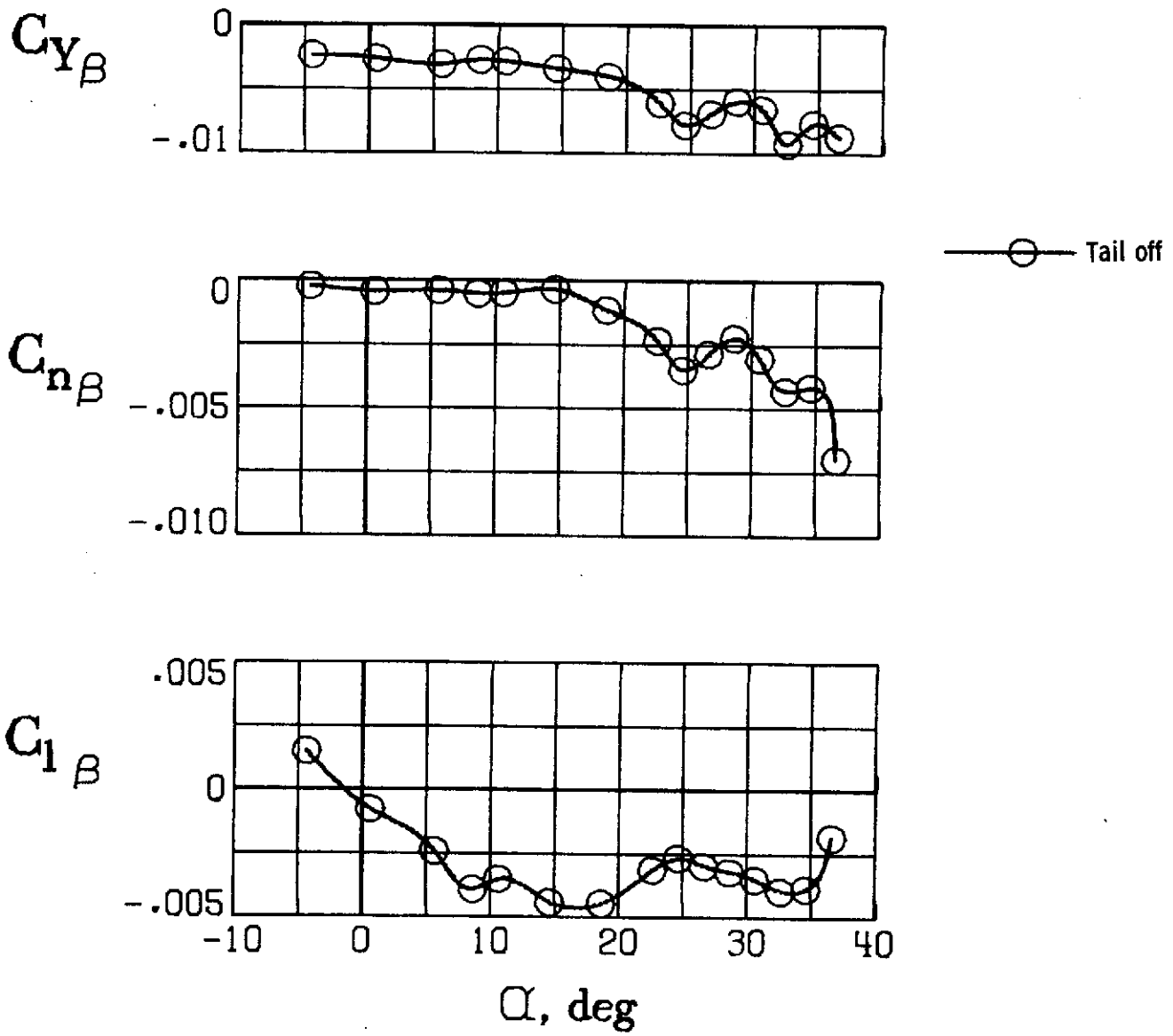

Figure 33.- Lateral-directional stability derivatives of basic strake configuration. $\Lambda = 20°$. $\delta_f = 14°/28°$.

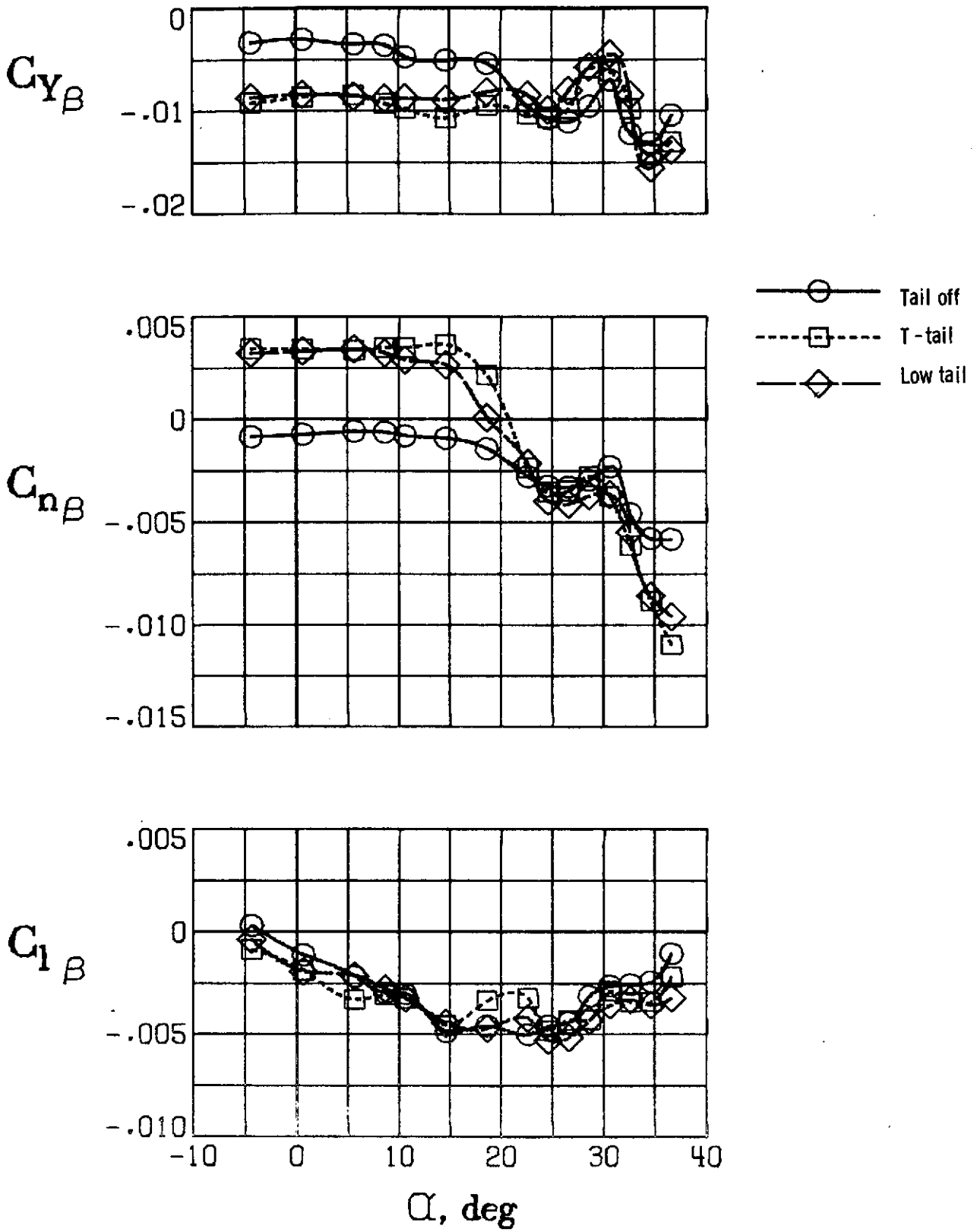

(a) $\delta_f = 14°/28°$.

Figure 34 . - Lateral-directional stability derivatives of slatted-strake configuration. $\Lambda = 20°$.

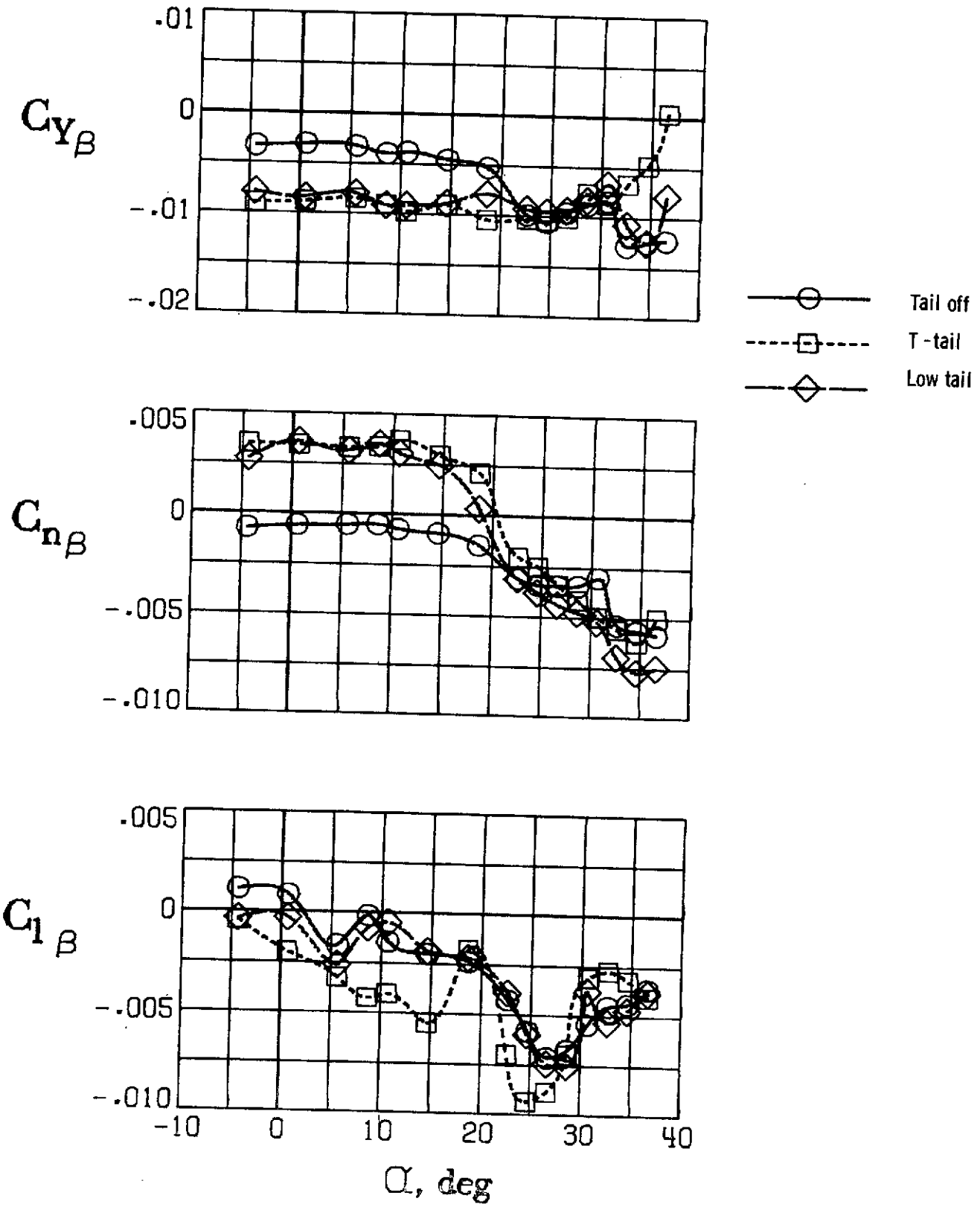

(b) δ_f = 30°/50°.

Figure 34. - Concluded.

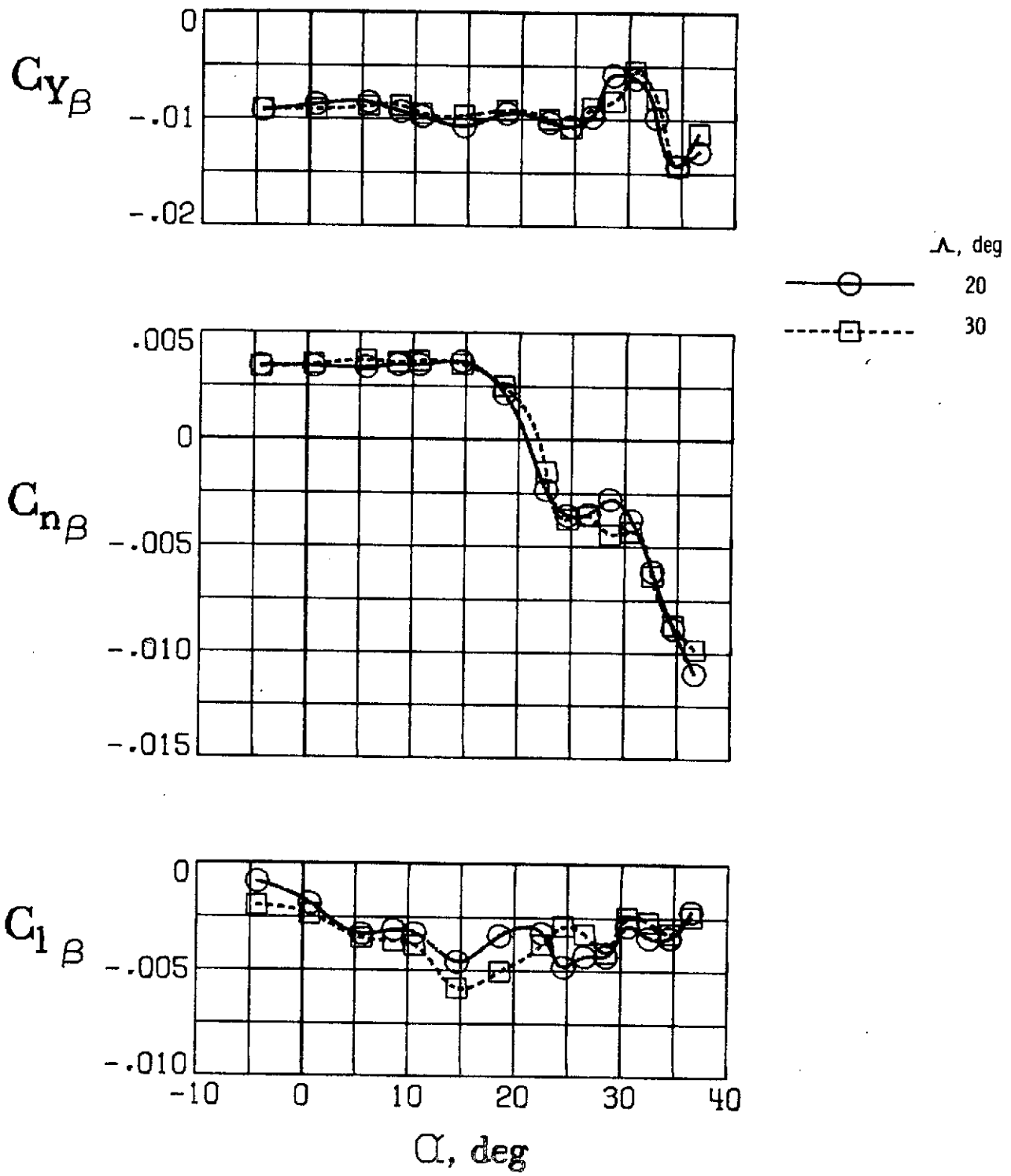

Figure 35. - Lateral-directional stability derivatives of slatted strake configuration for two wing sweep angles. $\delta_f = 14°/28°$.